ABSTRACT

Title of Thesis: AN ALTERNATIVE TO HYDRAULIC FRACTURING: AN EXPLOSIVELY DRIVEN MECHANICAL DEVICE

David T. Horst, Master of Science, 2018

Thesis Directed By: Professor William L. Fourney
Department of Mechanical Engineering

Hydraulic fracturing is currently used to extract natural gas from shale formations in the U.S, but there are major concerns regarding the environmental impact. As an alternative method of well stimulation, a mechanical device driven by explosive loading was developed. The goal of the device is to control the orientation of crack growth, in an unfavorable in situ stress field. Small scale model testing was conducted in PMMA, simulating an unconventional reservoir. A hydraulic press was used to simulate the in situ stress and high speed cameras were used to capture images of detonation, device function, and crack development. Variations were made to device geometry and the resulting crack growth is visually compared. Optimal device dimensions for fracture initiation are determined, and the effect of borehole characteristics on crack formation is discussed. Scaling recommendations for testing the device at full scale are provided.

AN ALTERNATIVE TO HYDRAULIC FRACTURING: AN EXPLOSIVELY DRIVEN MECHANICAL DEVICE

by

David T. Horst

Thesis submitted to the Faculty of the Graduate School of the University of Maryland, College Park, in partial fulfillment of the requirements for the degree of
Master of Science
2018

Advisory Committee:

Professor William L. Fourney, Chair

Professor Amr Baz

Professor Hugh Bruck

Acknowledgements

I would like to start to by thanking my advisor, Dr. William Fourney for his endless support and patience. Throughout the many challenges I faced, I knew I could count on Dr. Fourney's expertise and advice to help me along the way. I will always be thankful for the opportunities he has given me and the lessons he has taught me.

Next, I would like to thank the Center for Engineering Concepts Development (CECD) at UMD, for the financial support they provided to conduct this research. Without their backing, I would not have been able to pursue my research interests and benefit from the experiences I have gained during this project.

Also, I would like to thank my committee members, Dr. Amr Baz and Dr. Hugh Bruck, for their valuable input and flexibility to help. Their eagerness to help and contributions towards this thesis are highly appreciated.

I would like to give a special thanks to Mike Perna from the UMD Aerospace Machine Shop. His machining expertise and advice were crucial to my research. He was always willing to take a break from his busy day to help me out and teach me something new. I could not have done it without him.

Last but not least, I would like to thank Dr. Uli Leiste and Leslie Taylor. The two friendly faces that make the Dynamic Effects Laboratory the place that it is. Over the years I have received a healthy balance of friendly banter and expert advice from Uli and Les. Their presence is lab is irreplaceable and greatly improved my experience at UMD.

Table of Contents

List of Figures

Chapter 1: Introduction and Background

1.1 Introduction

In recent years, the role of natural gas has become increasing important for the United States energy sector. In 2016, natural gas was the largest source of primary energy production accounting for 33% of U.S. domestic energy production [1]. The increase in production of natural gas is mostly due to the access of unconventional reservoirs. The distribution of natural gas production by source can be seen in Figure 1 [2].

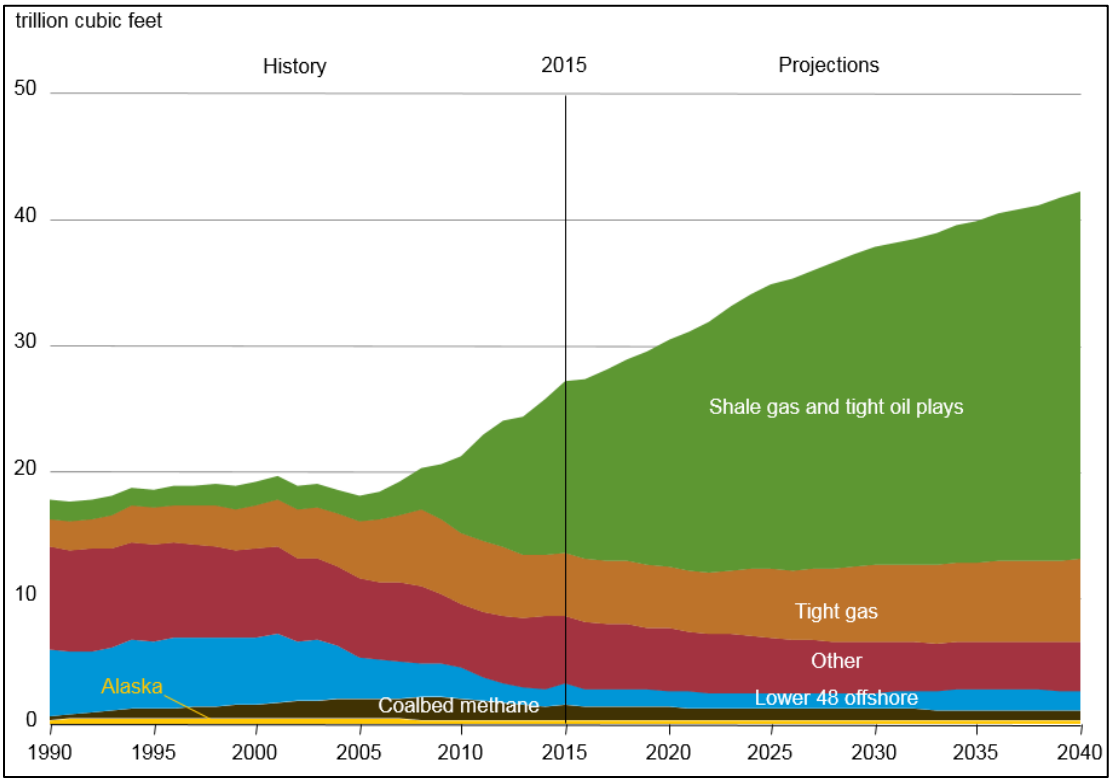

Figure 1: U.S natural gas production by source [2]

The historical data is presented along with a projection of future performance, as of 2015. As can be seen in Figure 1, gas production from shale and other low permeability

formations (tight gas) has seen a drastic increase in recent years. The increasing role of gas production from shale reservoirs can be attributed to developments in drilling and fracturing technologies, allowing for economic potential in low permeability reservoirs [3]. Three important factors leading to the economic viability of shale gas production are advances in horizontal drilling, hydraulic fracturing, and increasing prices in natural gas [3]. Horizontal drilling creates wells with much greater reservoir exposure compared to that of vertical wells due to the lamina structure of shale [3][4] . Hydraulic fracturing is a formation stimulation technique used to increase permeability in a producing formation, allowing gas to flow more readily to the wellbore [5][6].

1.2 Overview of the Current Hydraulic Fracturing Method

The process of hydraulically fracturing a shale formation begins after a suitable reservoir has been selected and a horizontal wellbore has been drilled. Before any fracking can occur, a steel pipe is inserted into the vertical section of the wellbore to serve as a protective casing. Additionally, a casing composed of either steel or concrete may be inserted into the horizontal section of the wellbore, depending on the structural integrity of the rock formation. Cement is then used to secure the casing and bond it to the adjacent rock surface. The casing provides structural support for the wellbore, preventing unwanted collapsing and acting as a protective barrier for the rock, separating the fracking fluid from entering protected zones such as aquifers [3][7] . Due to the length of the exposed wellbore, it is usually impossible to effectively pressurize the entire borehole at once [8]. Instead, the majority of the well is plugged, isolating a small

portion called a stage. Stages are fractured sequentially until the entire well has been stimulated [9]. For each stage, small shaped charges called perforators are placed in a helical/screw pattern around the borehole wall [7]. These explosive charges are detonated next, in order to rough up the borehole and create small cracks that will later be repressurized to cause further crack growth. Then, a liquid commonly known as "frack fluid" is inserted into the wellbore. As seen below in Figure 2, frack fluid is primarily composed of water and a proppant (sand), with a small volumetric percentage being chemicals that are used to alter specific performance characteristics of the fluid. The exact chemicals used will vary depending on the well operator, but some common uses are acid for dissolving minerals and expanding fractures, biocide for eliminating corrosion causing bacteria, and gelling agents to aid the suspension of the proppant [3]. The proppant is an essential component of the frack fluid, holding open fractures and allowing gas to flow back into the wellbore. After the frack fluid fills the borehole and existing cracks, it is pressurized with high power pumps from the surface. The high pressure fluid is forced outwards, expanding fractures vertically into the shale and allowing access to natural gas. After the cracks have arrested, the fluid is treated with chemicals to lower viscosity. The fluid is then pumped back up to the surface leaving the proppant behind to hold open fractures. When the fluid is removed, the wellbore becomes lower in pressure than the gas held within the shale formation and gas begins to flow back up to the surface for production. An overview of a horizontal well after hydraulic fracture is presented in Figure 3 [7].

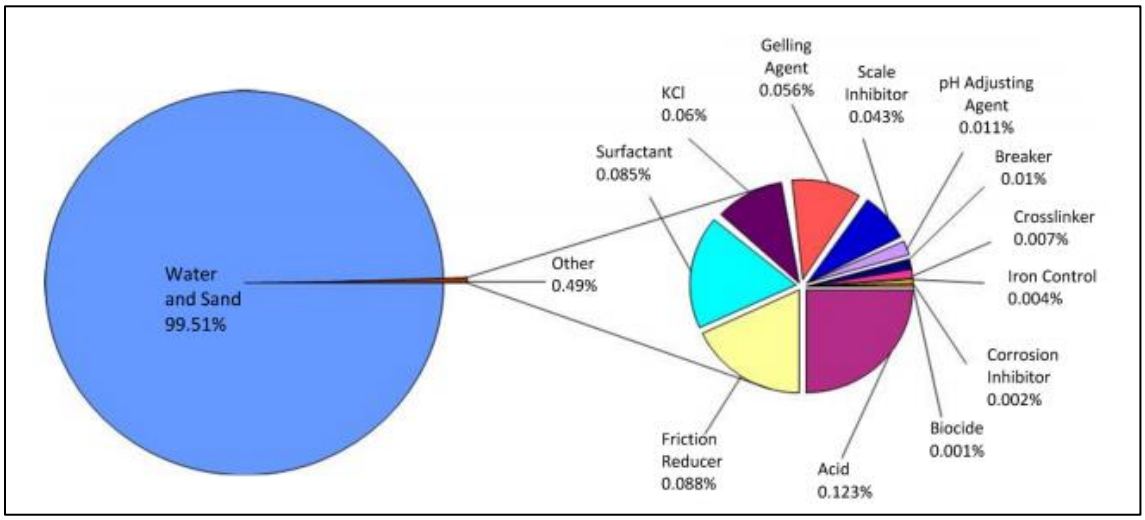

Figure 2: Volumetric composition of a generic fracture fluid [3]

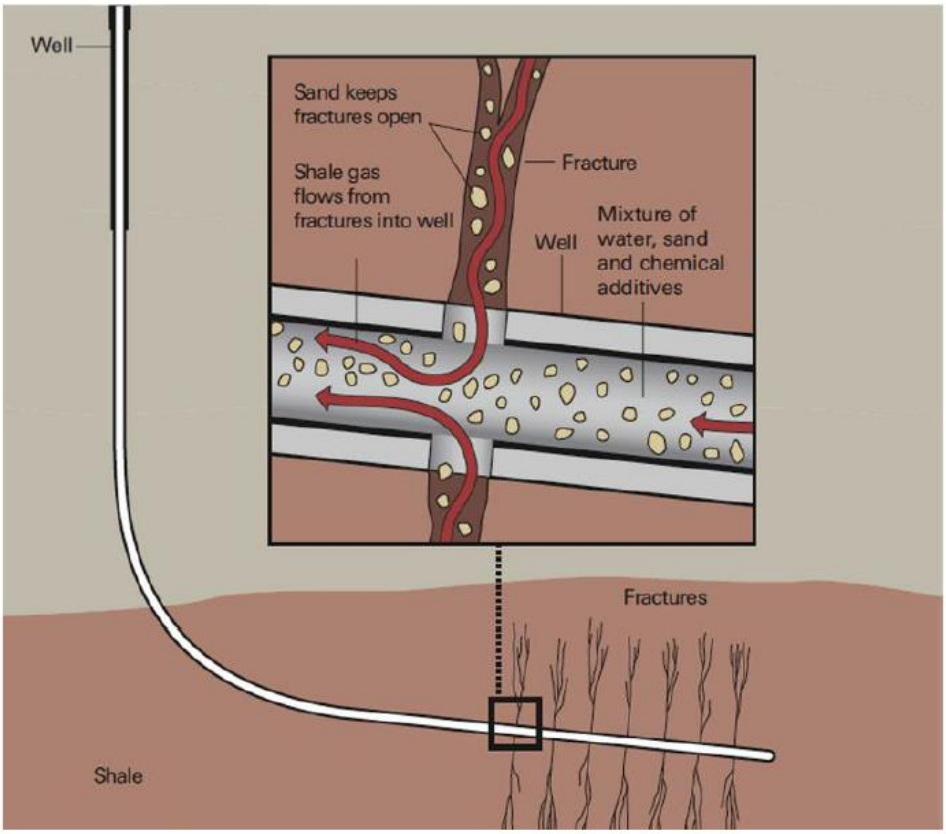

Figure 3: Vertical section view of a hydraulically fractured horizontal well [7]

1.3 Drawbacks of Current Method

Although hydraulic fracturing has been used successfully from an economic perspective, there are concerns over the environmental costs of the method [13]. A study by D. Zhang et al. on the environmental impacts of hydraulic fracturing of shale formations found that there is potential to consume fresh water resources, contaminate surface and groundwater, induce earthquakes, and pollute air. However, the water usage, as well as the intensity, are lower than conventional oil. Additionally, the earthquakes induced are non-destructive micro-earthquakes below 2 in magnitude [12]. It is likely that the reported earthquakes induced by fracturing and were larger than 3 in magnitude were a result of existing faults prior to fracturing [14]. The air pollution caused by hydraulic fracturing comes from pollutant emissions and gas leakage during extraction and transportation [12]. Some estimations place the greenhouse gas footprint of shale gas being greater than conventional oil [13], while other estimations expect the emissions to be significantly lower [15]. The environmental impacts stated above are substantial, but comparable to conventional reservoir extraction methods. The most distinctive and controversial environmental concern associated with hydraulic fracturing is water contamination. Studies have shown possible contamination risks from both stray natural gas [16][17] and wastewater leakage [18].

The environmental impacts presented have led to regulatory and social repercussions for the practice of hydraulic fracturing. Government agencies have restricted the practice and completely banned it in some states [10]. Other regions have seen large-scale rejection of the practice from angered citizens due to groundwater

pollution. D. Evensen et al. conducted a national survey on the support or opposition to both the terms "fracking" and "shale gas development." The results showed that nationally only 46% of the survey participants supported "fracking," while 62% of the participants supported "shale gas development" [11]. The author suggests that these results are most likely influenced by the language and connotation associated with each phrase. The media often uses fracking in a negative sense, while the media often uses developing the shale in a positive sense. This survey data could also be interpreted to mean that the method of fracking has large social rejection, while the idea of accessing the shale in general is more acceptable. Furthermore, this shows that citizens of the U.S. are not satisfied with the current hydraulic fracturing procedure and developing a new, more environmentally method of accessing unconventional reservoirs could be highly desirable.

1.4 Background

The researchers at the Dynamic Effects Laboratory at the University of Maryland have previously had success modeling boreholes in small-scale fracture testing. PMMA models have been tested using various well stimulation techniques. It was found that the results can be used to qualitatively predict results in full-scale testing of nonhomogeneous material [19][20] . The field conditions and stress states acting on the borehole dictate crack propagation and orientation. Model testing has been conducted showing the effects of the in situ stress field on a horizontal wellbore. Also, the use of machined flaws or notches as well as the influence on crack initiation and orientation due to variations in

flaw geometry, numbers of flaws, and locations of flaws has been studied. Notching techniques have been used to successfully control the orientation of crack growth [21]. The significance of the pressure versus time loading profile has been explored and variations in pressure magnitude and duration have been determined to be an important parameter for quantity and quality of crack development [22][23] .

Additional work has been performed to investigate the method of fracture initiation and the influence of borehole conditions. An immensely important and well documented concept for hydraulic fracturing is the in situ stress imposed by the overburden rock above a horizontal wellbore. This stress field acts as a vertical compressive stress on the borehole, making it very difficult to grow cracks in the horizontal plane. The in situ stress makes the direction of preferred fracture propagation parallel to the compressive stress and perpendicular to the least principle stress [24][25][26].

Mechanisms of brittle fracture in rock has been studied and a fracture theory has been developed. A relationship between crack velocity, driving energy, crack propagation, and crack roughness has also been established [24]. The principle of applying explosive energy in a borehole to initiate rock fracture has been studied and a method for finding borehole pressure generated from a detonation has been determined. The mechanism of how the resulting borehole pressure causes fracture growth is known [26]. The volume of reservoir accessible by a fracture network has been established as a metric for effectiveness. Increased surface roughness is desirable as it increases the volume of rock accessed and aides in keeping the crack open without the use of proppant.

Explosively driven cracks are driven at a higher speed and result in a higher crack roughness making them a superior source of crack propagation when compared to quasi-static loading [21]. One concern of explosively loading a wellbore is the formation of a residue stress cage after detonation is complete. Too much explosive can crush the immediate area around a borehole, where plastic effects cause the resulting fractures to close and resist opening to allow gas flowback. Filling the borehole with a fluid such as water has been shown to be an effective method of minimizing unwanted crushing [23][26]. The relationship between fluid medium, coupling ratio, and borehole pressure generation has been studied [26].

Another source of unwanted crack development can be discontinuities in the borehole. It has been found that circumferential cracks form at the ends of the borehole or at a change in diameter. Stress wave theory has been investigated and applied to fracture initiation by explosives [26]. The crack development at discontinuities can be attributed to a doubling in pressure wave magnitude and duration of loading due to reflection at the discontinuities [23].

This paper strives to use the established principles of controlling fracture growth, and apply them to developing a device that can be inserted into a wellbore. With the previous methods of fracture control, there is no practical way to reproduce results at full-scale due to the challenges of manufacturing flaws and notches in deep horizontal wells. The goal of this device is to replicate the successful fracture control demonstrated with notching techniques, by implementing a new mechanism of fracture initiation. The

recognized fracture theory will be applied to design a device capable of producing desirable crack characteristics for natural gas extraction.

1.5 Developing an Alternative Method of Crack Initiation

At the Dynamic Effects Laboratory at the University of Maryland, small-scale model testing is conducted to simulate hydraulic fracturing. A mechanical device driven by explosives was designed to initiate cracks in wellbores. The purpose of this device is to replace the need for chemical additives in frack fluid, reducing ground water pollution, and initiating cracks in any desired orientation within the shale formation. The device was manufactured and inserted into PMMA blocks, a transparent and brittle material, allowing for monitoring of crack formation. Variations in device design and geometries were investigated to find the optimal configuration. An analysis was performed on crack growth with high speed camera footage and post-mortem photography. A discussion of scaling the device to full-scale is presented and a final recommendation of device geometry for future testing is provided.

1.6 Small-Scale Testing

The small-scale explosive testing performed at the Dynamic Effects Laboratory at the University of Maryland has advantages over large-scale testing. The most obvious advantage of scaled testing is the amount of money that is required to conduct tests. The reduction in scale of explosives and other materials used saves a considerable amount of funds. Another benefit offered is that the time required for testing is much lower. When

developing a device or method, custom manufacturing can be very time consuming. Conducting these tests at small-scale means less time and materials are needed for manufacturing and drilling.

An important requirement of small-scale testing is that the results have some real meaning and implication for the real scenario. The Dynamic Effects Lab and other organizations investigating fracture mechanics of rock have provided field verification showing that small-scale testing in PMMA blocks can provide data with significance for full-scale testing. Specifically, the results found in small-scale testing provide qualitative information about how cracks will form from different techniques and loading scenarios [19][20]. With scaled testing it is important to look for general patterns of crack formation. Exact repeatability and scaling is not to be expected. This is due to small and randomly distributed cracks and flaws within materials that impact the development of the fracture system [24].

A common method for scaling blast waves is cube root scaling. The scaling law from Hopkinson's scaling states that for any distance R, the peak pressure blast will be proportional to the cube root of the weight of explosive [27][28]. A common form used from these scaling laws is given by the following equation:

$$\frac{R}{R_1} = \left(\frac{w}{w_1}\right)^{\frac{1}{3}}$$

In this equation, R is distance from the charge and w is the weight of the charge [29]. The subscript 1 denotes the new explosive. An example of this scaling can be applied to a change in borehole diameter. If an explosive charge of 250 mg is detonated in a 1 inch

borehole, an equivalent charge mass for a 4 inch borehole would be 16 grams of explosive.

Chapter 2: Overview of Device Design

As stated above, the Dynamic Effects Laboratory has had success controlling crack growth orientation under a large compressive load simulating in situ stress by using machined notches. However, it is not practical to use this method in a horizontal well due to the challenges of manufacturing. Instead, a device was designed to reproduce the results of notches while remaining compact and capable of being inserted. The design requirements are that the device must be manufactured and assembled at the surface, and also be capable of being inserted into a horizontal borehole and then detonated to initiate fractures.

Shale reservoirs are an anisotropic media with a laminar structure, generally oriented in the horizontal plane. Natural gas is contained within these layers of the shale. For this reason, the horizontal plane will be the desired orientation of crack growth, as it will allow for a greater volume of natural gas access when compared to growth in the vertical direction. Access to the reservoir in the vertical direction is limited by the thickness of the shale reservoir. Fracture growth in the horizontal direction has the potential to be extended a much greater distance, but this is not possible with current methods due to the in situ stress field acting on the formation. The primary concern for horizontal crack growth is the vertical compressive stress imposed by the overburden rock. A compressive stress in the vertical direction impedes horizontal crack growth and makes the vertical direction the preferred direction of fracture initiation. The device

developed must be capable of overcoming the unfavorable conditions imposed by this compressive stress, and initiate crack growth in the horizontal direction.

The premise of this device is based around using hardened steel wedges with a tapered edge (3 degrees), which will be explosively driven into the side of the wellbore. A thin-walled aluminum rod with slots is used to hold and align the wedges. A tapered steel pin with a matching degree of taper (3 degrees) to the wedges is inserted and epoxied into the rod and wedge subassembly. The assembly of the three components are then inserted into a 15/16 inch diameter by 5.5 inch long borehole within a PMMA block. PMMA is chosen due to its transparency, allowing internal deformation to be monitored more easily. Additionally, PMMA has been replicated in field testing, proving it serves as an effective qualitative model of anisotropic rock. An explosive charge composed of PETN and lead azide is placed in close proximity to widest end of the steel pin and wires are run out of the block to an external firing box, and then a plug is inserted into the borehole and bonded with an adhesive. Finally, the entire block is inserted into a hydraulic press where a significant load is applied perpendicular to the plane of desired cracking to model the in situ stress. An exploded top view of a computer-aided design

model for an assembled block can be seen below in Figure 4.

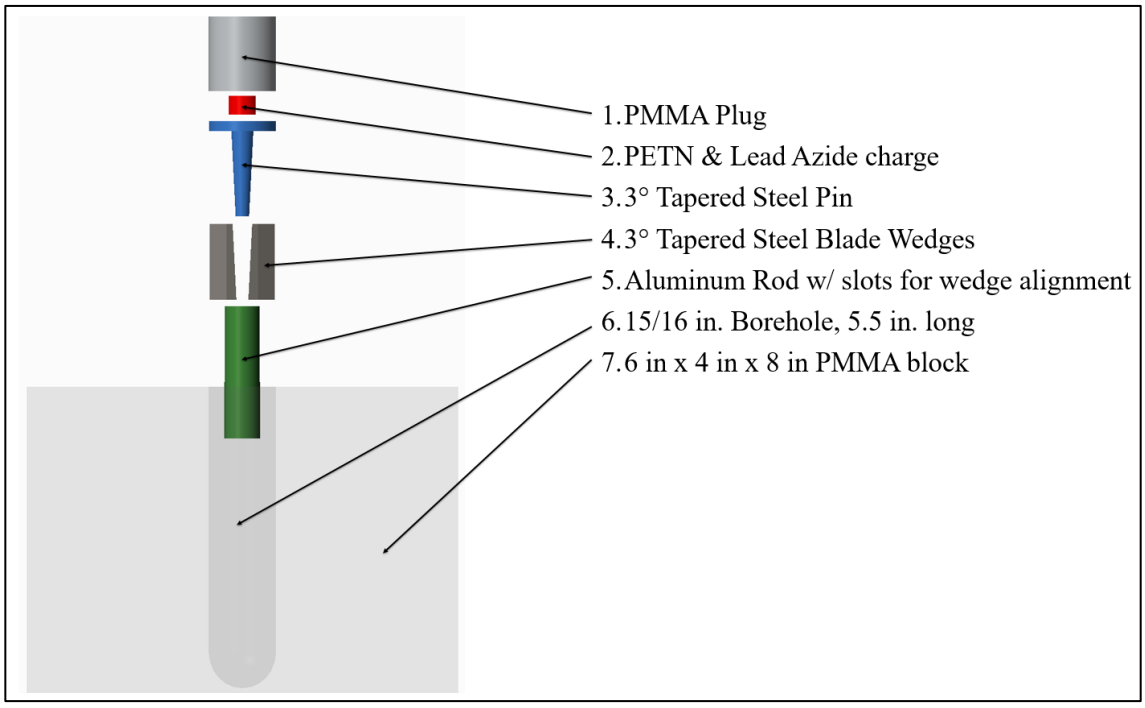

Figure 4: Exploded top view of CAD model for preliminary design

To initiate the test, a high voltage is applied to the firing cables causing a detonation of the charge. The detonation causes pressure to build up within the borehole, driving the pin down through the wedges. Due to the taper on the wedges, they are driven outward into the wellbore wall and embed themselves within it. This deformation, combined with the pressure build up in the borehole, initiates a crack in the orientation of the blades. This method successfully overcomes the preferred direction of cracking caused by the applied compressive stress and allows controlled crack orientation.

To further expand the initial fractures, a second stage of testing is performed on the same block. The plug and device are removed from the borehole and the borehole is drilled fresh again to ensure no unwanted material is left behind. A second smaller

charge is inserted and the borehole is filled with water. The borehole is plugged again and reinserted into the hydraulic press under the same compressive load. The charge is detonated and the initial fractures are expanded farther horizontally.

A third and final stage of testing is conducted. Now that the dynamic fracturing potential has been performed via explosive loading, the block is connected to a hydraulic pump to further expand the cracks by quasi-static loading. A steel plug with NPT threads is bonded into the borehole, the borehole is filled with hydraulic oil, and the block is reinserted into the hydraulic press. The hydraulic pump applies a slow incremental pressure increase until the fracture grows. One of the cracks initiated by explosive loading (the most well defined crack) will continue to grow until it reaches an outer surface of the block and loses pressure.

It is worth noting the reasoning and implications of using hydraulic oil as a pressurization medium. The first and most obvious reason is that it was an inexpensive fluid compatible for use with the hydraulic hand pump. However, the high viscosity of the hydraulic oil is also advantageous. The increase in viscosity helps pressurize major flaws, while avoiding the fluid from pressurizing and extending minor flaws. In a porous material such as rock, a high viscosity fluid will avoid leakage and flow into unwanted areas. Furthermore, most of the current fluids used in hydraulic fracturing at full-scale are very viscous, so using a viscous hydraulic oil will be an effective model for small-scale testing.

Chapter 3: Materials and Methods

3.1 Testing Equipment

In order to conduct small-scale explosive testing, there are equipment requirements and test preparation is needed. Specifically, there is explosive equipment needed for conducting detonations, optical equipment needed for recording and observing models, and preparation equipment needed to assemble models and modify their characteristics. A detailed discussion of the typed of equipment needed and the methods of test preparation are provided.

3.1.1 Explosive Equipment

The most obvious and fundamental equipment for explosive testing are the charges themselves. For initial testing, premanufactured charges from a large-scale distributor were purchased. However, an iterative design process was used for early testing in order to quickly narrow down device geometry and charge sizing. During this period, it was determined that using fixed size charges purchased in bulk from retailers were not economically feasible. Instead, creating custom charges was preferred. This option offers flexibility in charge sizes between tests and the ability to manipulate charge mass with ease. An overview of an unassembled custom charge can be seen below in Figure 5.

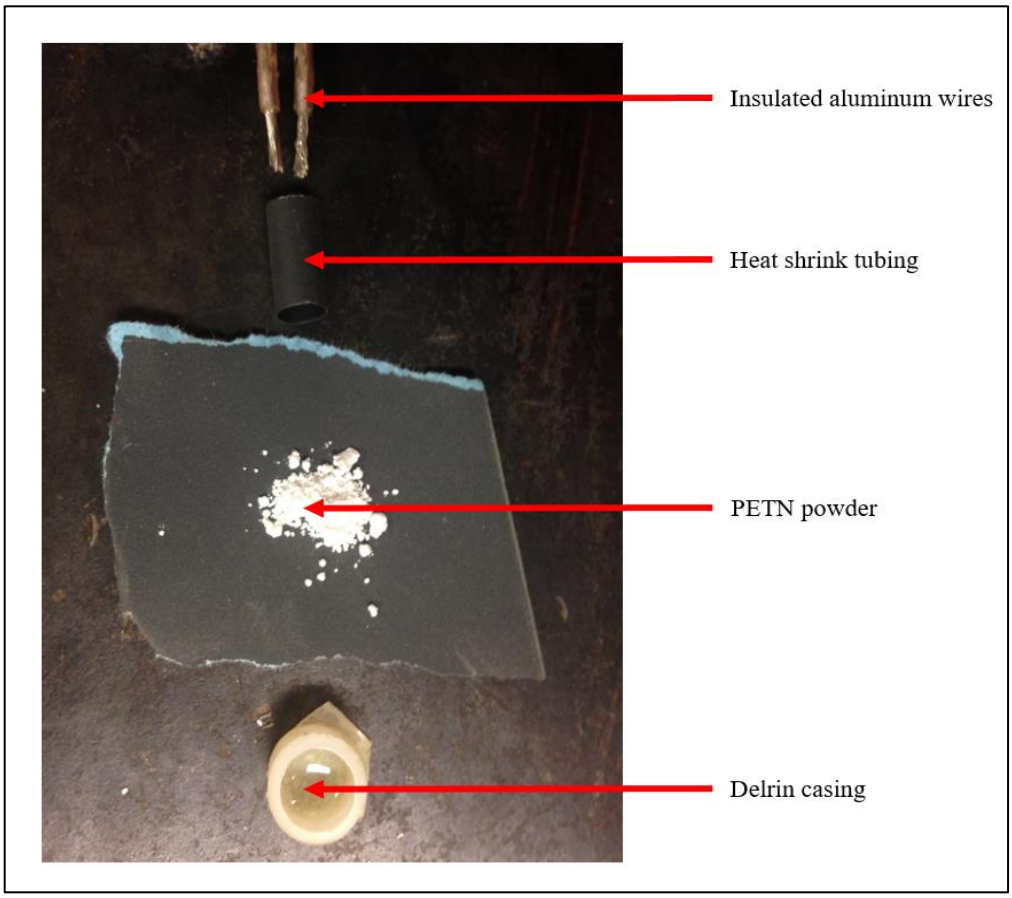

Figure 5: An overview of a custom explosive charge

Manufacturing an explosive charge begins with two 18 AWG aluminum wires. One end of each wire is stripped and fastened together to form a single length of wire. This is a safety precaution taken to avoid an unintentional voltage difference from static build up when in contact with sensitive initiating explosive. The other ends of the wires are stripped to expose roughly 3 mm of the inner aluminum core. The exposed lengths of wire are separated by a small gap, about a millimeter in width. A heat shrink tube with a diameter of 5 mm (0.196 in) is placed around the exposed sections and a heat gun is applied. The heat shrink tube secures the wires together while holding the gap at a fixed distance. The heat shrink tube now has the structure of a small firm cylinder which will

house the initiating explosive, lead azide. 10 milligrams of lead azide is carefully packed into the heat shrink, filling the gap between the two aluminum wires. This assembly functions as a detonator for the charge. A Delrin tube with an OD of 9.52 mm (0.375 in) and an ID of 7.39 mm (0.291 in) serves as a casing for the charge. The Delrin casing is epoxied to a sheet of paper, closing one end of the tube. The other end of the casing is filled with the desired amount of powdered PETN. The end of the aluminum wires with heat shrink tubing and lead azide are inserted into the casing and embedded in the PETN powder. The rest of the casing is filled with epoxy and the adjacent wires are coated in epoxy as well. This provides a waterproof seal and structure integrity for the assembled charge. Figure 6 shows a completed charge.

Figure 6: Completed custom explosive charge

To initiate the custom charge, the free ends of the wires are unfastened and a high voltage difference is applied to them. This causes an arc to occur across the small gap located at the opposite end, inside the charge. The arc causes a spark which initiates a detonation in the sensitive lead azide. A chain reaction occurs, setting off the PETN powder and detonating the remainder of the charge.

In order to provide a high voltage in a controlled and safe manner, a firing system is necessary. For the purpose of these tests, the FS-10 control unit was obtained from Reynolds Industries Systems Incorporated. The firing system is capable of supplying 4,000 volt energy source to the explosives, creating a significant arc and spark. An additional feature of the firing system, is its capability to simultaneously send a trigger signal to other electrical equipment upon firing. This is a very useful tool for timing the high speed camera that is used to record images after detonation. The FS-10 firing system can be seen in Figure 7.

Figure 7: FS-10 Firing System

3.1.2 Optical Equipment

To observe the function of the device and the resulting growth of cracks, a Phantom v12.1 high speed camera was used. The camera was equipped with a Nikon Nikkor 50 mm lens for optimal image quality. The Phantom camera was placed upon an adjustable tripod that allowed for fine tuning of position. Figure 8 shows the camera with the lens attached, and mounted on the adjustable tripod. The camera sensor allows for a maximum resolution of 1280 x 800 pixels. However, in order to obtain higher frame rates, the resolution is often reduced. Due to the high speed nature of explosive and fracture development, the frame rate most commonly used for testing was 91,056 frames per second. This framerate allows for an image to be recorded every 11 microseconds. The resolution of the images recorded were 256 x 184 pixels. With the chosen frame rate

and image size, the camera is then positioned to have the area of interest within the field of view. Then, the attached lens can be focused by hand to find the highest clarity image. An Ethernet cable is connected between the camera and a computer allowing for remove control and managing various settings. Also, a cable is attached between the firing system and the camera to provide a trigger signal upon detonation.

Figure 8: Phantom v12.1 high speed camera

One challenge with high speed photography is generating enough light to illuminate the area of interest and reach the sensor. At high frame rates the sensor is not exposed to light for very long, so the images appear darker. To account for this, additional lighting is provided by two incandescent 250 W lamps. Two lights were positioned to shine light at the model within the hydraulic press. This proved to be an effective way of illuminating cracks as they formed and grew during testing. Additional lighting is also useful for inspecting and analyzing models after conducting tests. A combination of the incandescent lights and a custom LED array were used to illuminate the cracks. The custom LED array is shown in Figure 9.

Figure 9: LED array for analyzing crack development after loading

3.1.3 Loading Equipment

An essential component for this model testing was a hand-operated hydraulic press. This piece of equipment was responsible for simulating the in situ stress field generated by overburden rock. The press is pictured in Figure 10. The assembled model

PMMA block is inserted with the borehole oriented horizontally and parallel to the loading platens. A steel plate is placed between the loading platens and both sides of the block, to evenly distribute the applied load. It features a hand lever, using mechanical advantage to generate incremental increases in load. A gauge measuring force is mounted at the top of the press to monitor the current load. Once a desired load it reached, the press will maintain it until a release value is opened. The maximum load capacity of the press is 88.9 kN (20,000 lbf), but in the interest of the longevity of the press, the load was restricted to 80 kN (18,000 lbf) during testing.

Figure 10: Hydraulic hand press used to simulate in situ stress

As mentioned in the discussion of the preliminary design and testing process, the third pressurization of the model borehole is performed using quasi-static loading. This

loading is applied by the hydraulic hand pump shown in Figure 11. The pump features a hand lever, giving the user mechanical advantage. There is also an attached pressure gauge that provides readings of the current pressure being applied. The output of the pump is through a 3/8 inch NPT thread. A tapered thread is an effective method for maintaining a seal for high pressure applications. The threads are wrapped in Teflon pipe sealing tape and inserted into a threaded steel plug bonded within the model block.

Figure 11: Hydraulic hand pump used for quasi-static loading

3.2 Method of Model Assembly and Testing

3.2.1 First Stage of Testing

The process of preparing for a test begins with a PMMA block machined to the desired dimensions. The machined surfaces of the block are then sanded with 600 grit water proof sand paper while wetted. The surfaces must then be polished to remove any remaining surface flaws. The result is a smooth and transparent model that allows for

easy monitoring of internal deformation and crack growth. The final dimensions of the model block can be seen in Figure 12. Note that that the displayed units are in inches. The model has a cross section of approximately 102 mm (4 in) by 152 mm (6 in). The length of the model is approximately 203 mm (8 in). A borehole with a diameter of 23.8 mm (15/16 in) is machined at the center of the cross section, extending 140 mm (5.5 in) in total length. This leaves 63.5 mm (2.5 in) between the bottom tip of the borehole and the bottom surface of the block. From preliminary testing, it was determined that this spacing was necessary to ensure that the bottom portion of the block does not blow out when the borehole is loaded. There is some variation in borehole roughness throughout the manufactured blocks. This is due to deterioration of the condition of the drill bit over time. The effect of borehole roughness on crack growth is analyzed and discussed.

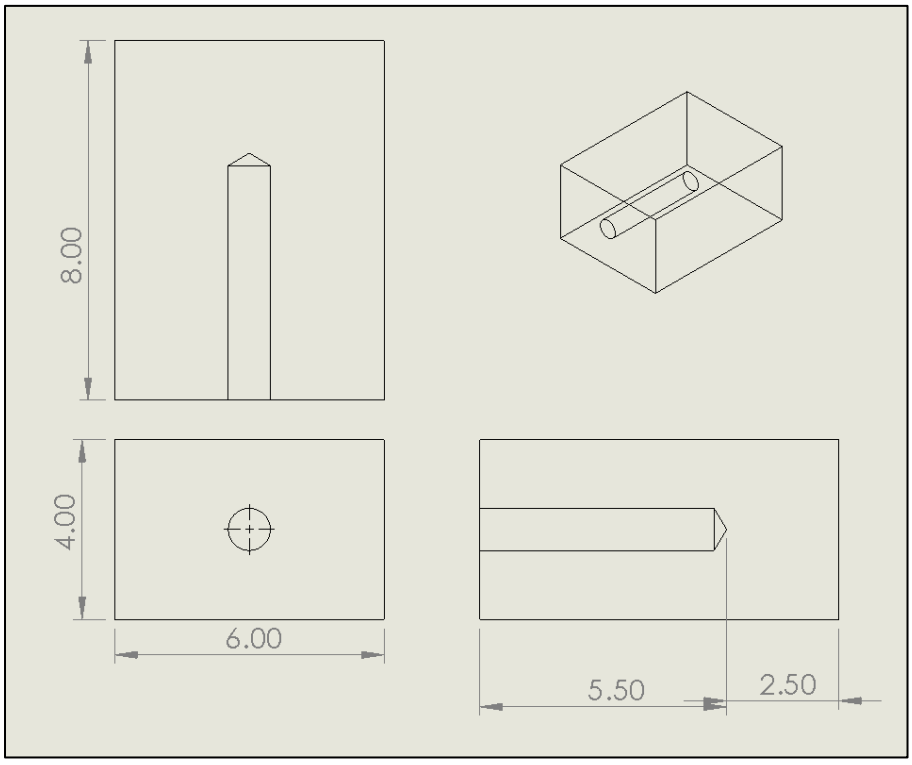

Figure 12: Engineering drawing of model block

The next step of assembling a block for testing is putting together the aluminum rod and steel tapered wedge subassembly. The wedges are a critical component of the device since they are directly responsible for causing deformation and causing crack growth in the borehole wall. The wedge geometry was changed between tests to see how the variations affect the success of crack formation. A general schematic for the tapered wedge component is presented in Figure 13, the listed dimensions are inches. An important dimension for assembly and alignment is the 3.2 mm (1/8 in) thickness of the tapered end. This dimension remained constant throughout all tests. Similarly, the width of the two ends remained constant at 8.1 mm (0.32 in) and 9.4 mm (0.37 in) for all tests. This dimension determined the gap between the wedges and borehole wall when the model was assembled. The goal of this was to have a small consistent gap size that allowed for the wedges to be inserted without damaging the borehole prior to testing, while also remaining relatively snug within the borehole. If the gap is too large, the blades have a tendency to misalign during test preparation and can deviate from the desired orientation. The angle of the pointed side of the wedge was varied to observe its influence on crack growth. The angle was tested at 10°, 20°, and 30°, and the resulting crack formation was studied. The mass of each wedge is 1.58 g, 2.8 g, and 3.39 g respectively. Additionally, the length of the wedge was varied to study its impact. One test was conducted at half the normal length of 25.4 mm (1 in) with an angle of 30° and a mass of 1.61 g.

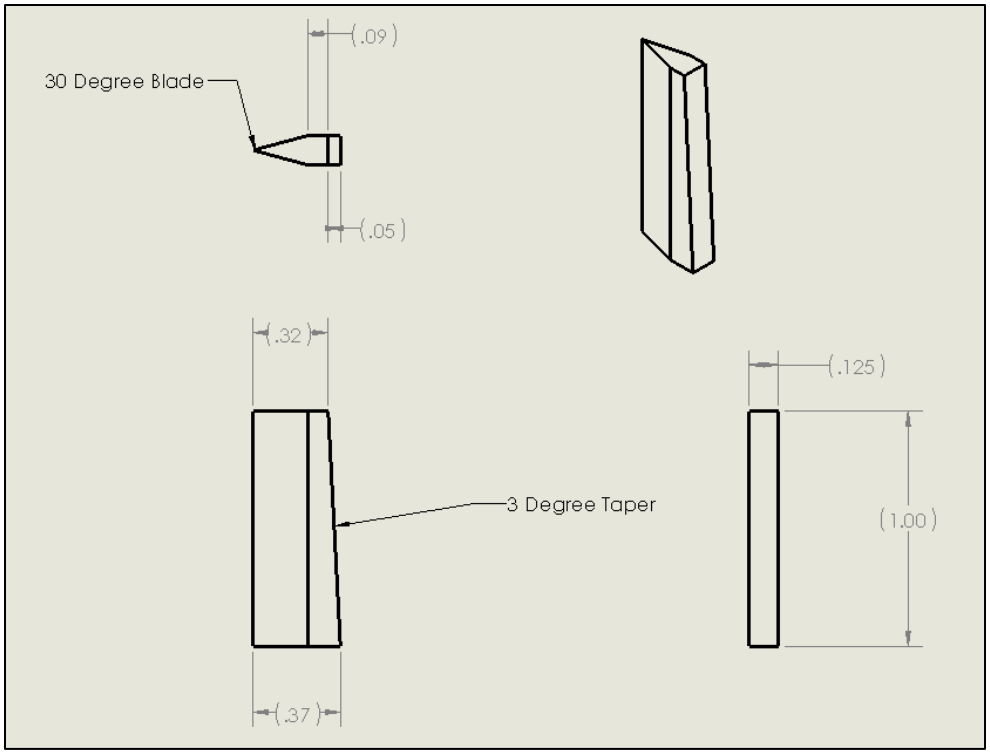

Figure 13: Engineering drawing of tapered wedge blades

In order to provide a controlled method of alignment, the wedges are assembled into a slotted rod. The aluminum rod can be seen in Figure 14, dimensioned in inches. As noted above, the tapered wedges have a constant thickness of 3.2 mm (1/8 in). The rod has a corresponding slot with a gap size of 3.2 mm (1/8 in). If machined correctly, the slot and wedge will fit with an interference fit. Occasionally, adjustments are necessary and a thin steel file is used to remove burrs or open the gap by a small amount. Once the wedge can be inserted into the rod's slot, it is aligned so the distance from the outer tip of each wedge's blade is 23.4 mm (0.92 in). This is an appropriate distance for providing a small gap between the wedges and borehole wall when inserted. After the wedges are aligned, quick set epoxy is applied. The epoxy does not serve any structural purpose during testing, but is helpful in maintaining the desired alignment while

assembling the remainder of the model. The completed subassembly composed of the aluminum rod and steel tapered wedges can be seen in Figure 15.

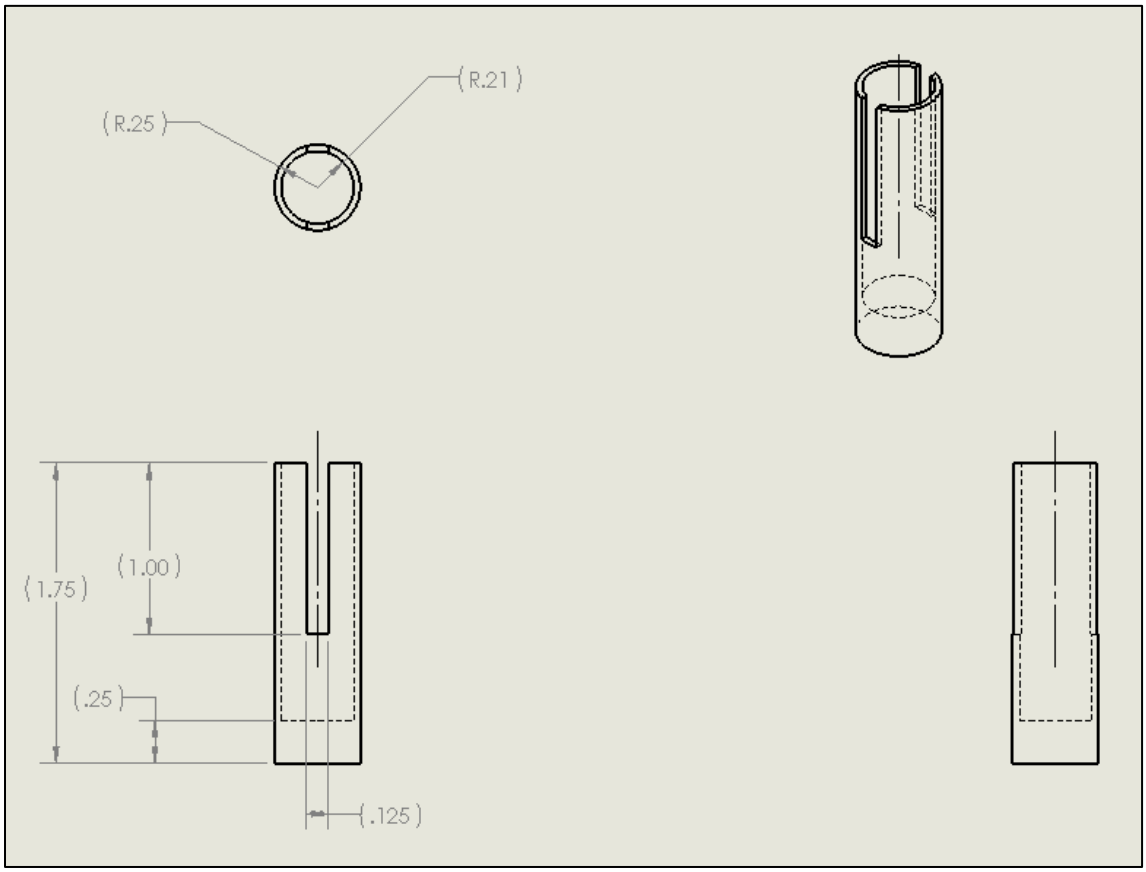

Figure 14: Engineering drawing of slotted aluminum rod

Figure 15: Aluminum rod and steel wedges subassembly

The tapered steel pin is the next component to be assembled. A dimensioned drawing of the pin with units of inches, can be seen in Figure 16. The pin features a 3° taper on its side to match the tapered edge of the wedges. This is helpful for alignment purposes, but is also responsible for driving the wedges outward into the borehole wall upon detonation. For assembly, the pin is inserted into the rod and wedges subassembly. The pin's tapered sides rest upon the tapered ends of the wedges which centers the pin within the rod. The small end of the pin reaches the midpoint of the wedges when assembled, which is 12.7 mm (0.5 in) from the top surface of the aluminum rod. Similarly to the assembly of the wedges, once the pin is in the desired position it is secured with quick set epoxy. The assembled device containing the pin, rod, and wedges is shown in Figure 17. Another important dimension of the tapered pin is the 23.4 mm (59/64 in) diameter top surface. This dimension was chosen to be sized just under the

diameter of the borehole, allowing for a tight fit without impeding assembly. When detonation occurs, this tight fit will restrict the rapidly expanding gases from the charge, generating pressure on the pin's top surface. The pressure drives the pin which initiates the movement of the wedges and the resulting crack growth. The last noteworthy feature of the pin is the 1/4 -20 threads machined in the top surface. The threads serve as an alignment tool once the device is inserted into the borehole. When the device is inserted, a screw can be lightly threaded into the top of the pin and used to fine tune the alignment of the wedges.

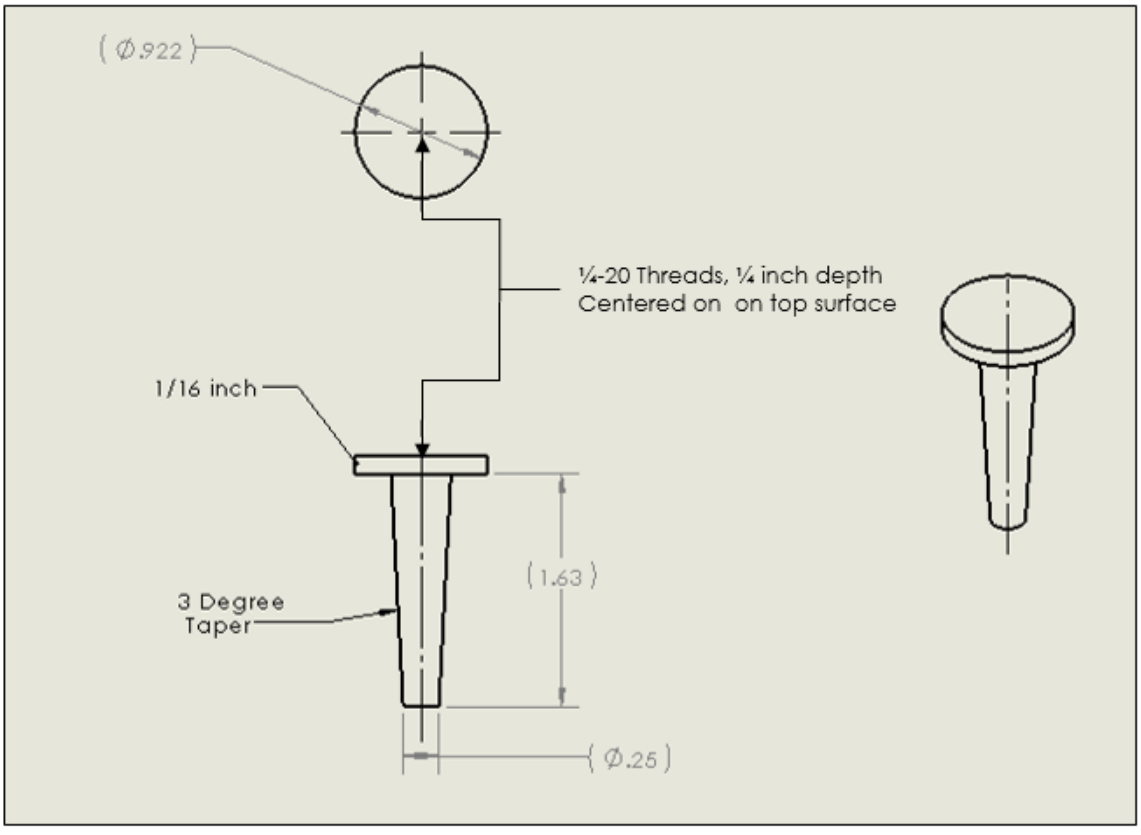

Figure 16: Engineering drawing of tapered steel pin

Figure 17: Assembled device (pin, rod, and wedges)

The final step of assembly is inserting a charge and plugging the borehole to hold pressure upon detonation. The charge size used for this stage of testing is 250 mg of PETN and 10 mg of lead azide as an initiating explosive. The plug material used is PMMA for earlier stages of testing or Polycarbonate (PC) for later tests. The material type is not critical; the switch to PC was made solely for easier manufacturing. The geometry of the first stage plug remained constant throughout all tests and can be seen in Figure 18. The 7.9 mm (5/16 in) through hole is for running wires from the explosive to the external firing system. The larger diameter hole at the bottom of the plug is used to center the explosive charge. The outer surface of the plug has a diameter of 23.75 mm (0.935 in), providing a very close fit to the borehole wall. The outer surface is roughed with coarse sand paper and cleaned with a degreaser safe for plastic use, such as isopropanol alcohol. The same surface treatment is applied to the borehole wall where the plug will be in contact. This technique increases the bonding strength by increasing

the surface area and removing trace amounts of oil from machining, which can potentially interfere with bonding. The adhesive used for bonding is 3M Scotch-weld instant adhesive, model CA8. This is a great choice for high pressure sealing of plastics. The 3M adhesive acts more similarly to a plastic weld than a traditional glue. The process of applying begins with first coating each surface with the adhesive via paint brush. This method allows the adhesive to seep into the roughed up surfaces and improve bonding. After, the plug is coated in the adhesive and inserted into the borehole. Although the adhesive sets quickly, it was given 12 hours to gain strength prior to testing. Additionally, the 7.9 mm (5/16 in) hole allowing the wires to run through the plug is sealed with epoxy at the top surface. A completely assembled and ready to test model is shown in Figure 19.

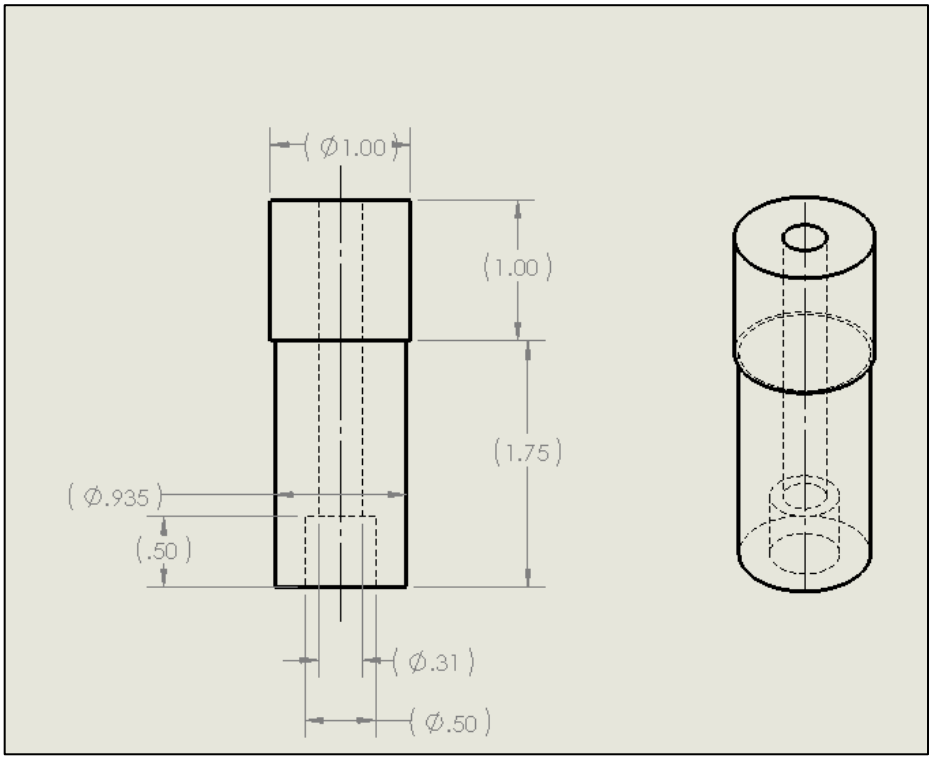

Figure 18: Engineering drawing of first stage plug

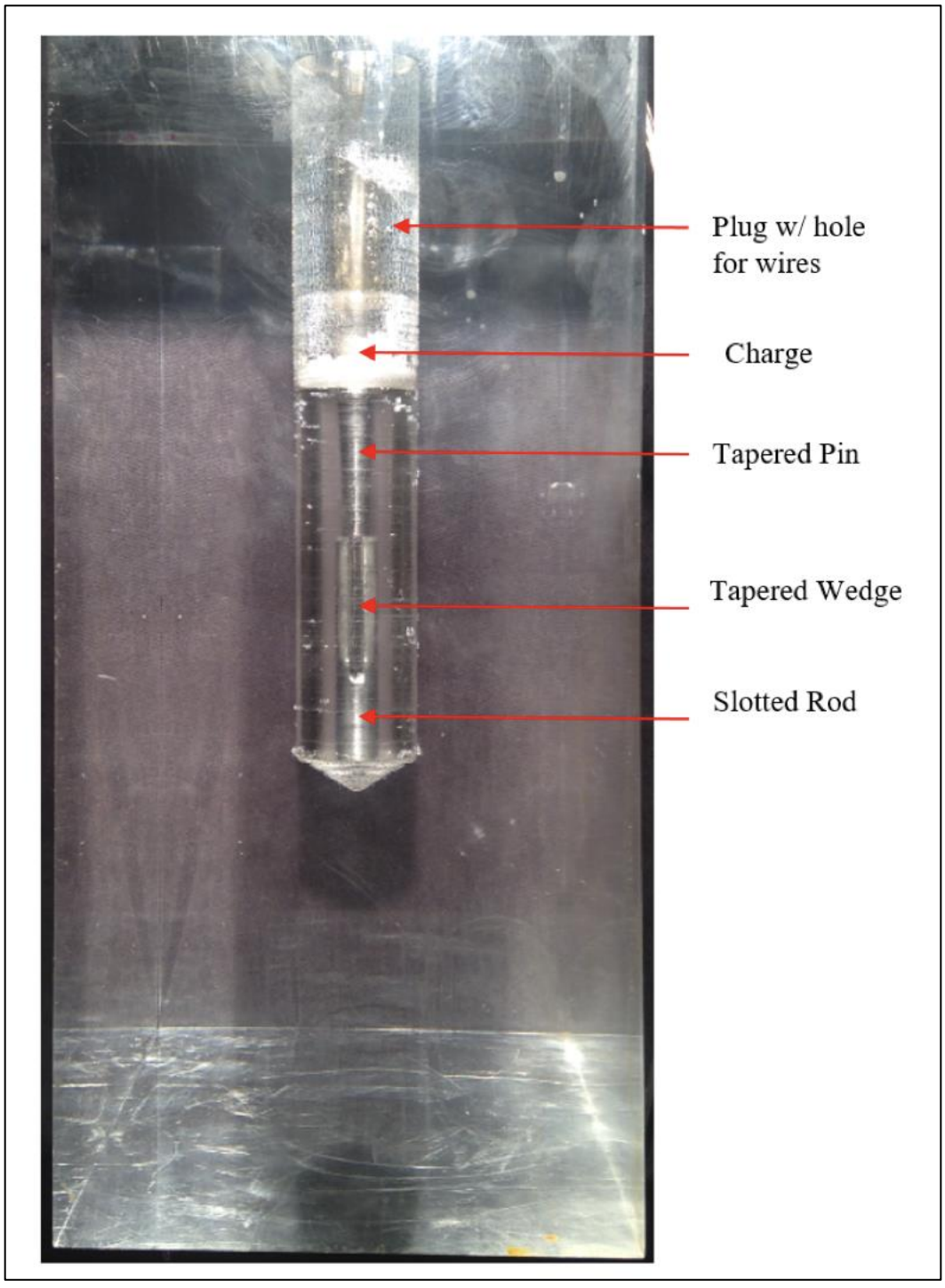

Figure 19: Assembled model prepared for first stage of testing

After the bonding adhesive has had sufficient time to cure, the model is ready to be tested. The assembled block is inserted into the hydraulic press with the borehole oriented in the horizontal plane. In this orientation, the press is loaded and 80 kN (18,000 lbf) of compressive force is applied in the vertical direction, perpendicular to the horizontal plane. The charge is detonated and the results are analyzed.

3.2.2 Second Stage of Testing

After the results of the first stage are measured and recorded, a second stage of testing is conducted to expand the initial fractures. In order to prepare for the second stage of testing, the plug and device from the first stage must be removed. The plug occasionally dislodged from the borehole when testing, but typically was drilled out. Significant changes in borehole size from the first stage does not occur, but to remove unwanted adhesive or surface abnormalities, the borehole is drilled again. After removal of the plug, the rod, pin, and wedges are all removed from the borehole. A new charge with 100 mg PETN and 10 mg lead azide is then prepared. The charge is inserted in the borehole, positioned around the horizontal fractures initiated in the first stage of testing. The 3M scotch-weld is painted on the inside of the borehole to seep into the prepared surface and cover any unwanted cracks. The borehole is then plugged with a new, longer PMMA or PC plug. The additional length is useful in providing additional strength and plugging any unwanted cracks that developed at the bottom of the first stage plug. Aside from the length, the new plug is dimensioned and prepared in the same manner as the first stage plug. An engineering drawing for the second stage plug is shown in Figure 20.

The dimensions shown are in inches. The surface preparation method is repeated, sanding and degreasing the bonding surfaces of the plug and the borehole. The 3M Scotch-weld instant adhesive is applied and given at least 12 hours to cure. After the 3M scotch-weld has set, the borehole is filled with water through the hole in the plug and then sealed with epoxy. The water serves to efficiently pressurize the borehole while minimizing unwanted crushing. The model block is then reinserted into the hydraulic press with the same orientation for a second detonation. The constant load of 80 kN (18,000 lbf) is applied vertically. The charge is detonated and the results from the second stage are analyzed and recorded.

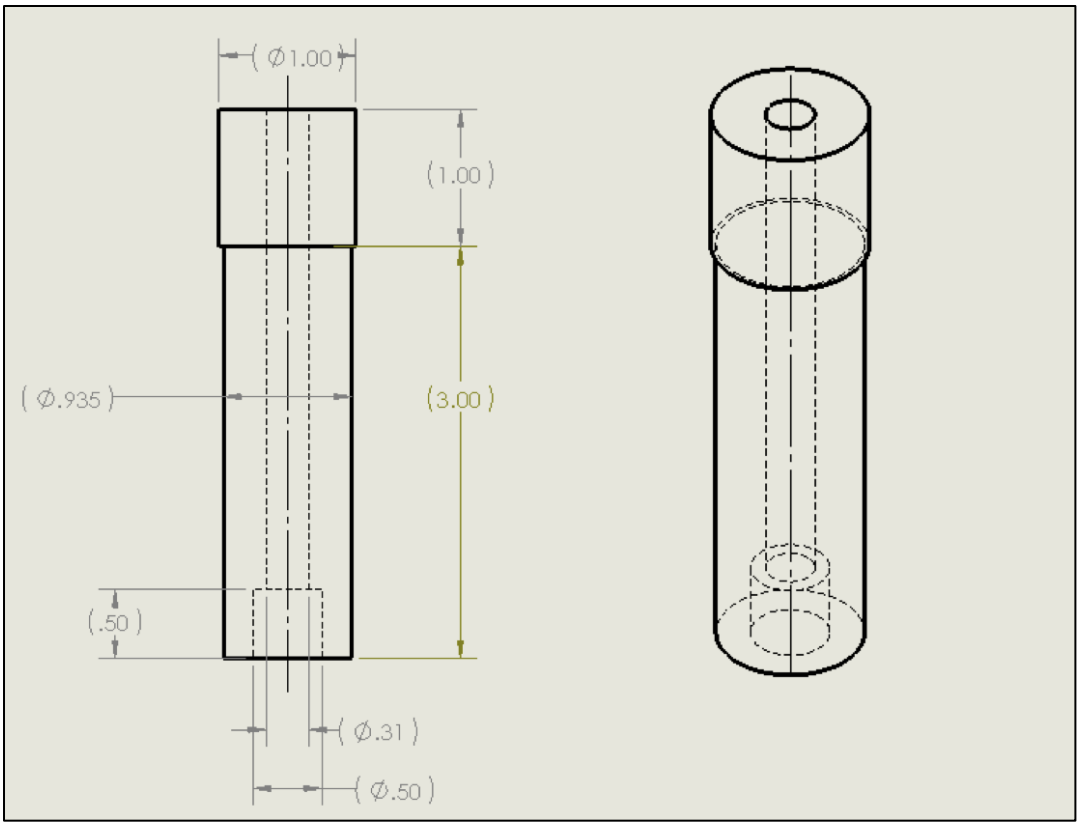

Figure 20: Engineering drawing of second stage plug

3.2.3 Third Stage of Testing

To prepare for the third and final stage of testing, the second stage plug is removed and the borehole is drilled fresh again. This time, a steel plug with internal 3/8 inch NPT threads is used. A schematic of the plug can be seen in Figure 21, the dimensions provided are in inches. The use of steel as the material for this component is important, as plastic threads are prone to leakage and failure for this high pressure application. The plug's bonding surface is prepared by etching with a steel file and degreasing with a cleaner. The borehole wall is prepared by using sand paper and isopropanol alcohol, in the same manner as the previous stages. Once again, the 3M scotch-weld is applied to the inside of the borehole and the plug is inserted. After the plug has set, the borehole is filled with hydraulic oil, identical to the type used in a hydraulic pump. Then, Teflon tape is applied to the matching male 3/8 NPT threads of the hydraulic hand pump. The threads are inserted into the steel plug protruding out of the assembled model block and secured with a wrench. The block is then reinserted onto the loading plate of the hydraulic press and the constant load of 80 kN (18,000 lbf) is reapplied. The Phantom v12.1 high speed camera is positioned to record both crack growth and the pressure gauge located on the hydraulic pump. This allows for a pressure reading at the time of failure. The hydraulic hand pump is then loaded in a quasi-static manner. Load is slowly applied in small increments until a crack is extended to a free surface, losing pressure within the borehole.

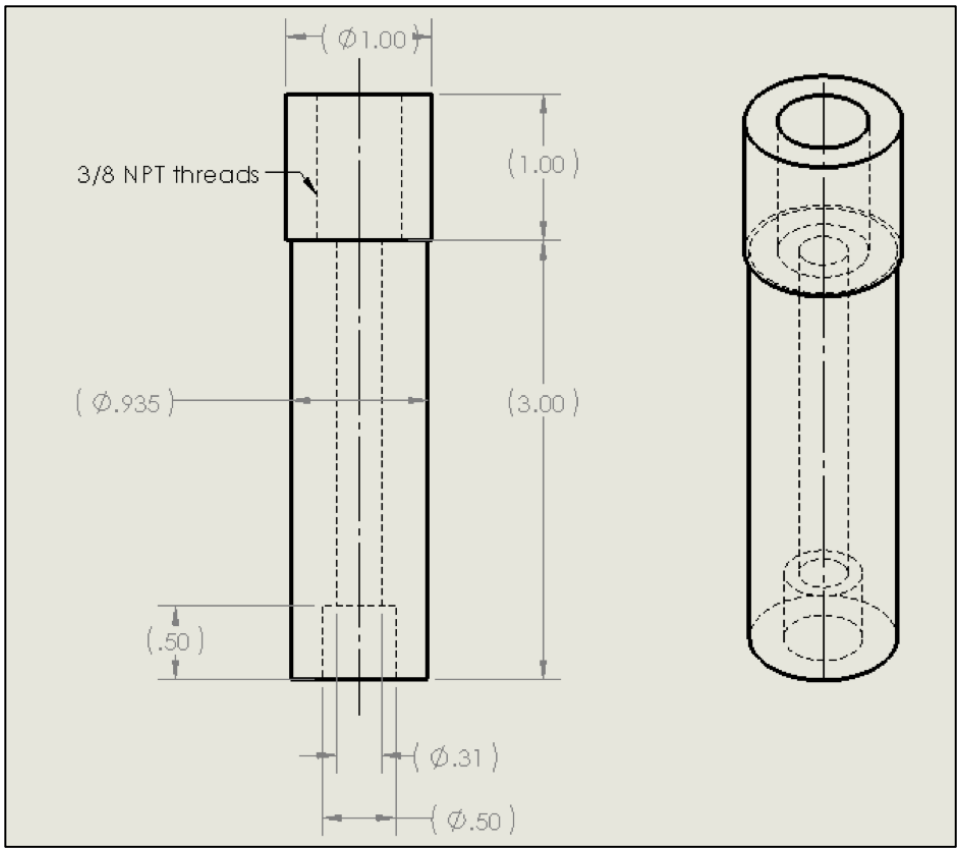

Figure 21: Engineering drawing of third stage plug

Chapter 4: Experimental Results

4.1 Preliminary Testing and Design Iteration

In order to develop with the current functioning device, some basic preliminary testing was conducted. These tests used different mechanisms for attempting to mimic the results of notched boreholes and did not have as much success controlling crack initiation. Although the mechanisms were not directly relatable, the results gave insight into sizing of explosives, sizing of borehole diameter, method of sealing, and selecting the appropriate detonation medium for each testing stage.

The first tests done started with a deformation mechanism of creating flaws in ductile rods, inserting explosives, and detonating. Hoping that the flaws could control the deformation of the rods, resulting in an impact on the borehole wall and crack growth. In order for this method to work, the rod needed to be a similar diameter to the borehole and an excessive coupling ratio was achieved. A picture of the resulting crack formation is shown in Figure 22. Learning from the mistakes of this mechanism, the borehole diameter was increased. A new mechanism was attempted, placing steel blades inside an alignment rod and driving them outward with explosives detonated from within the rod. This mechanism initially used O-rings as a method for containing borehole pressure, but this was unsuccessful. The next iteration in design involved incorporating threaded plugs at the top of the borehole. A CAD drawing of this is shown in Figure 23. Note that the borehole diameter was increased again (to the current size of 15/16 in) to reduce unwanted cracking and to provide larger threads for better structural support. This design iteration proved to be an improvement, but still had problems with thread failure and

consistent ejecting of blades. It was at this point that reinforcing pins introduced as an aide of restraining the plug within the block. The pins were inserted through the thickness of the block (102 mm or 4 in) and into a groove machined circumferentially through half the plug thickness. Additionally, the wedge and pin design of the current device, shown in Figure 13 and Figure 16 were implemented. These changes showed improvement, however, with the successful containment of the pressure there was an increase in crushing and the blades still failed to consistently eject into the borehole wall. It was determined that using a water filled borehole allowed the pressure to transmit around the pin at detonation, pressurizing the borehole to failure instead of ejecting the wedges. Subsequent tests used air filled boreholes which helped in driving down the pin and ejecting the wedges. The only problem remaining with the device was the stress concentration due to the restraining pins. The holes drilled through the block that the pins were inserted into were a weak point and caused unwanted fractures to grow. The pins and threads were removed from the design and adhesive secured plugs were introduced, leading to the current device being tested.

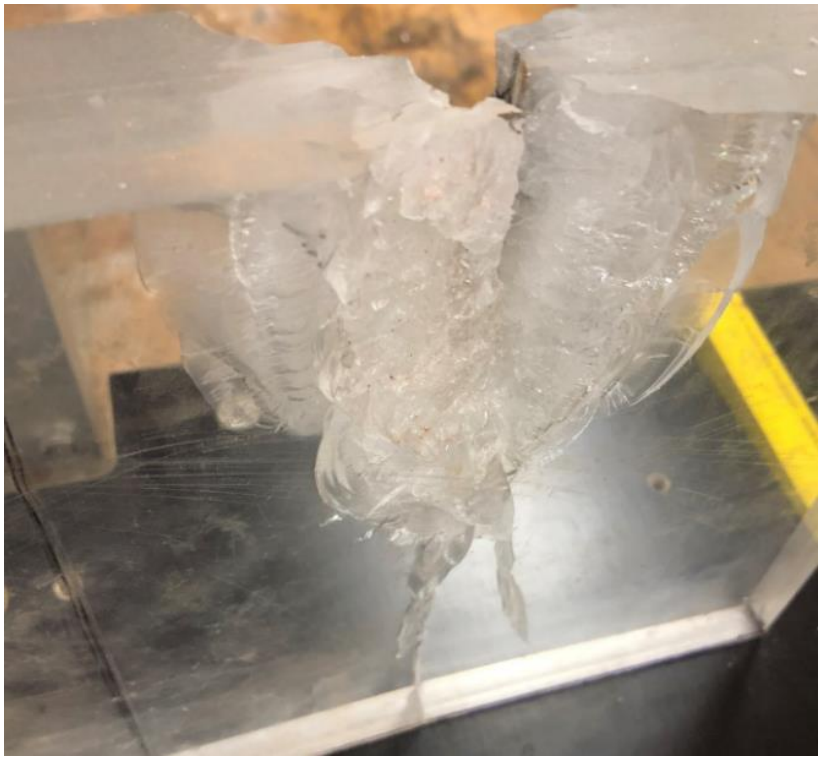

Figure 22: Unsuccessful Preliminary Test

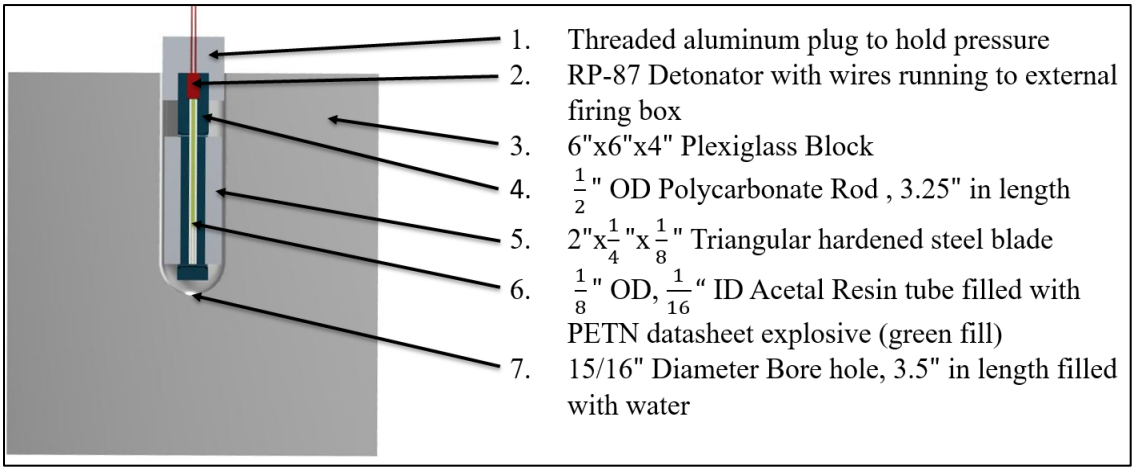

Figure 23: CAD Drawing of Section Design Iteration

4.2 Establishing Planes of Reference

Prior to presenting results, it is convenient to introduce a coordinate system to make referencing orientation simpler. In Figure 24, a photograph of a block is presented looking in the normal direction to the front surface. Each edge is labeled with the name of the block side it represents.

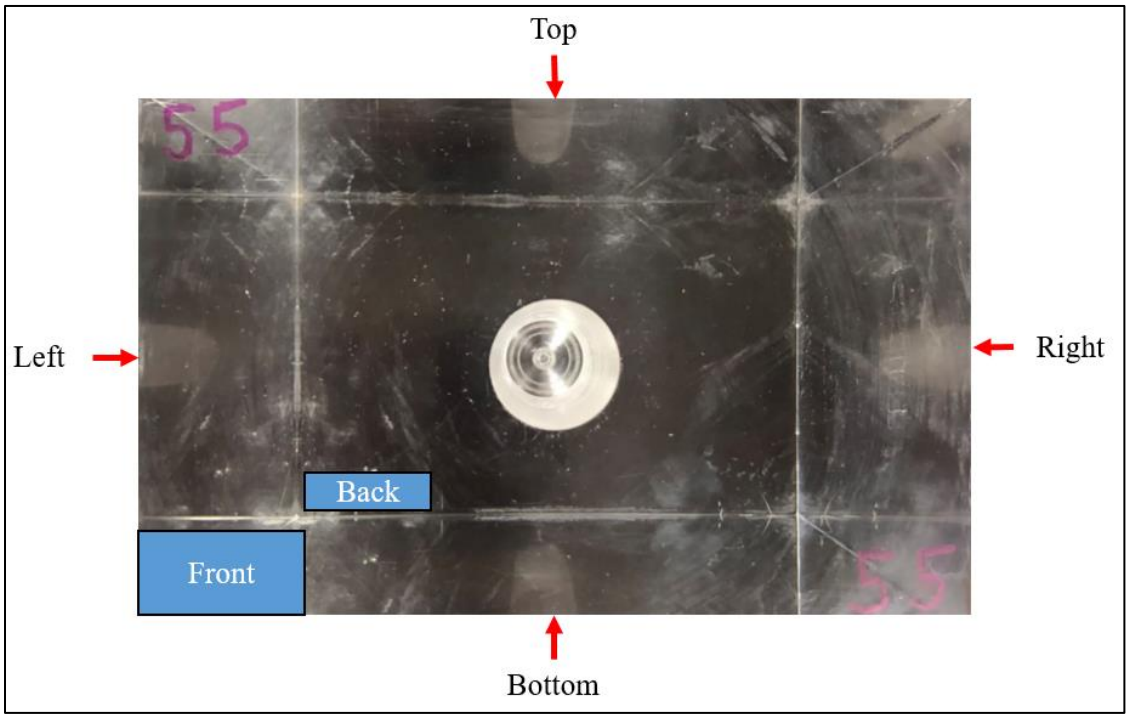

Figure 24: Front view of a block prior to testing

Note that we are looking onto the 102 mm x 152 mm (4 in x 6 in) cross section and that the borehole is machined into the front plane. The surface 203 mm (8 in) in distance, but parallel to the front surface is referred to as the back surface, denoted by the blue square and white text. When the device is inserted into the borehole, the wedges are

oriented in the left and right direction. The block is placed in the hydraulic press and pressurized in the top and bottom direction, which is parallel to gravity. This means the left and right directions represent the horizontal plane in the model. Crack growth left or right may be referred to as horizontal. While growth in the top and bottom directions will be referred to as vertical. Growth towards the front and back will be referred to as longitudinal.

4.3 Resulting Crack Growth from Test 1

4.3.1 Test 1, Stage 1

Test 1 was conducted with the standard component geometry presented in the material and methods section. This included a 102 mm x 152 mm x 203 mm (4 in x 6 in x 8in) PMMA block and tapered wedges that feature blade angles of 30° and a length of 25.4 mm (1 in). The resulting crack growth from the first stage of testing is shown from a top view in Figure 25. This picture provides a good overview of the developed cracks, displaying both desired cracks in the horizontal direction and other undesired cracks.

Figure 25: Top view of Test 1, Stage 1

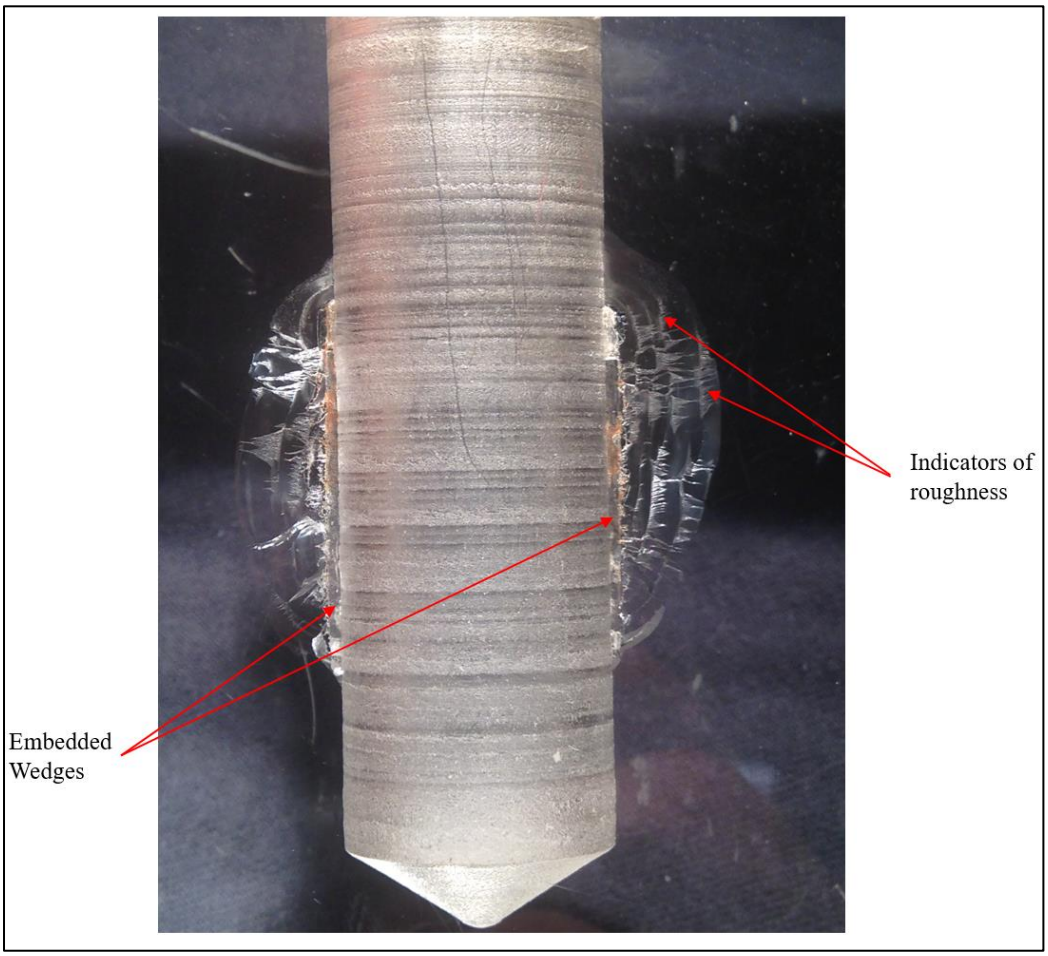

Figure 26: Top view, close up of horizontal cracks at bottom of borehole

Figure 26 shows a close up of the bottom of the borehole, offering a detailed view of the horizontal crack development. The rectangular crack extending from the borehole wall is a direct result from the wedges ejecting and embedding within the borehole wall. The initial cracks caused by this deformation are extended both horizontally and longitudinally by the pressure within the borehole. The left side crack reaches a maximum distance from the borehole wall of 9.7 mm (0.38 in). The longitudinal length is 36.8 mm (1.45 in). The horizontal crack on the right side of the borehole features a slightly smaller peak of 8.3 mm (0.325 in), but has a similar length of 36.3 mm (1.43 in).

The right side crack is centered about the embedded wedge, while the left side crack favored growth towards the front plane. An important characteristic of both cracks are the roughness they have developed. Observed in Figure 26, the indicators of roughness are noted. In addition, the cracks feature a ripple pattern extending outwards horizontally which is also indicative of a high energy and high roughness crack. As previously stated, the roughness is an indicator of a high driving energy and high crack speed, a characteristic of explosively driven cracks. This is a desirable crack characteristic and will aide in extraction from shale [21].

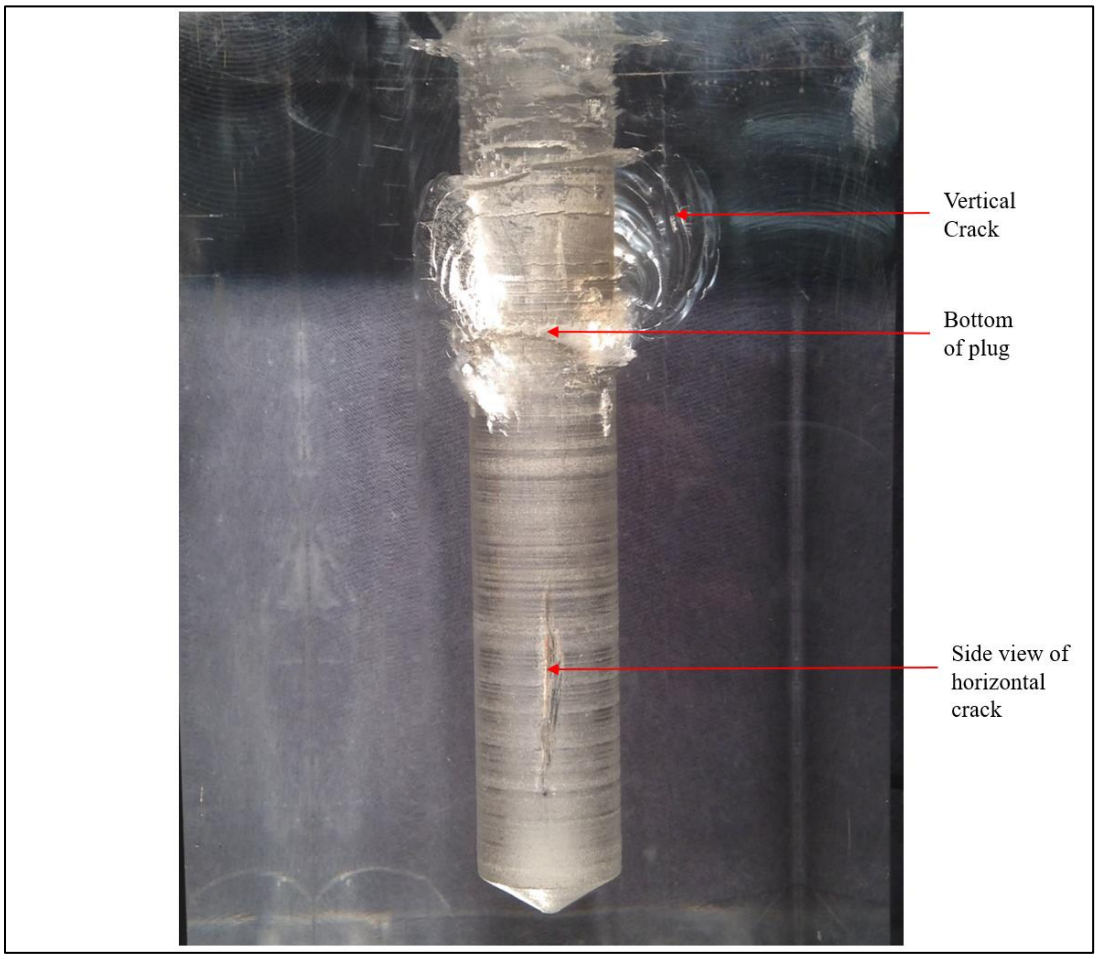

Figure 27: Right view, detailing side profile and unwanted vertical cracks

For analyzing vertical crack development and localized cracking around the detonation point, a side view is presented in Figure 27. The bottom of the plug is located 44.5 mm (1.75 in) from the front surface. The charge is detonated immediately below this point. The area in close vicinity to the charge experiences a high pressure during detonation. This effect combined with the shockwave reflection at the plug bottom causes unwanted cracking in this area. The majority of the cracking is a high number of short, ill-defined cracks extending less than 5 mm (0.2 in) outward. However, there are two fractures in the vertical direction that are undesirable and noted. The largest vertical crack extends 15 mm (0.6 in) outward and has a longitudinal length of 19.6 mm (0.77 in). This crack is substantial, but is not problematic. In stage two it will be completely covered by the plug preventing any future growth. It does however give insight into the effect of the in situ stress. The fact that there is zero significant horizontal fractures around the point of detonation, but two vertical ones, clearly indicates the effect the compressive stress has on crack orientation.

4.3.2 Test 1, Stage 2

A bottom view displaying the horizontal plane can be seen in Figure 28. Note that this is the bottom view instead of the top view from stage 1, the right and left side are reversed. Recall that stage 2 is performed with a fluid filled borehole and a smaller charge mass. The use of water increased coupling, generating a higher ratio of borehole pressure to expand the existing horizontal fractures [26]. The horizontal cracks resulting from stage 1 are greatly expanded in both the longitudinal and horizontal directions. The

left and ride side cracks each span the entire effective borehole length (63.5 mm or 2.5 in), reaching from the bottom of the stage 2 plug, to the bottom of the borehole. The right side crack shows the most significant growth in the horizontal direction. It expands outward symmetrically, reaching a peak distance from the borehole wall of 28.7 mm (1.13 in). The left side experienced a similar magnitude of crack propagation. The maximum peak reached 27.7 mm (1.09 in) from the borehole wall. The outline of the cracks developed in stage 1 are identified in Figure 28, so the relative size of the cracks can be compared. The results show that reapplying pressure to the borehole is an effective way to enhance crack growth in the desired orientation. It is also important to analyze the effect of stage 2 on the undesired crack growth.

The plug inserted and bonded to the front most 76 mm (3 in) of the borehole was effective at preventing additional growth of the undesired cracks developed in stage 1. The two significant cracks developed in the vertical direction did not experience any further growth. Additionally, the cracks that resulted from local effects in stage 1 are not pressurized to a noteworthy degree during stage 2. This is important, because if the vertical cracks are allowed to grow to a significant degree and reach the outer surface, the horizontal cracks will not be able to be pressurized and grow further. In the second stage of testing, additional non-horizontal cracks developed. Figure 29 shows a view from the backside of the block, detailing radial fracture growth around the borehole. The two largest cracks in the horizontal direction can be used as a scale to analyze the growth of other cracks. In the vertical direction, there are cracks developed that reach slightly below 12.7 mm (0.5 in) in length. For the purpose of model testing, it is desired to minimize this growth to show directional control and ensure that the vertical cracks do

not interfere with further expansion of the cracks during stage 3. However, when testing in the field, minor cracking in the vertical direction would also contribute to shale access and would not be considered an undesired result.

The results from stage 2 also highlight the effects of discontinuities in the borehole. Two significant circumferential cracks have developed around the borehole. One originating at the bottom of the plug, and one at the bottom of the borehole, where there is a change in diameter due to drilling. As previously discussed, this is due to the reflection of the pressure wave at the boundaries. It is a noteworthy result, but not problematic for controlling fracture orientation.

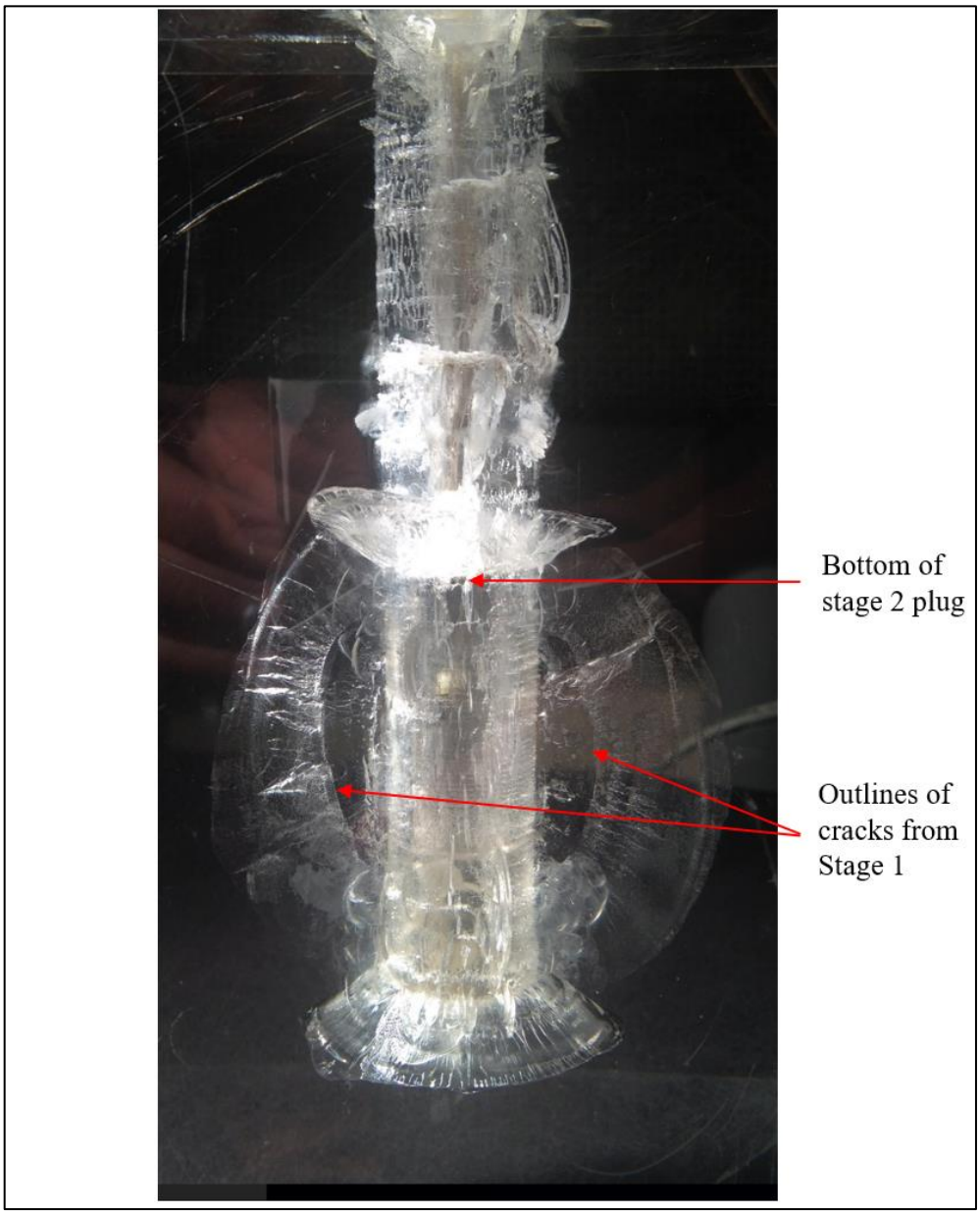

Figure 28: Bottom view of Test 1, Stage 2

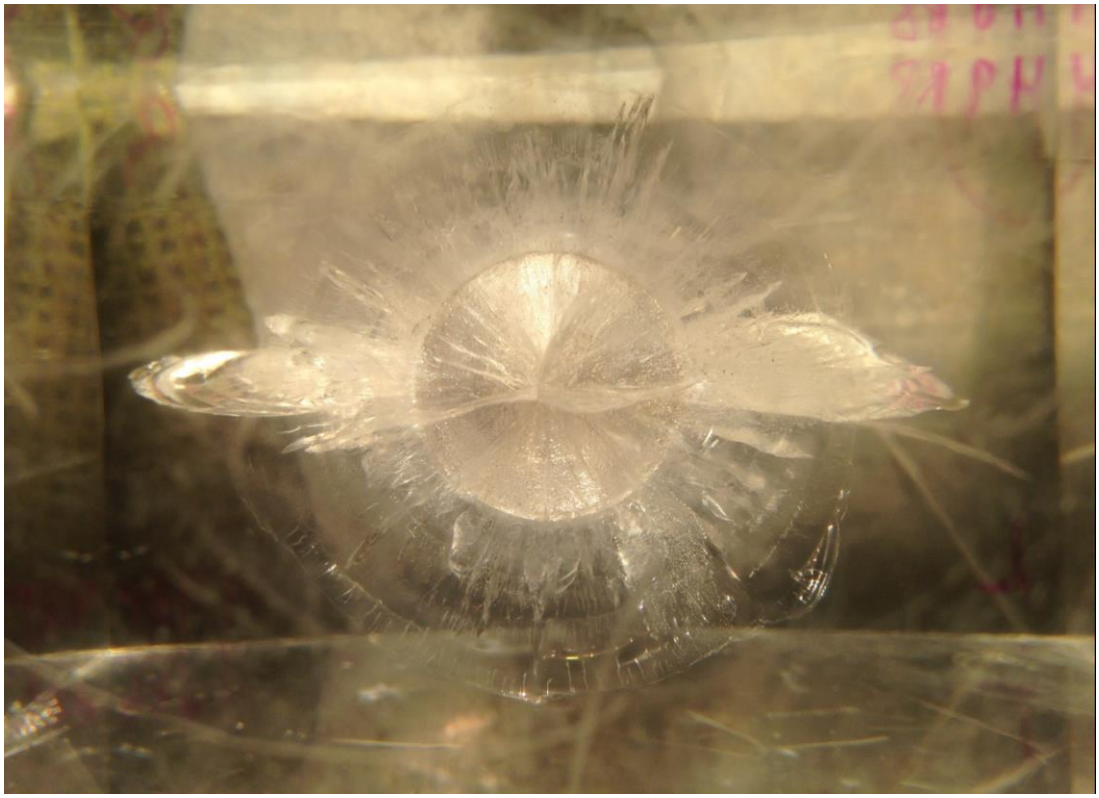

Figure 29: Back view of Test 1, Stage 2

4.3.3 Test 1, Stage 3

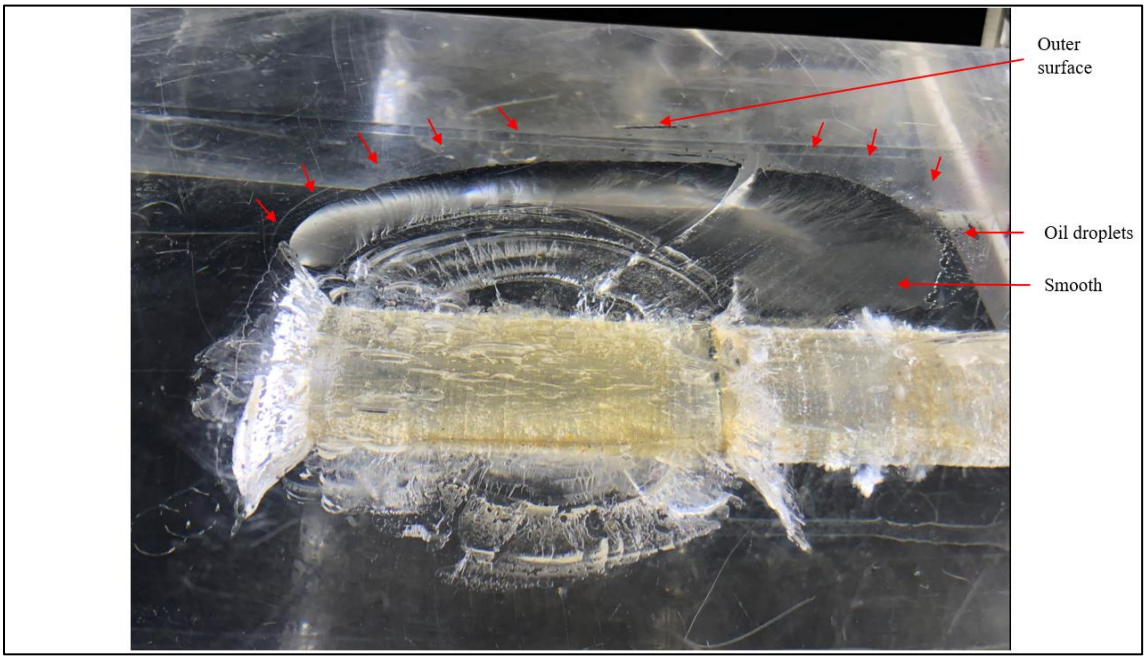

Figure 30: Top view of Test 1, Stage 3 results

The third and final stage results are presented in Figure 30. When the quasi-static loading reached 9 MPa (1,300 psi), the stress in the right horizontal crack reached a critical value and crack propagation began. This shows the well-defined horizontal crack beat out the many ill-defined cracks in the vertical direction. The horizontal crack expanded outward until it reached the outside right surface of the block, losing pressure. The resulting crack expanded significantly in both the longitudinal and horizontal directions. The longitudinal expansion reached the bottom circumferential crack before stopping, and extended up the borehole reaching 27.9 mm (1.1 in) from the front surface of the block. The longitudinal distance peak to peak is 118.5 mm (4.67 in). After pressure is removed from the borehole, the outer edges of the statically driven cracks close up and are very thin. This presents challenges for viewing in pictures. The outside

profile of the crack is marked with red arrows on the block. The smoothness of the statically driven cracks can also be observed in Figure 30. The cracks resulting from stage 3 testing do not have the ripples or other small branch shaped cracks that indicate roughness. They appear to be thin and mostly transparent, as they do not alter the structure and optical qualities of the block as much as rough cracks do.

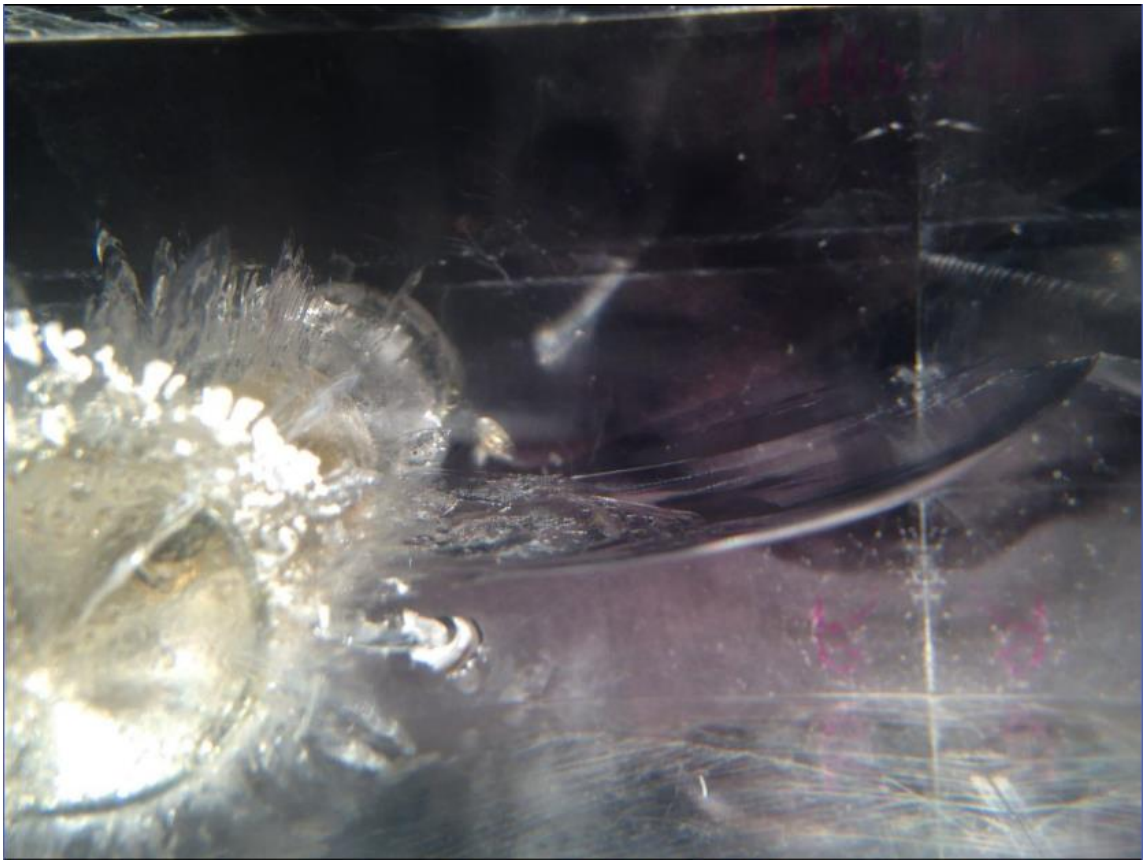

Figure 31: Back view of Test 1, Stage 3 results

The results from stage 3 also showcase the effects of the in situ stress on crack growth. In Figure 31, the curvature of the statically driven crack can be noted when comparing its orientation to that of the horizontal, dynamically driven crack. The stress concentration from the device in stage one, combined with the high pressure from

dynamic loading dominates the crack behavior in stage one and two. However, for stage 3 the energy and pressure of quasi-static loading is lower and making the in situ stress a more dominate factor as the fracture propagates away from the dynamically initiated cracks.

4.4 Model Repeatability

With test 1 showing great success at producing controlled crack growth in the desired orientation, proving these results could be repeatable is desired. Test 2 is conducted under the same process and the results are compared to test 1 to analyze model consistency.

4.4.1 Test 2, Stage 1

The resulting horizontal cracks from test 2 viewed from the bottom surface are shown in Figure 32. The horizontal crack development is very similar to that seen in test 1. The cracks begin with the embedded blades, with further crack growth extending outward from the borehole wall. The right side features a crack with a peak of 8.5 mm (0.334 in) and a longitudinal length of 34.5 mm (1.36 in). The left side crack is slightly larger in both length and extension. It features a peak extension of 8.9 mm (0.35 in) from the borehole wall and a longitudinal length of 5.8 mm (1.41 in)

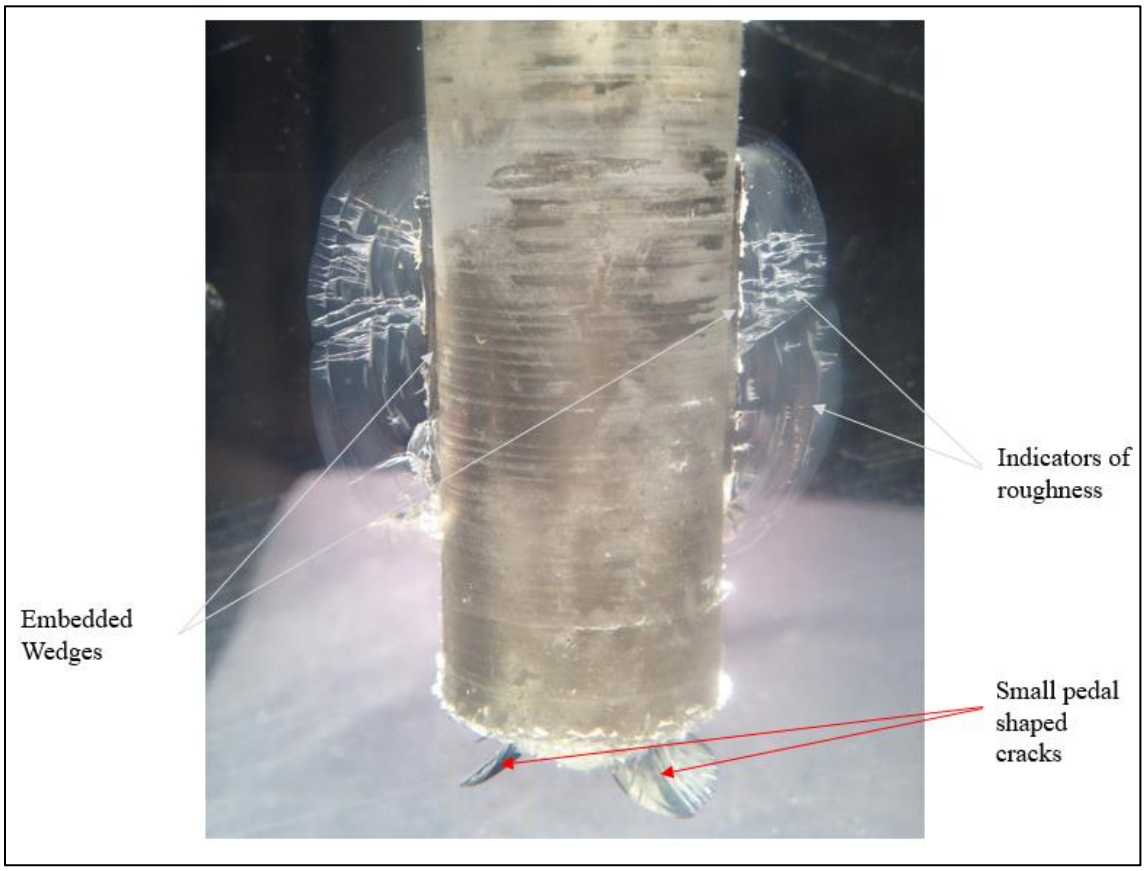

Figure 32: Bottom view of Test 2, Stage 1 horizontal cracks

The unwanted crack development for test 2, stage 1 is limited to mostly crushing around the detonation point. There are a large number of small radial fractures located at the bottom of the plug, where the charge was located. They are all limited to 5 mm (0.2 in) or less and will be insignificant for later stages of testing. It is worth noting there is an increased roughness of the borehole for this test. This is due to machining with a single flute drill bit that was not very sharp. This is most notable around the plugged section in Figure 33. This roughness may have helped in the surface bonding of test 2, as the plug remained bonded throughout the duration of testing. Only the epoxy that was used to plug the through hole for running wires was blown out. This may have had a

minor effect on increasing pressure build up and driving the pin. The pedal shaped cracks detailed in Figure 32 and Figure 33 are due to the impact of the pin hitting the rod, which in turn impacts the bottom of the borehole wall.

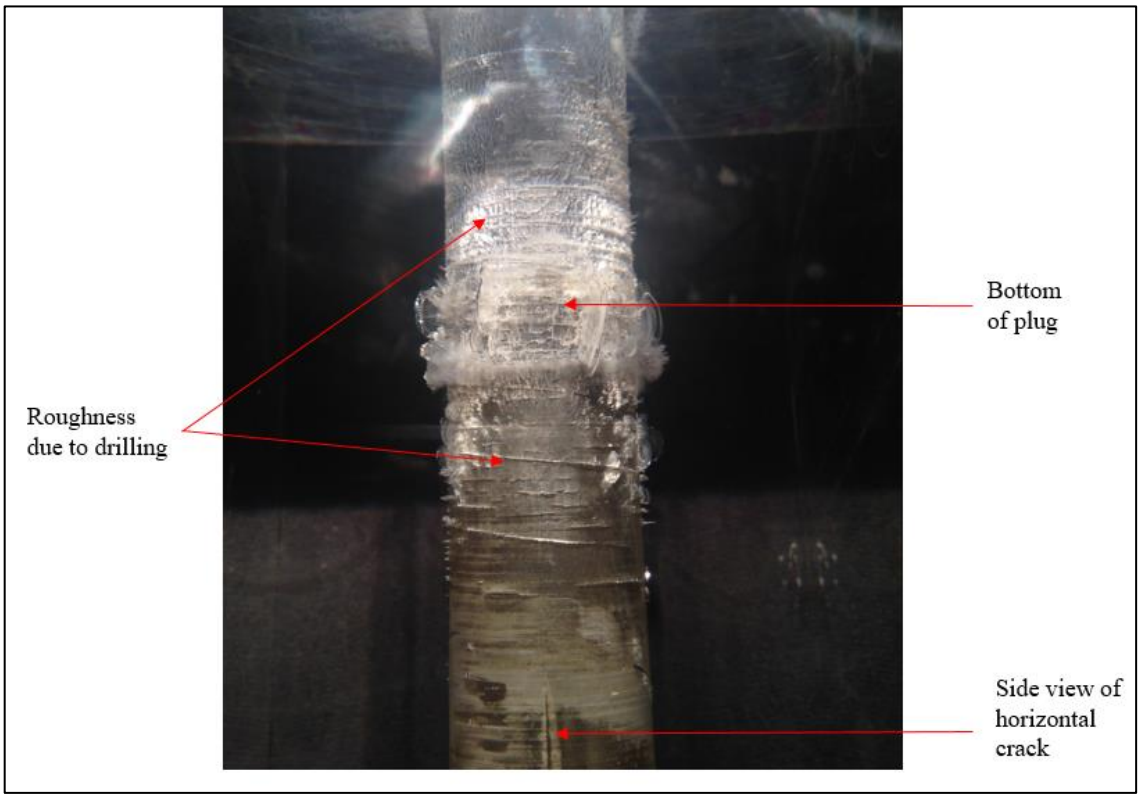

Figure 33: Right view of Test 2, Stage 1 detonation location

4.4.2 Test 2, Stage 2

The results from test 2, stage 2 are shown from a top view in Figure 34. There is substantial crack growth on both sides of the borehole. Both sides of the borehole have an arcing crack that extends from the flat end (above the beginning of the drill bit taper), to the circumferential crack originating at the end of the stage 2 plug. The right side of

the borehole has a horizontal crack with a longitudinal length of 59.2 mm (2.33 in). The shape of this crack is an almost symmetric arc, centered about the embedded blades. The maximum extension out from the borehole wall is 38.1 mm (1.5 in). The left horizontal crack has an antisymmetric arcing shape that favors the front surface of the block. The longitudinal length of this major crack is also 59.2mm (2.33 in). However, the maximum extension from the borehole has a slightly smaller peak of 36.6 mm (1.44 in). A much smaller minor horizontal crack also formed on the left side. It originates at the circumferential crack at the base of the stage 2 plug and extends towards the front surface 23.6 mm (0.93 in). The peak extension of this minor crack is 11.2 mm (0.44 in). A noteworthy result regarding the orientation of the horizontal cracks is shown in Figure 35. The crack on the left side is oriented roughly 15° off of the horizontal plane. This is due a misalignment within the borehole. Confirmation that this is not an effect from the in situ stress is that the crack does not show curvature, it instead deforms in a straight line outward from the misaligned blade.

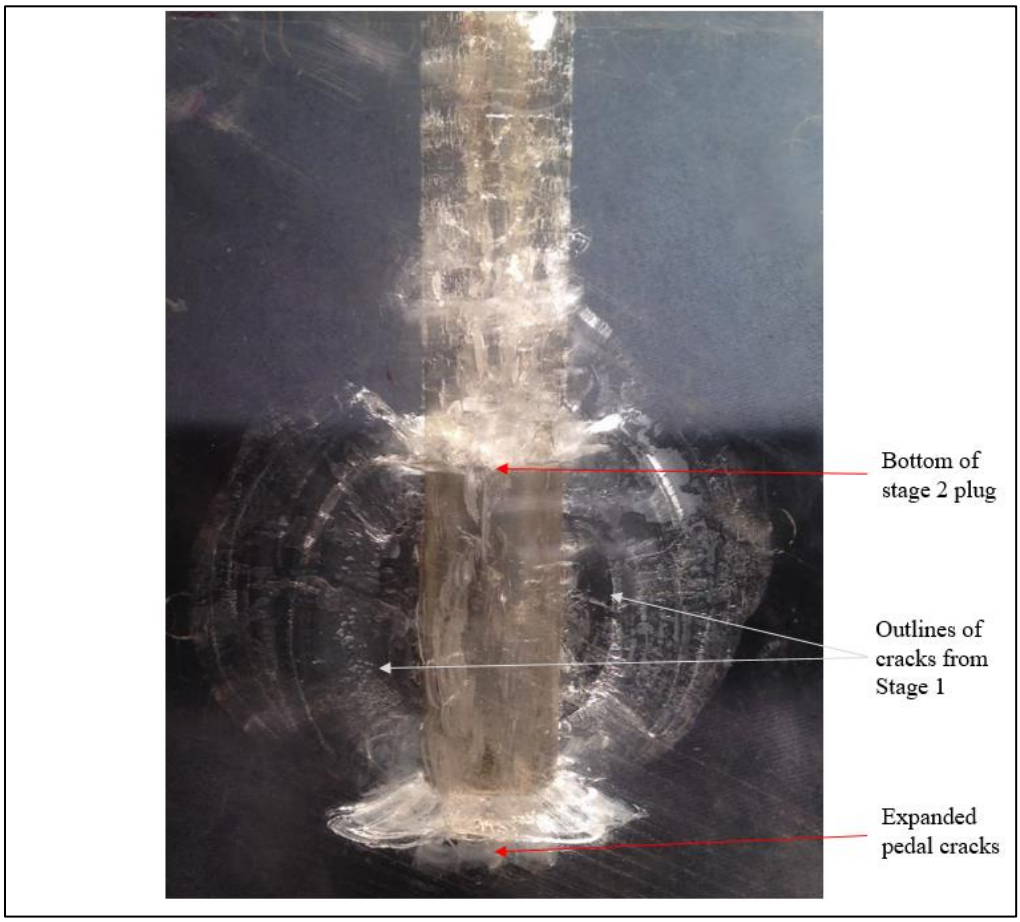

Figure 34: Top view of Test 2, Stage 2

The unwanted crack development from stage two is showcased best in Figure 35. There are significant radial cracks around the detonation point. The largest of these cracks extend outwards to 18.5 mm (0.73 in). The increase in magnitude of these unwanted cracks is likely due to the wall roughness within the borehole. The pedal shaped cracks originating in stage 1 are further extended, but not to a significant degree. As expected, there is a circumferential crack extending from the discontinuities at the bottom of the borehole and bottom of the stage 2 plug.

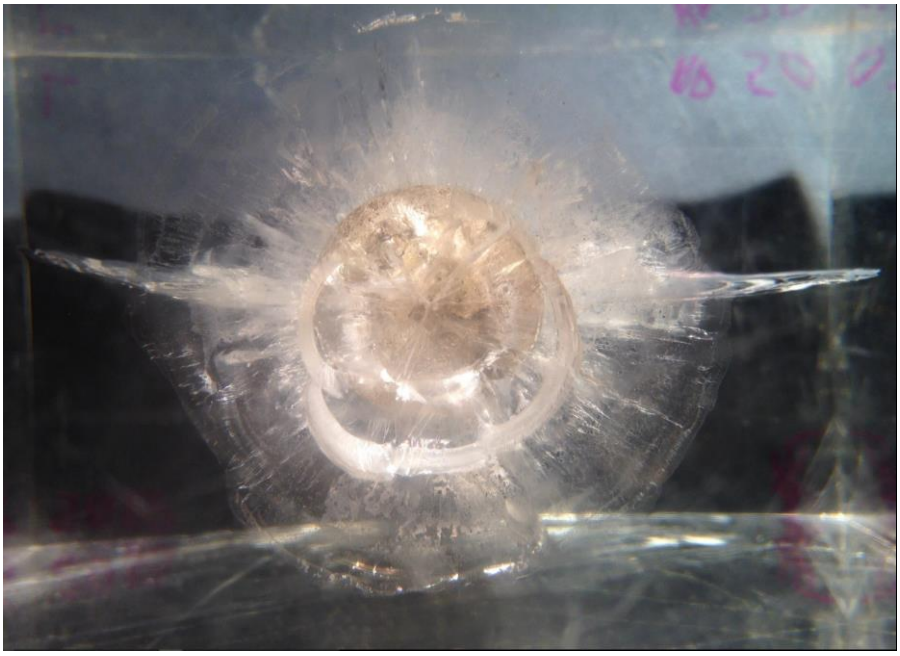

Figure 35: Back view of Test 2, Stage 2

4.4.3 Test 2, Stage 3

The quasi-static loading of test 2 reached 6.9 MPa (1,000 psi**),** causing crack growth on both sides of the borehole, before the left horizontal fracture reached the outer surface. The major crack growth of the left horizontal fracture is marked with red arrows on Figure 36. The fracture started expanding from around the peak distance and midpoint of the horizontal crack developed in stage 2. It extends longitudinally up the borehole towards the front surface, reaching 31.2 mm (1.22 in) from the front surface. This gives a total longitudinal length of 81.8 mm (3.22 in). The minor extension of the right side crack is labeled in Figure 36 as well. The fact this crack grew at a similar pressure implies that within an infinite medium, when enough resistance is provided for the left horizontal crack to arrest, the crack propagation is likely to switch to the right

side crack. The smoothness and curvature of the left side fracture is displayed in Figure 37. Although the dynamically driven crack was already oriented 15° off horizontal, there is a significant change in curvature once the crack is driven statically.

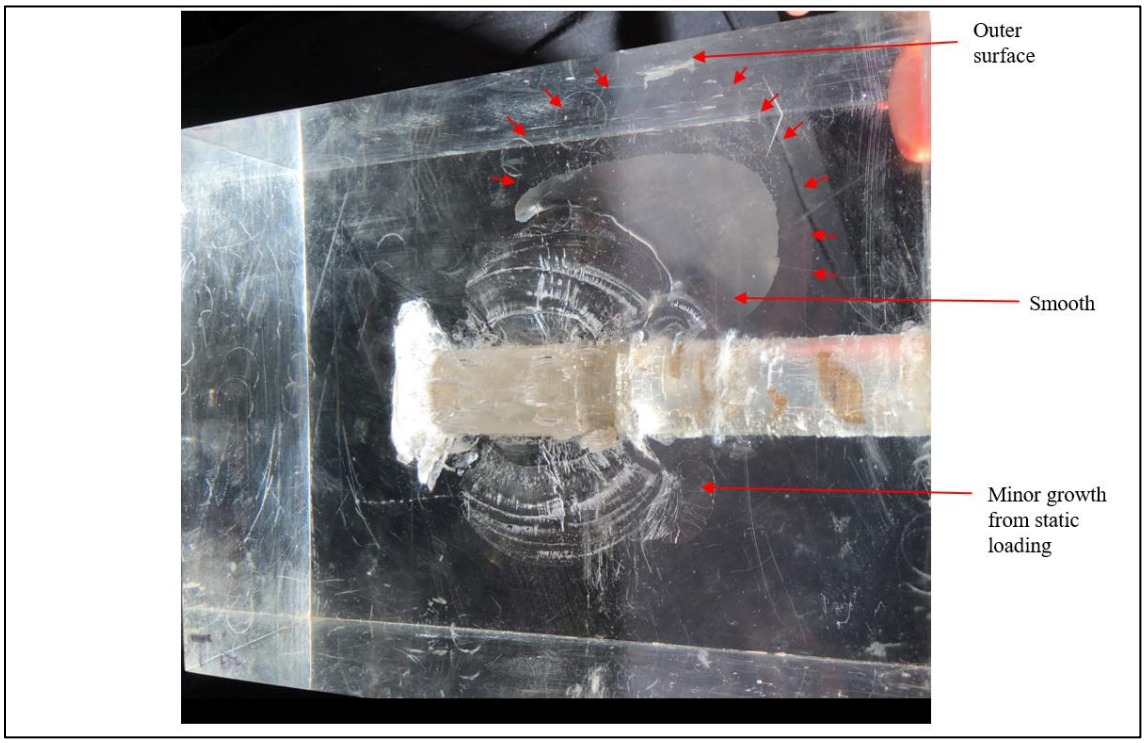

Figure 36: Bottom view of Test 2, Stage 3

Figure 37: Front view of Test 2, Stage 3 detailing curvature

4.4.4 Discussion of Repeatability

Comparing test 1 and test 2, it is apparent that the mechanism of fracture initiation is repeatable. The cracks formed directly from the function of the device in stage one are extremely similar in extension and length. When detonating a second charge during stage 2, some deviations in crack growth are observed, but this is expected. Crack patterns between specimens are expected to show variations due to randomly distributed flaws in materials [24]. This effect could be enhanced by the variations in borehole conditions,

specifically the change in roughness due to machining methods. Instead, if comparing the broad patterns and behaviors, tests 1 and 2 are very similar. The statically grown fractures are not identical in size and shape, but exhibit a similar trend. These fractures grow outward until reaching the surface, then lose pressure. Both fractures display smooth surfaces and an influence due to the in situ stress. The successful repetition and consistent behavior of crack growth show that the function of this device is repeatable.

4.5 No-Load Condition

Test 3 was conducted without the vertical load simulating in situ stress for two purposes. One, without the restriction of placing the model in the hydraulic press, high speed video of the device could be taken from a better angle. Allowing a top view to observe the wedge ejection and crack formation. Two, to observe the crack behavior without the in situ stress imposed. The geometry of the wedges, rod, and block remained the same, however, a new tapered pin was made. This pin retained all the same dimensions from the original design except an increased thickness of the 15/16 inch head. The thickness of the head was changed from 1.59 mm (1/16 in) to 6.35 mm (1/4 in). This was done to increase durability and allow multiple uses of the pin. The drill bit used to machine the borehole of this test caused significant roughness.

4.5.1 Top View of Functioning Device

The high speed camera was positioned to record form a top view during the test 3, stage 1. Selected images are presented in Figure 38, showing key moments in the function of the device. The first image presented takes place 44 microseconds after the time of detonation. The borehole is still saturated by light, but the outline of some deformation around the detonation point is evident. By 67 microseconds, the light produced by detonation has reduced enough to see the crushing formed around the borehole. The pin has yet to change position. The third image at 100 microseconds is the moment the pin begins to move down the borehole. At this point in time, the epoxy has failed at the top of the plug and pressure is no longer contained within the borehole. The frame taken at 144 microseconds shows progression in the failure at the top of the plug. The top, larger diameter section of the plug fractures and breaks off, however, the portion of the plug bonded to the borehole wall remains intact. Image 5 marks the moment when although no cracks have formed, the pin has moved enough to displace the wedges against the borehole wall. At 418 microseconds after detonation is triggered, the wedges have displaced outwards and horizontal crack growth has been initiated, favoring the right side of the block. In the seventh image, both cracks continue to grow, with the left crack beginning to catch up in size. At 605 microseconds, the pin and rod slam into the bottom of the borehole and initiate a circumferential crack. Both horizontal cracks and the circumferential cracks continue to grow until 680 microseconds, where the pin and rod are observed to bounce and begin to move back up the borehole. The last image at 726 microseconds is when all cracks arrest and the pin and rod have moved a noticeable

amount up the borehole. It is important to note during the last two images, the circumferential continued to see small amounts of growth.

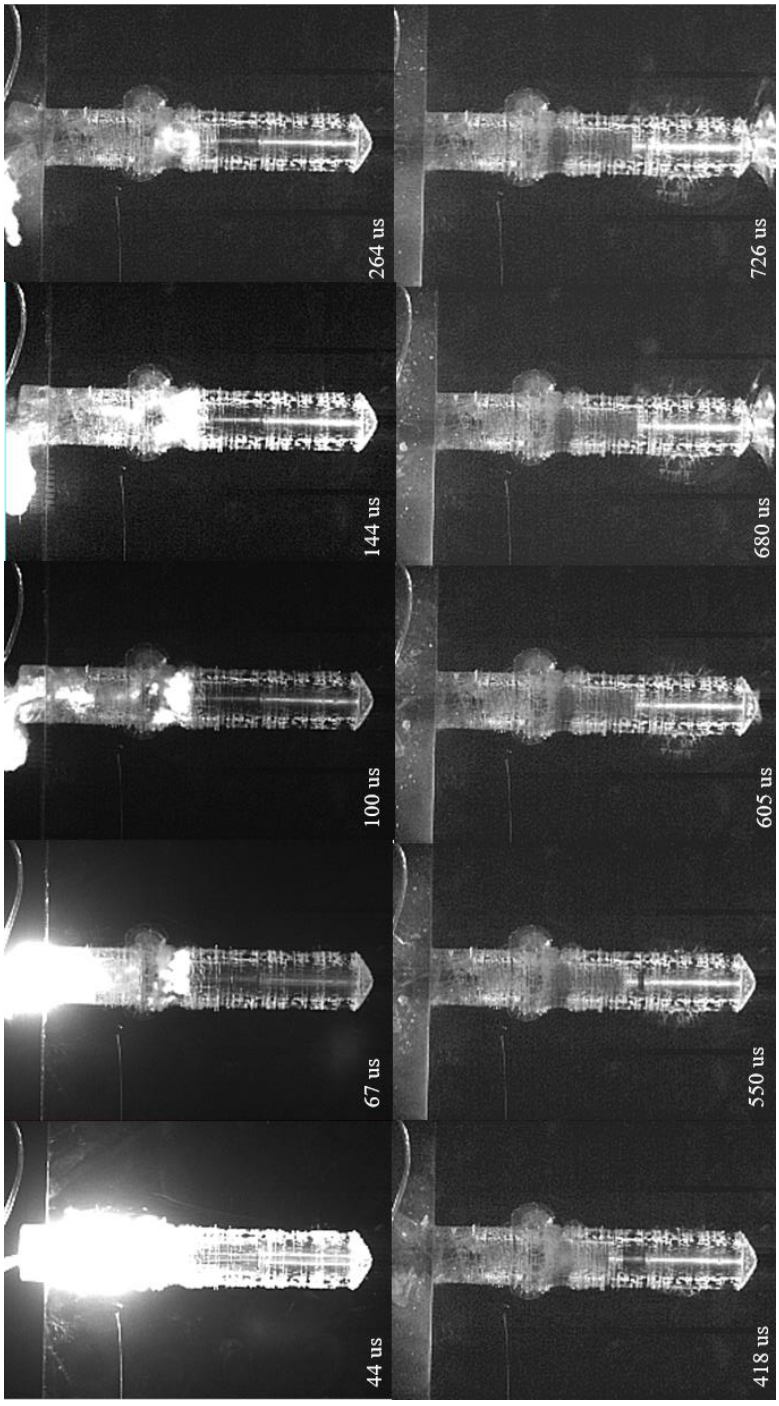

Figure 38: High speed images of functioning device

4.5.2 Test 3, Stage 1

Looking at the overview of crack growth presented from the top view in Figure 39, the overall crack growth is significantly larger. The largest horizontal crack develops on the right side of the block. The crack initiated around the embedded blade and propagated down to the beginning of the tapered section of the borehole. The total longitudinal length of the right crack is 43.2 mm (1.7 in). The crack reaches a maximum horizontal distance of 14.2 mm (0.56in) from the borehole wall. The left horizontal crack extends down the borehole toward the back surface, but does not reach the end of the borehole. The total length of the left crack is 40.9 mm (1.61 in). The crack's peak reaches 9.9 mm (0.39 in) outward from the borehole wall. The left horizontal crack is composed of three smaller cracks that line up in the same plane, whereas the right crack is a single continuous crack.

Looking at the detonation point, there is significant crushing around the borehole. Most of the cracks formed are randomly distributed radial cracks less than 3.2 mm (0.125 in) in length. There are a few radial cracks that exceed 3.2 mm (0.125 in), with the largest being oriented in the horizontal plane. The length of this crack is 9.1 mm (0.36 in). There is also a circumferential crack with a diameter of 55.9 mm (2.2 in) at the bottom of the borehole caused by the impact of the pin.

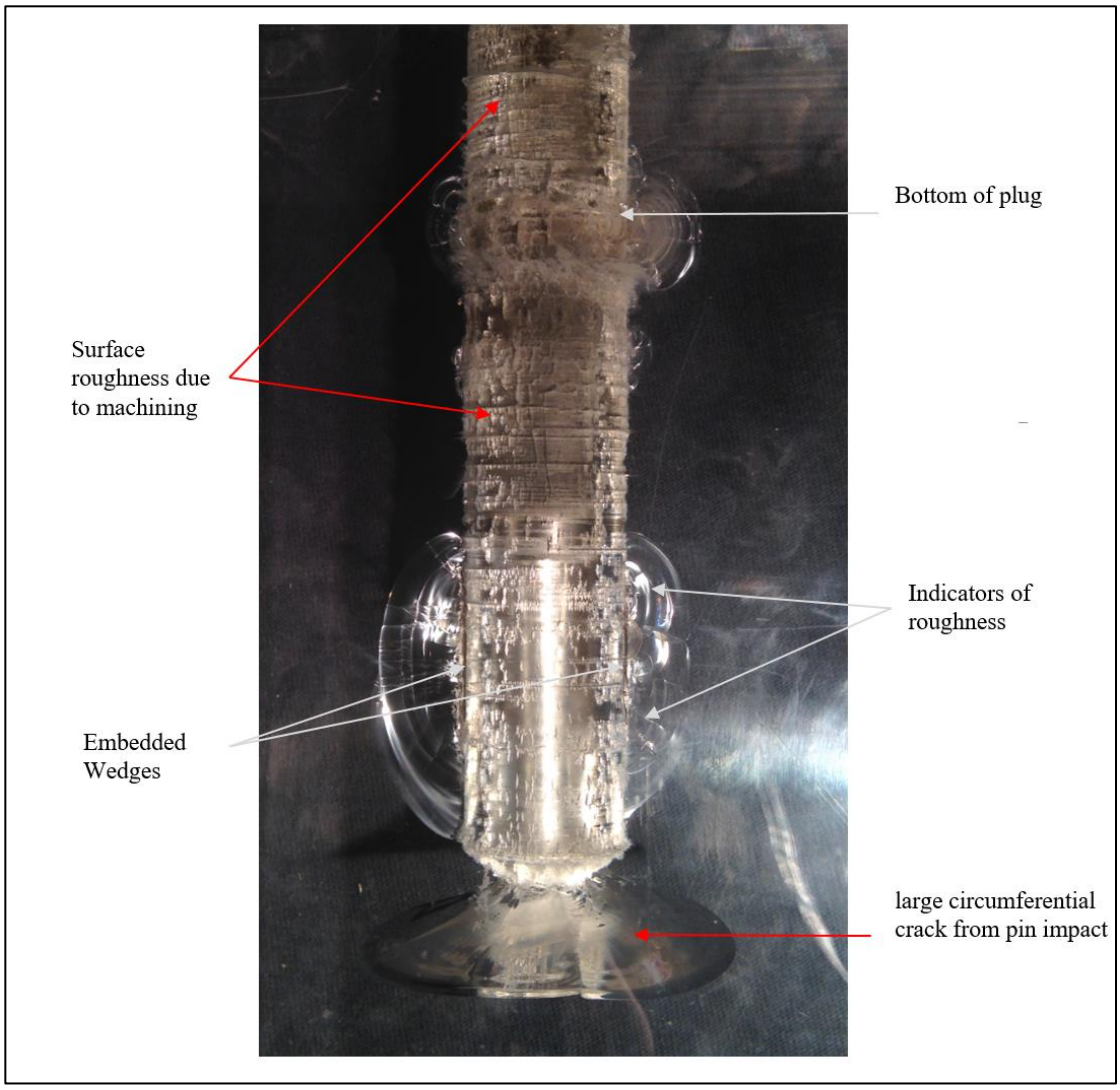

Figure 39: Top view of Test 3, Stage 1

4.5.3 Test 3, Stage 2

The results of the stage 2 are shown in Figure 40. The left horizontal crack has the most extensive crack growth resulting from the second stage of pressurization. The horizontal crack extends down the borehole to the circumferential crack closest to the back surface of the block. It also extends up the borehole and past the second stage plug,

merging with other smaller horizontal cracks. The combination of these horizontal cracks create a total longitudinal distance of 118 mm (4.67 in) in the horizontal plane. The maximum distance from the borehole of 34.5 mm (1.36 in) is reached at approximately the midpoint of where the blades were ejected. Although the left side has the largest over all crack growth, the right horizontal crack experienced the largest crack extension outwards from the borehole. The maximum distance from the borehole was 38.1 mm (1.5 in) and was also centered about the point of wedge ejection. Similarly to the left side, the right side extends down the borehole to the circumferential crack closest the back surface of the block. The horizontal crack on the right side extends up the borehole reaching the bottom of the stage 2 plug and merging with the circumferential crack formed at the boundary. There are multiple smaller horizontal cracks that formed on the other side of the stage 2 plug, but they did not connect with the main crack formed from the ejected wedges. The total longitudinal length of the right horizontal crack is 110 mm (4.34 in).

Despite the severe roughness of the borehole walls, it does not appear to affect the crack formation a significant amount. Around the detonation point some radial cracks have formed that seem to originate from visually rough areas of the borehole, but they are all ill-defined and short in length. The largest of these radial cracks in the vertical direction extends 8.4 mm (0.33 in) from the borehole wall. There are two significant circumferential cracks that have formed at the bottom of the borehole. The crack formed in stage 1 due to the impact of the pin has experienced additional growth. The diameter has grown slightly to 58.4 mm (2.3 in). The longitudinal size has grown considerably, extending towards the back surface of the block 7.4 mm (0.29 in). The second

circumferential crack initiated in stage 2 of testing due to the reflection at the discontinuity. It features a diameter of 45 mm (1.77 in).

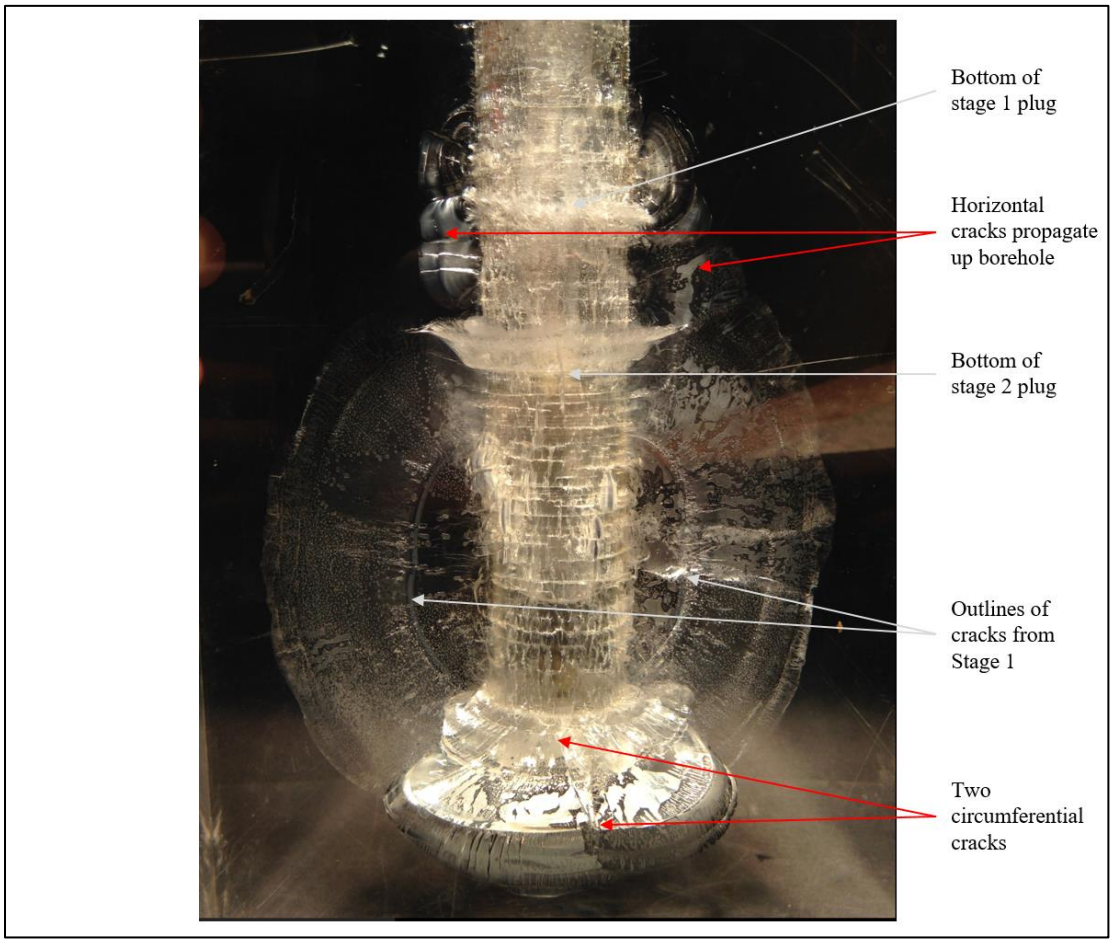

Figure 40: Top view of Test 3, Stage 2

4.5.4 Test 3, Stage 3

The crack growth resulting from stage 3 is best seen from the front view, as presented in Figure 41. The static pressure reached approximately 6.2 MPa (900 psi) before the right horizontal crack expanded to the outer right surface and lost pressure.

The outline of the major crack is marked with red arrows in the figure. The fracture growth in both the longitudinal direction and horizontal direction was drastic. The fracture growth extended longitudinally downward, past that of stage 2, extending past the largest circumferential crack by 7.4 mm (0.29 in). The crack also grew longitudinally up the borehole past the stage 2 plug and connected to the smaller horizontal cracks developed in stage 2. The total longitudinal length of the static crack peak to peak is 118 mm (4.65 in). When expanding outward horizontally the crack remained at a significant longitudinal crack length. When it reached the outside surface the crack was still 86 mm (3.4 in) in longitudinal length.

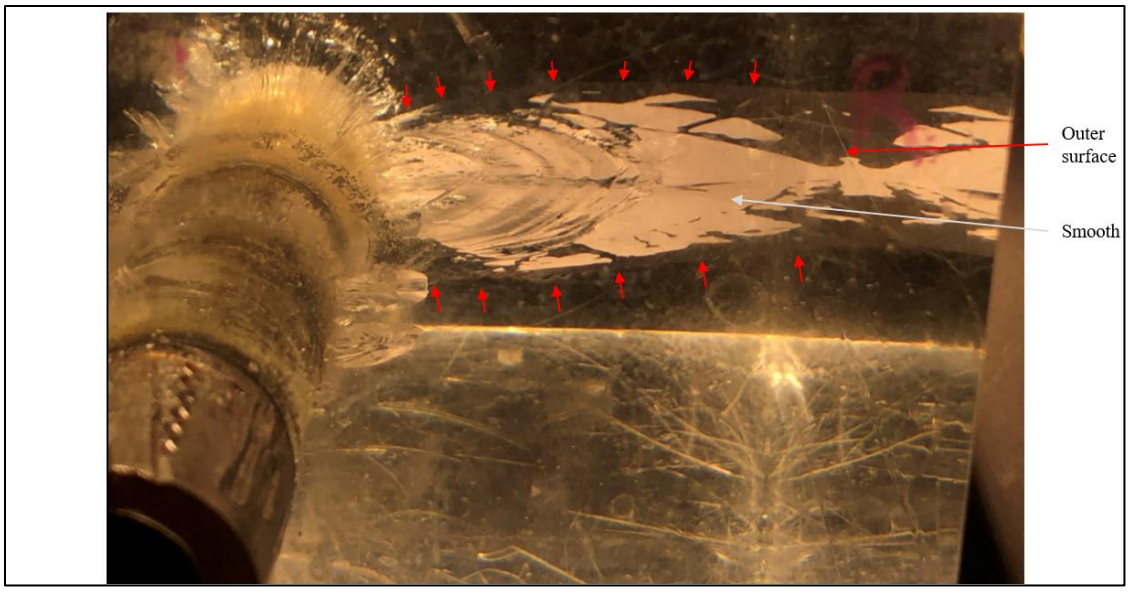

Figure 41: Front view of Test 3, Stage 3

4.5.5 No-Load Condition Discussion

The no-load condition provides insight into the magnitude in which the in situ stress affects crack development. In stage 1, the cracks developed around the detonation point are no longer largest in the vertical direction. This shows that without the influence of the in situ stress, the crack growth extends in whichever direction has the most significant surface flaws, likely randomized depending on manufacturing methods. Additionally, in all stages of testing, the crack development was to a greater magnitude in the horizontal direction, showing the device had better control over the orientation of growth.

In stage 2, the relationship between vertical radial fractures and in situ stress can be observed. The radial crack development in the non-horizontal directions around the detonation point were lower than that of the previous loaded tests, despite the increased surface roughness. This shows that without the constraints on horizontal crack growth provided by the large compressive stress, the driving energy from detonation is more efficiently used to expand the existing cracks. Stage 2 of testing also showed that cracks in the horizontal plane are more easily extended up the borehole, past the boundary of the plug. This is likely due to the randomly distributed horizontal cracks farther up the borehole, which connected to the wedge driven horizontal cracks. Other loaded tests have not seen any horizontal crack development, aside from the ones initiated by the device.

Stage 3 confirmed the earlier hypothesis that the curvature of the statically driven cracks is due to the in situ stress. Also, without the restraint on horizontal crack

development, the width and overall surface area of the crack was much larger than the loaded tests. The statically formed crack in stage 3 was 86.4 mm (3.4 in) when reaching the outer surface, compared to loaded tests that were closer to 25.4 (1 in) in longitudinal length at the outer surface.

4.6 Variations to Wedge Geometry

After establishing a functional device, three tests with varying wedge geometries were conducted to study the effect on crack growth. Test 4 features a 20° wedge angle and a length of 25.4 mm (1 in). Test 5 features a 10° wedge angle and a length of 25.4 mm (1 in). Test 6 remained at the same wedge angle as Test 1-3, but instead has a longitudinal length of 12.7 mm (0.5 in). All three tests used the original block and slotted rod geometry. The pins used in this test have the increased thickness of ¼ inch, as described in Test 3. Test 4 and Test 5 were machined with the same drill bit and surface roughness as Test 3. For Test 6, a new bit was used that resulted in significantly reduced roughness. The impact of roughness and other borehole characteristics will be discussed in Section 4.8.

4.6.1 Test 4, Stage 1

The resulting cracks from stage 1 are best seen by looking at both Figure 42 and Figure 43. The horizontal cracks developed are difficult to see from the top view, so they have been traced with red arrows. On both the right and left sides of the borehole two

cracks developed. Each side has a small vertical crack oriented 10° from the vertical plane pointed towards the top surface. Extending a maximum distance of 3.2 mm (0.125 in) from the side of the borehole wall and running a longitudinal distance of 25.4 mm (1 in). The vertical oriented cracks are both aligned about the embedded wedges. The horizontal cracks that developed on each side are equal or greater in magnitude than the vertical cracks. The horizontal crack on the right side of the borehole is the largest. It extends 5.6 mm (0.22 in) outward from the borehole and has a longitudinal length of 28 mm (1.1 in). Looking at Figure 43, it is evident that the horizontal cracks are not strictly in the horizontal plane. The right crack is approximately 30° offset in the direction of the top surface. While the left side crack is oriented approximately 40° offset in the direction of the top surface. The horizontal crack on the left side of the borehole is also smaller in size than the right side. The crack is composed of two smaller cracks that are aligned in the same plane to form a single larger crack. This extends a maximum distance of 3.2 mm (0.125 in) from the borehole wall and has a combined longitudinal length of 28 mm (1.1 in).

Figure 43 also highlights the roughness of the borehole and some unwanted crack development. There are a high number of very small ill-defined cracks that have grown off the borehole, largely in the vertical direction. Small pedal shaped cracks have also developed at the bottom of the borehole due to the impact of the pin. Figure 44 shows a close up from the right side of the block, detailing the deformation around the detonation point. There is some crushing around the borehole and one significant vertical crack. The large vertical crack extends 14 mm (0.55 in) outward from the borehole. The longitudinal length of the vertical crack is 26.2 mm (1.03 in)

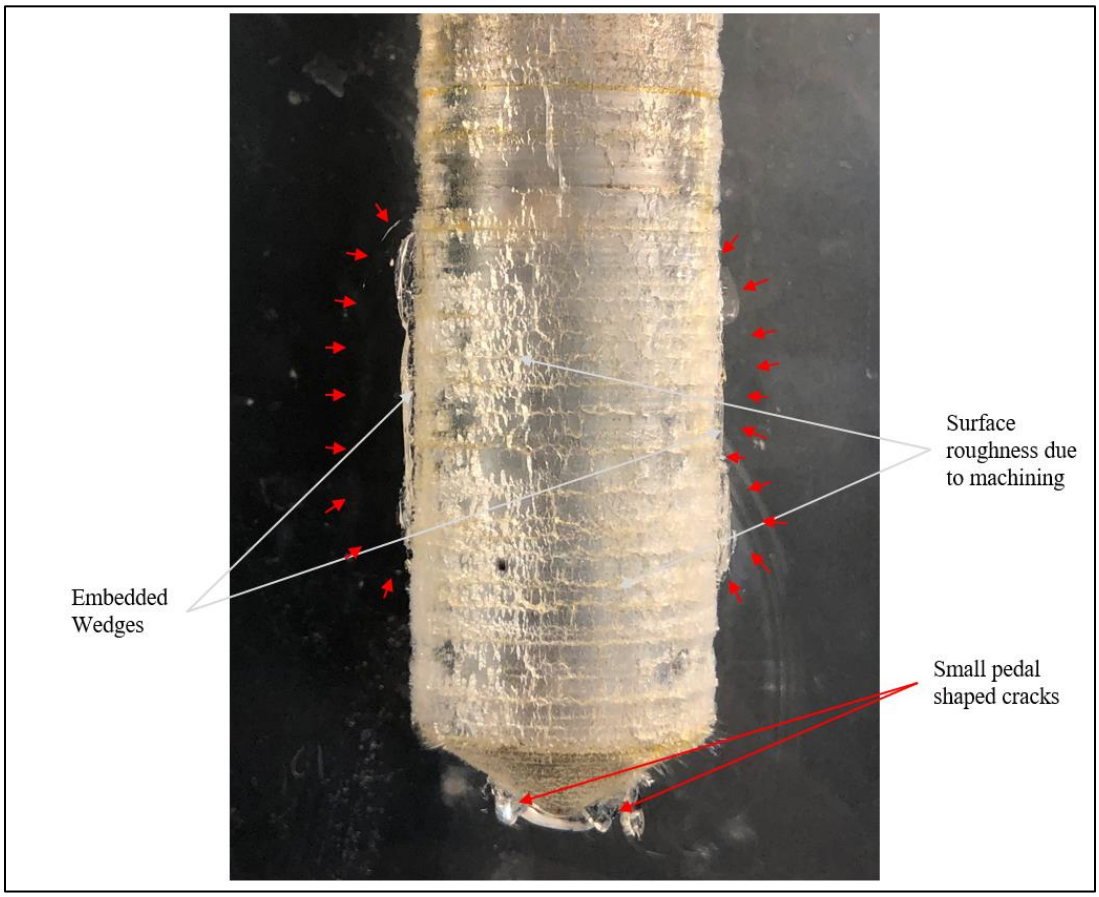

Figure 42: Top view of Test 4, Stage 1

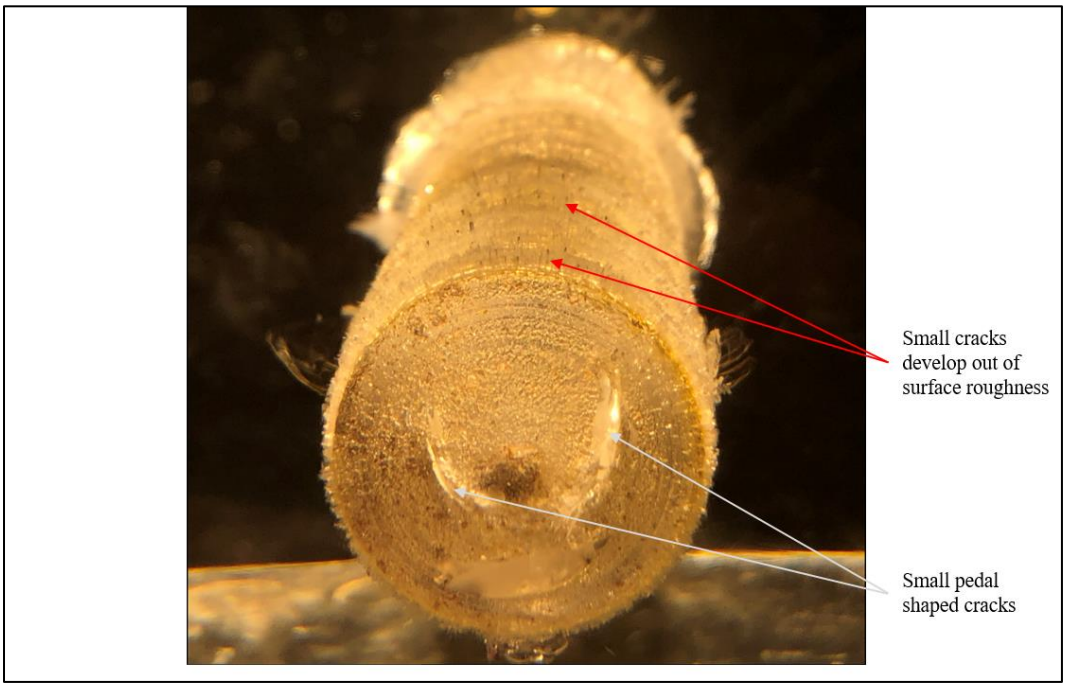

Figure 43: Back view of Test 4, Stage 1

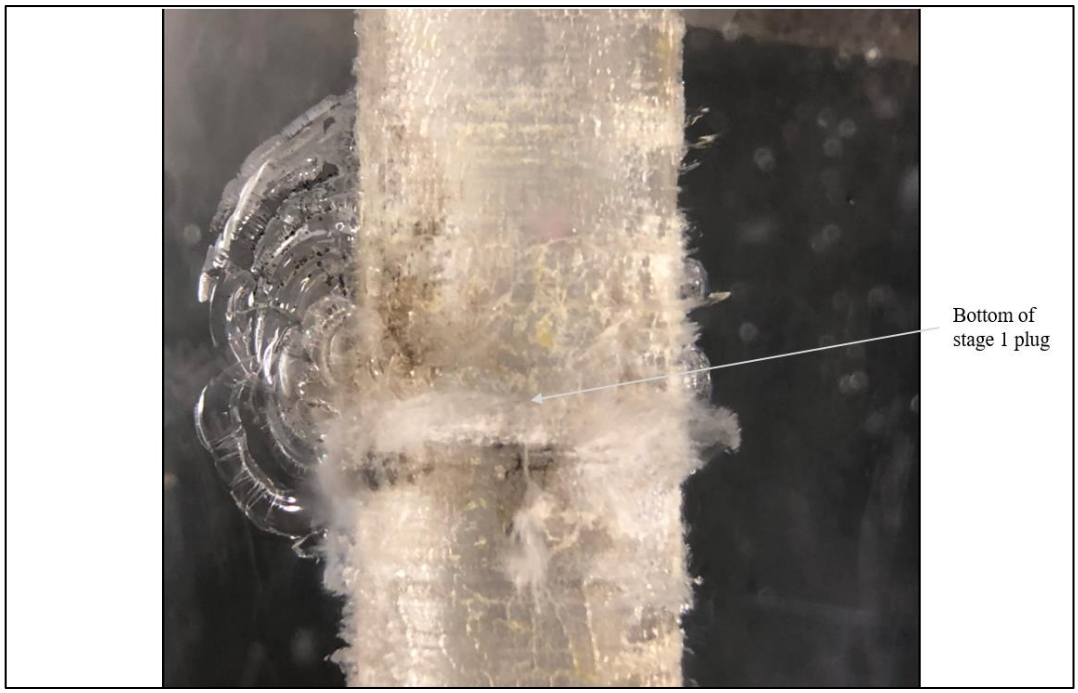

Figure 44: Right view close-up of detonation point, of Test 4, Stage 1

4.6.2 Test 4, Stage 2

The results of stage 2 can be seen from a top view in Figure 45 and a back view in Figure 46. There was significant growth in the horizontal and vertical direction. An important result shown in Figure 46, is the device initiated cracks have grown in the horizontal direction, whereas the resulting horizontal cracks in stage 1 were out of plane a notable amount. The horizontal cracks on the left side of the borehole experienced the most growth. As said in stage 1, there are two separate cracks, each experiencing extension. The maximum horizontal extension from this coalescence of cracks is 32.3 mm (1.27 in) outward from the borehole. The combined longitudinal length is 65 mm (2.56 in), reaching from the circumferential crack at the bottom of the borehole to the bottom of the stage 2 plug. The right side crack is smaller in both extension and length. The maximum extension in the horizontal direction is 22.6 mm (0.89 in). The crack does not extend as far down the borehole, stopping where the borehole begins to change diameter due to the drill bit, instead of extending all the way to the circumferential crack. It does extend all the way up the borehole to the second stage plug, totaling in a peak to peak longitudinal length of 55.2 mm (2.17 in).

The vertical crack development is best seen in Figure 46. There are numerous vertical cracks developed, almost reaching the maximum extension of the device initiated horizontal crack. The largest crack in the vertical direction reaches an extension from the borehole of 30.2 mm (1.19 in). These cracks are likely to be caused by the surface roughness, and are grown from the small cracks displayed in Figure 43.

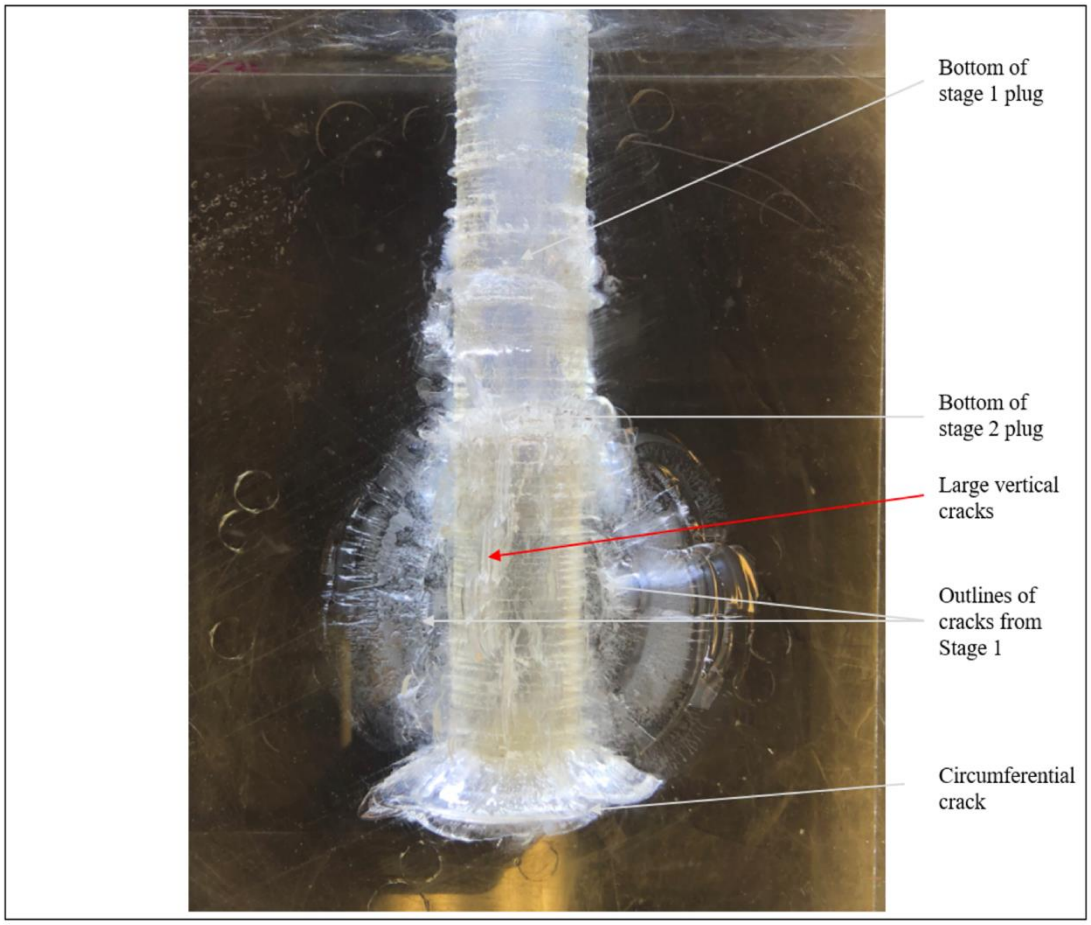

Figure 45: Top view of Test 4, Stage 2

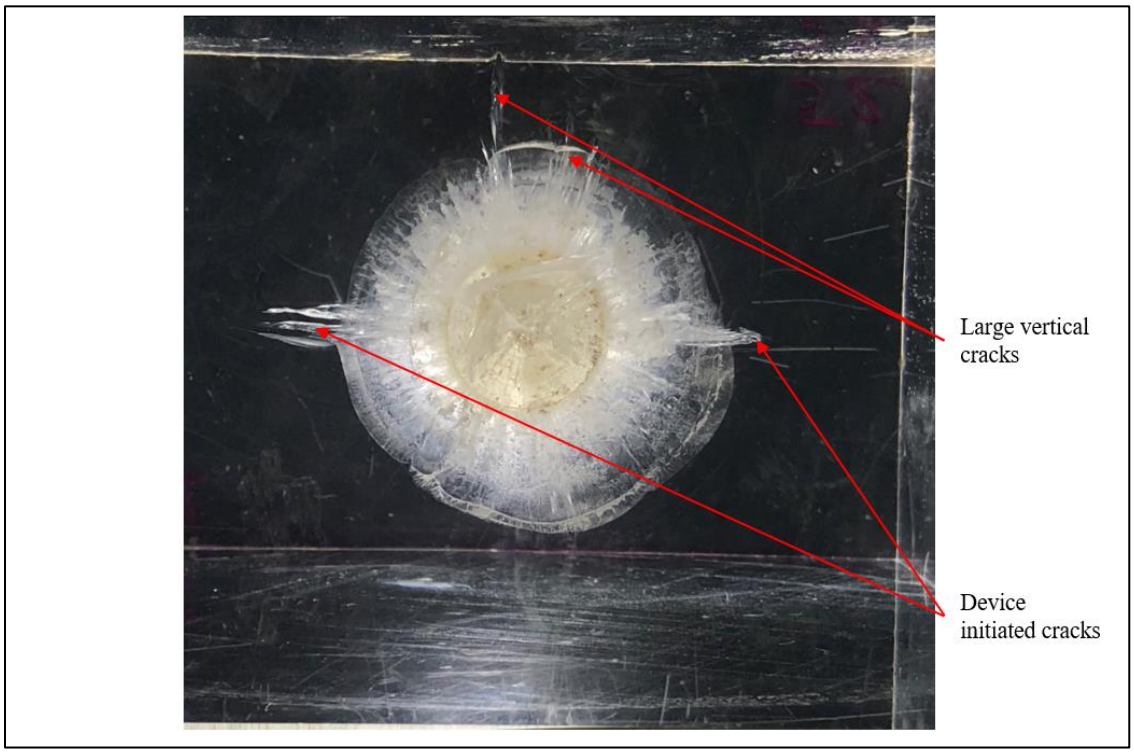

Figure 46: Back view of Test 4, Stage 2

4.6.3 Test 4, Stage 3

The results from stage 3 are displayed from a top view in Figure 47. The pressure in the borehole reached 7.58 MPa (1,100 psi) prior to a fracture on the left side reaching the outer left surface of the block and losing pressure. The crack does not extend down the borehole longitudinally, but it does increase up the borehole to a total longitudinal length of 85.9 mm (3.38 in). The shape of the crack as it extends horizontally is marked with red arrows in Figure 47. The longitudinal length of the crack when it reaches the outside surface is 26.4 mm (1.04 in). The curvature of the statically driven crack is

shown in detail in Figure 48. Note that the curvature is opposite of the original offset of the blades in stage 1.

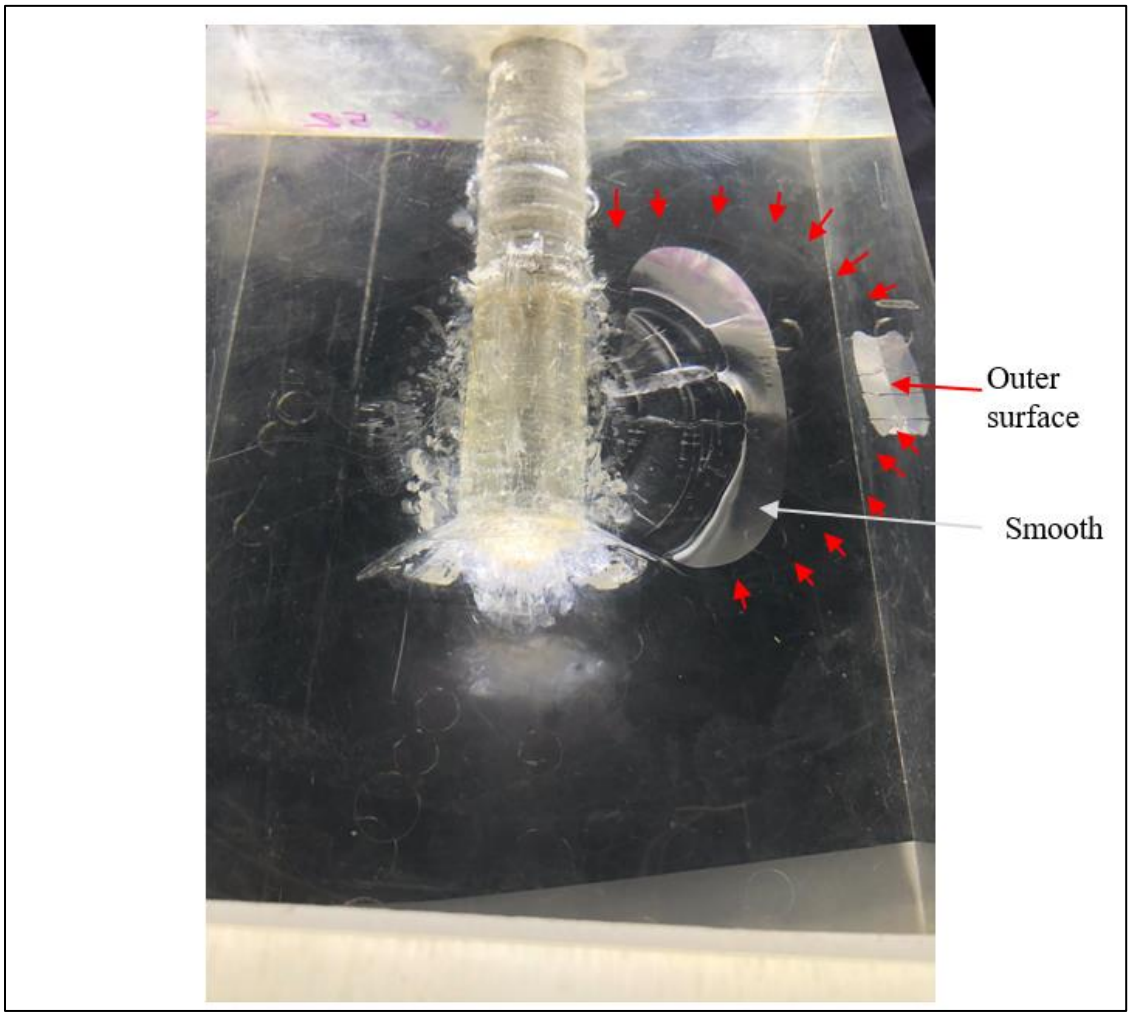

Figure 47: Top view of Test 4, Stage 3

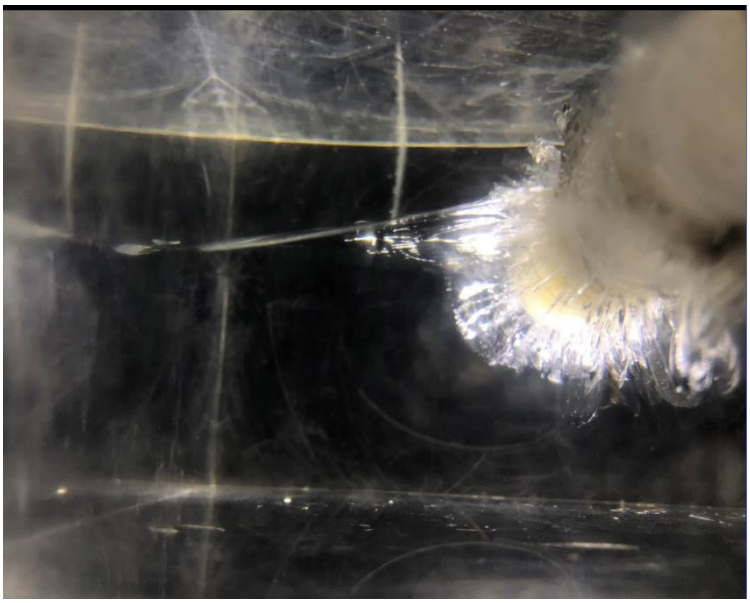

Figure 48: Front view of Test 4, Stage 3

4.6.4 Test 5, Stage 1

The results show the 10° blade to be an ineffective wedge at initiating crack growth. The blades buckled during the test and have negligible penetration of the borehole wall. The small cracks developed are shown in Figure 49. Both the left and right sides of the borehole have crack development that extends less than 1 mm (0.04 in) from the borehole. The left side has a series of very small cracks that cumulatively make up around 19 mm (0.75 in) in total longitudinal length. The right side has crack development of negligible size. Figure 50 shows a left side view. It can be seen that no significant crack is developed from the device, but the borehole has been scored where the wedges impacted and buckled.

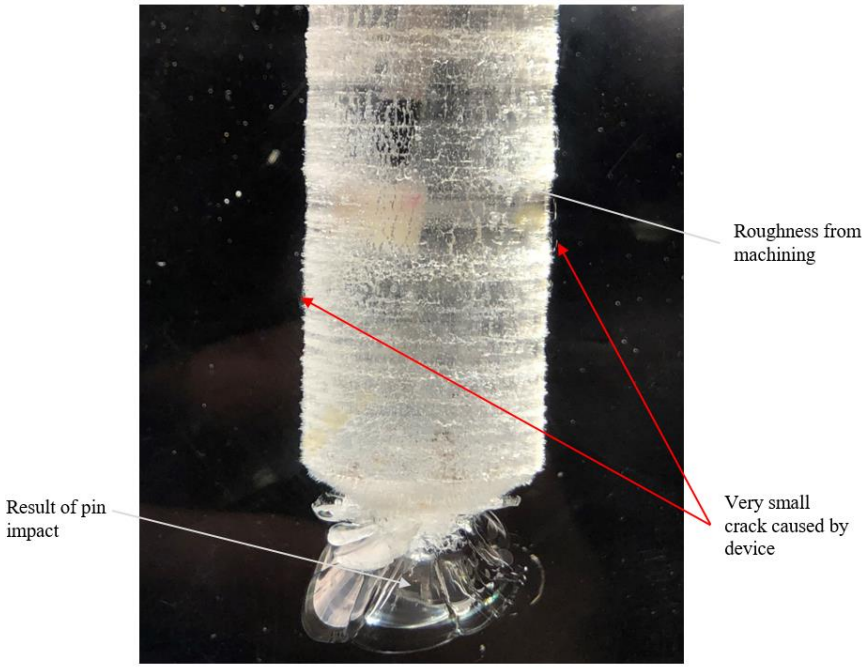

Figure 49: Top view of Test 5, Stage 1

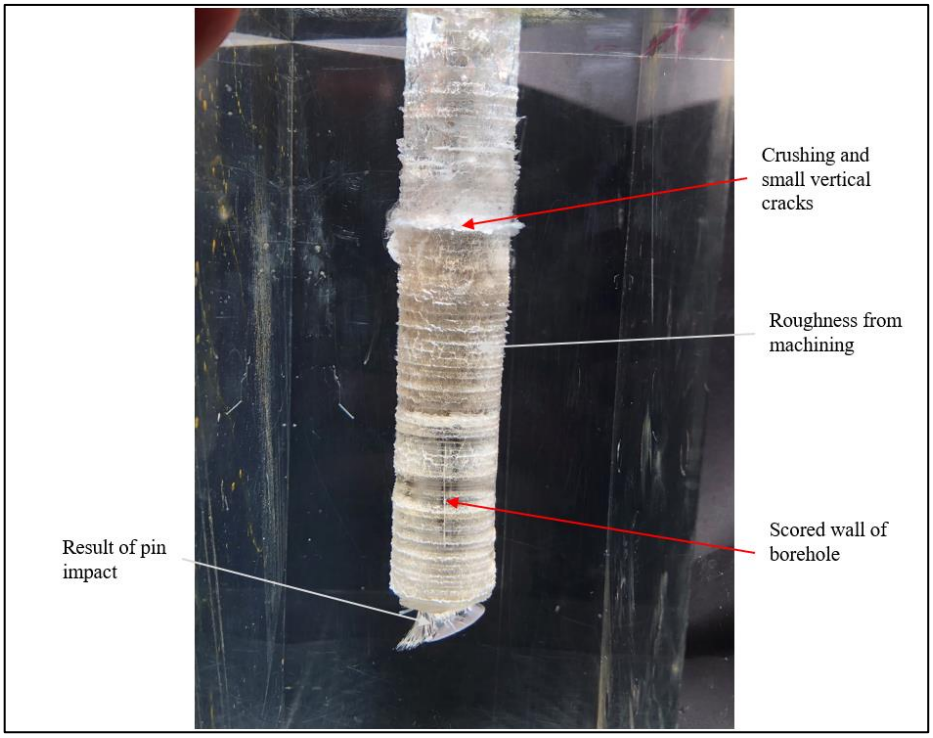

Figure 50: Left side view of Test 5, Stage 1

4.6.5 Test 5, Stage 2

Referring to Figure 51 and Figure 52, it is evident that horizontal cracks did not form in stage 2 of testing. The scored borehole wall from stage 1 was left unchanged and only vertical cracks experienced significant growth. Stage three was not conducted, as there were no horizontal cracks capable of being expanded by quasi-static loading.

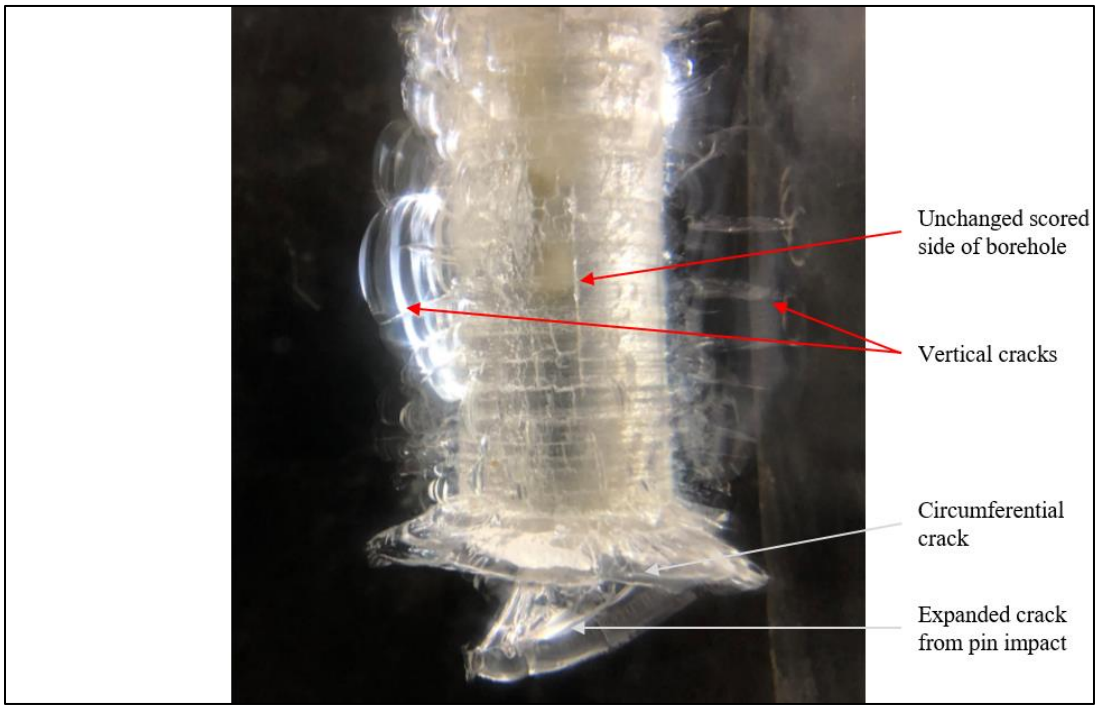

Figure 51: Left side view of Test 5, Stage 2

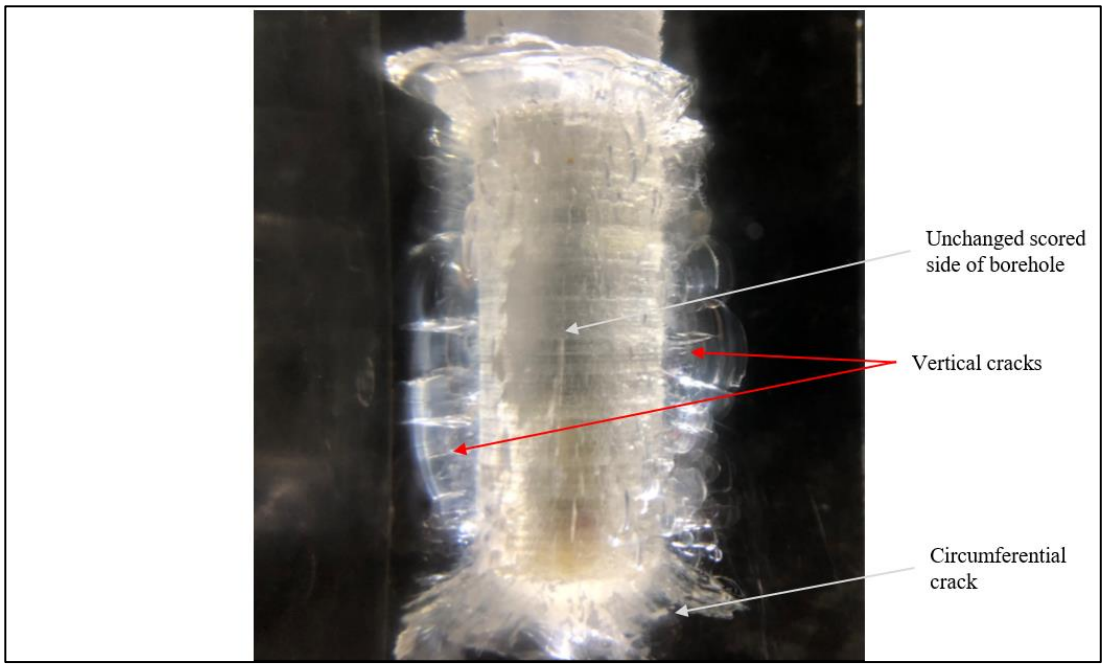

Figure 52: Right side view of Test 5, Stage 2

4.6.7 Test 6, Stage 1

The horizontal crack development from the half inch, 30° wedges used in Test 6 can be seen in Figure 53. It is also worth noting the significant reduction in surface roughness in Test 6, due to the use of a new drill bit during machining. The bottom tip of the borehole is now at an angle of approximately 80° instead of the standard 118°. The two wedges have ejected and formed significant horizontal cracks on each side of the borehole. The right side of the borehole displays the largest crack formation, composed of one large crack, and a smaller crack superimposed to form a single arcing fracture. The total longitudinal length formed is 24.6 mm (0.97 in). The maximum extension outward from the borehole wall is 8.6 mm (0.24 in). The left side crack is composed of

five smaller cracks, failing to coalesce to the same degree as the right horizontal crack. The maximum horizontal distance reached on the left side of the borehole is 6.9 mm (0.27 in). The longitudinal length spanned by the series of small cracks reaches 22.6 mm (0.89 in).

The impact of the pin on the bottom of the borehole creates large pedal shaped cracks as shown in Figure 53. The quantity and magnitude of these pedals is far more significant than the other loaded tests. The cracks together span a horizontal distance of 46.4 mm (1.83 in) peak to peak. The right most pedal also has a longitudinal length of 13.7 mm (0.54 in). A single large vertical crack is shown in Figure 54. After reviewing high speed video footage, it was determined that this crack was formed by the pin dragging along the borehole wall. The longitudinal length is 33 mm (1.3 in) and the peak extension from the borehole in the vertical direction reached 14.7 mm (0.58 in). As expected, there is also some minor crack development and crushing local to the detonation point, limited to radial fracture length of 5 mm (0.2 in). It is worth noting that when the epoxy blew out of the top of the plug, the plug head (section with 25.4 mm (1 in) diameter) fractured radial and blew out the top of the block. Due to the bonding between the plug and borehole wall, some cracking forming in the block as well, the effect of this is labeled in Figure 54.

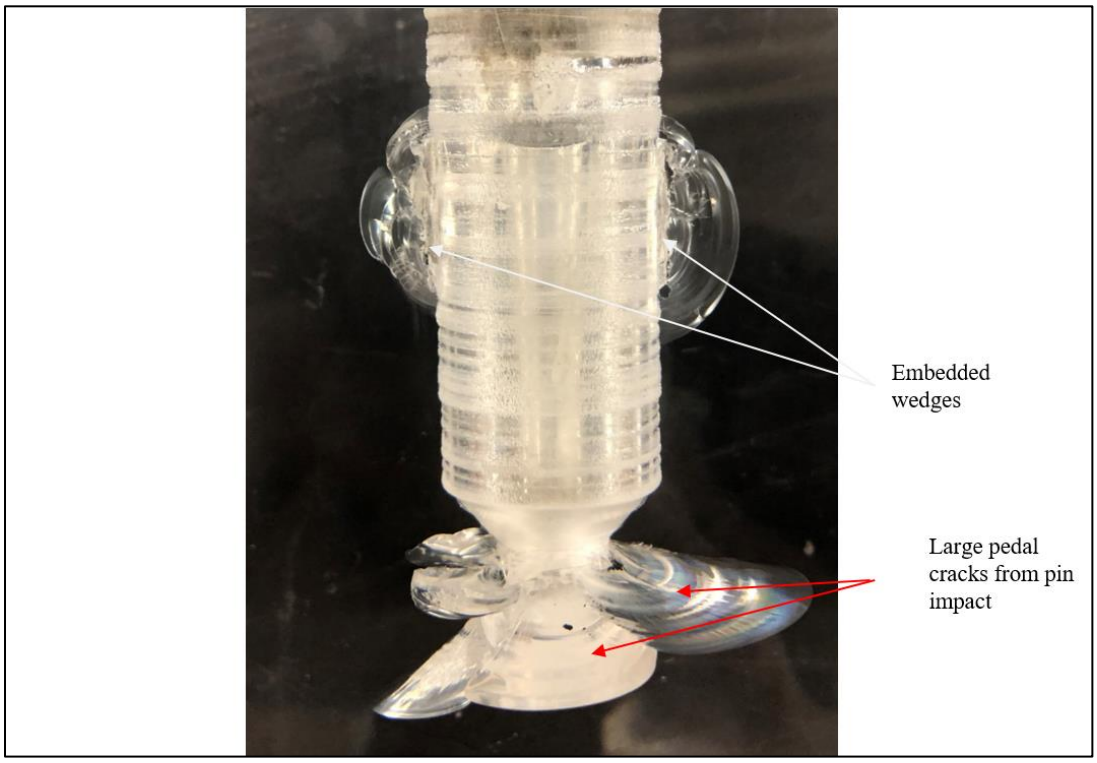

Figure 53: Bottom view of Test 6, Stage 1

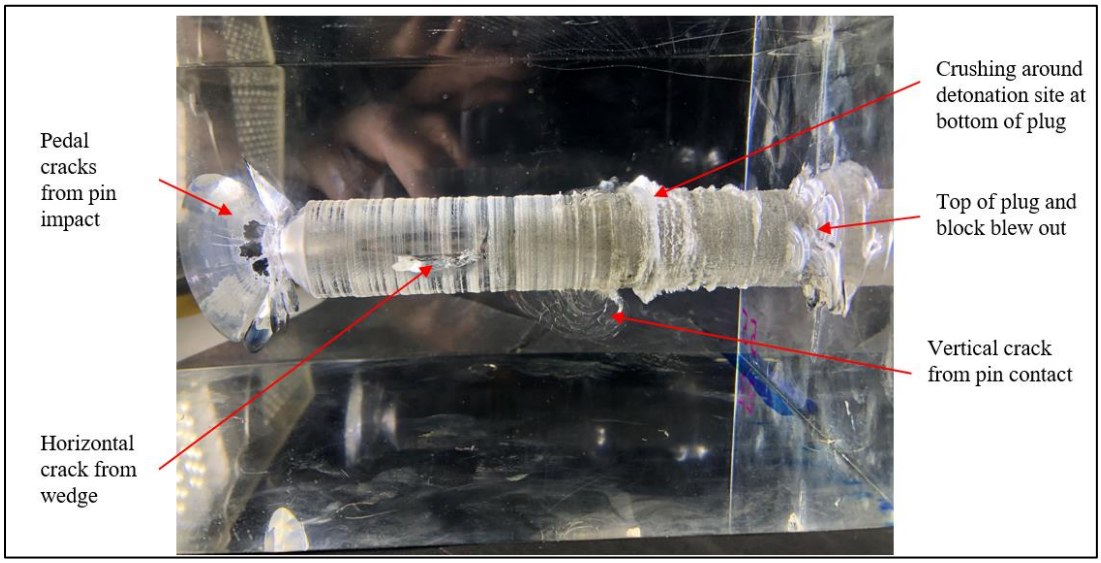

Figure 54: Left side view of Test 6, Stage 1

4.6.8 Test 6, Stage 2

Note that the stage 2 plug used for Test 6 was inserted an extra 5mm (0.2 in) in an effort to plug the vertical crack developed in stage 1. The cracks growth due to stage 2 is presented from a top view in Figure 55. The well-defined arcing horizontal crack from stage 1 on the right side undergoes the largest expansion. This crack extends the full length of the borehole until it reaches the circumferential crack at each discontinuity, reaching a total longitudinal length of 54.9 mm (2.16 in). The two cracks from stage 1 fully merged and extend outward horizontally to a peak of 34.5 mm (1.36 in). The horizontal cracks on the left side of the borehole experience a much smaller degree of growth. The series of small cracks formed in stage 1 extend individually in stage 2, instead of merging. This is labeled in Figure 56. The lack of coalescence is detrimental to the cracks ability to propagate outward. The maximum distance from the borehole achieved is 18.2 mm (0.72 in). The cracks do not span the entire longitudinal length of the borehole. They reach the circumferential crack at the bottom of the stage 2 plug, but only extend downward a total of 43.9 mm (1.73).

Highlighted in both Figure 55 and Figure 56, the large vertical crack initiated in stage 1 merges with newly formed vertical cracks from stage 2. It is likely that the pre-existing flaw aides in the vertical development of new flaws in stage 2, as the other locations experience relatively uniform radial crack growth, not exceeding 7.6mm (0.3 in). The vertical cracks do not reach farther than the 14.7 mm (0.58 in) developed in stage 1, but the longitudinal length of the series of vertical cracks reaches a total of 66 mm (2.6 in). A new circumferential crack forms at the bottom of the borehole and the

bottom of the stage 2 plug. The pedal shape cracks formed in stage 1 expanded and merged into a large cone shaped circumferential crack. The new diameter reaches 55.9 mm (2.2 in) and the longitudinal length expanded to a peak distance of 19.3 mm (0.76 in) towards the back surface. The cracking due to the fracture of the stage one plug remains unchanged.

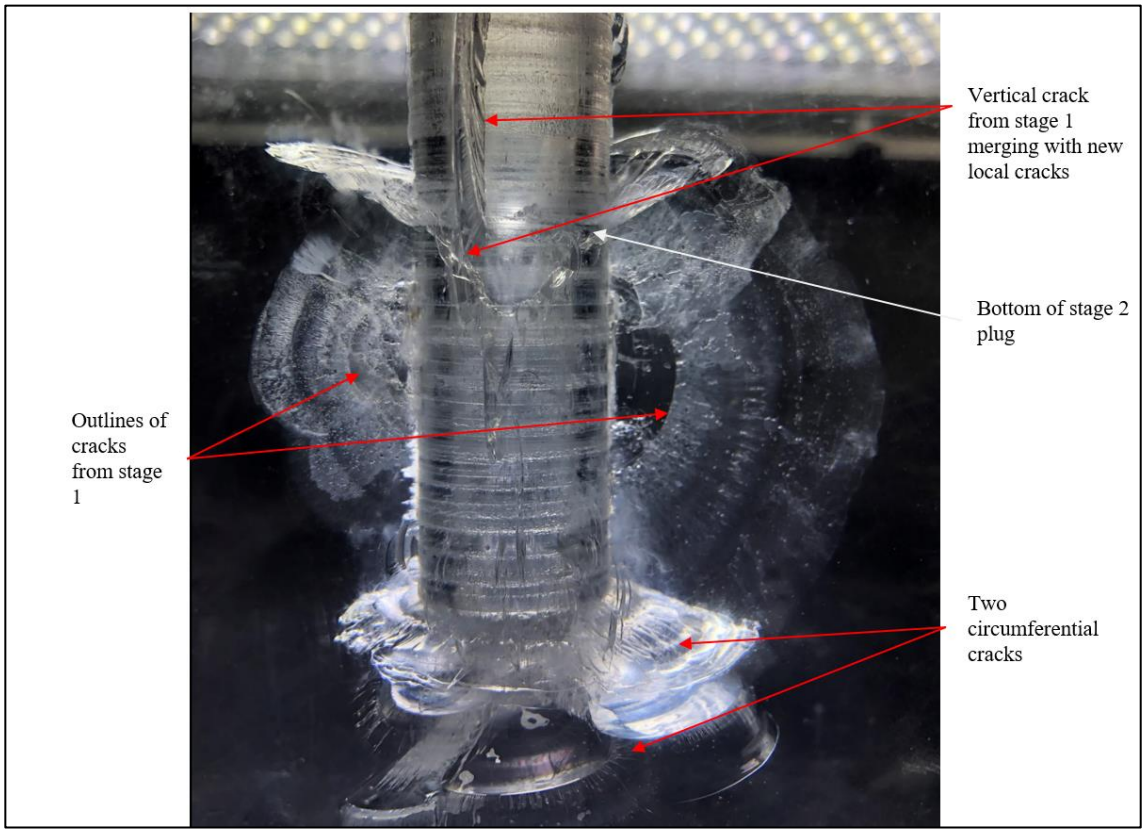

Figure 55: Bottom view of Test 6, Stage 2

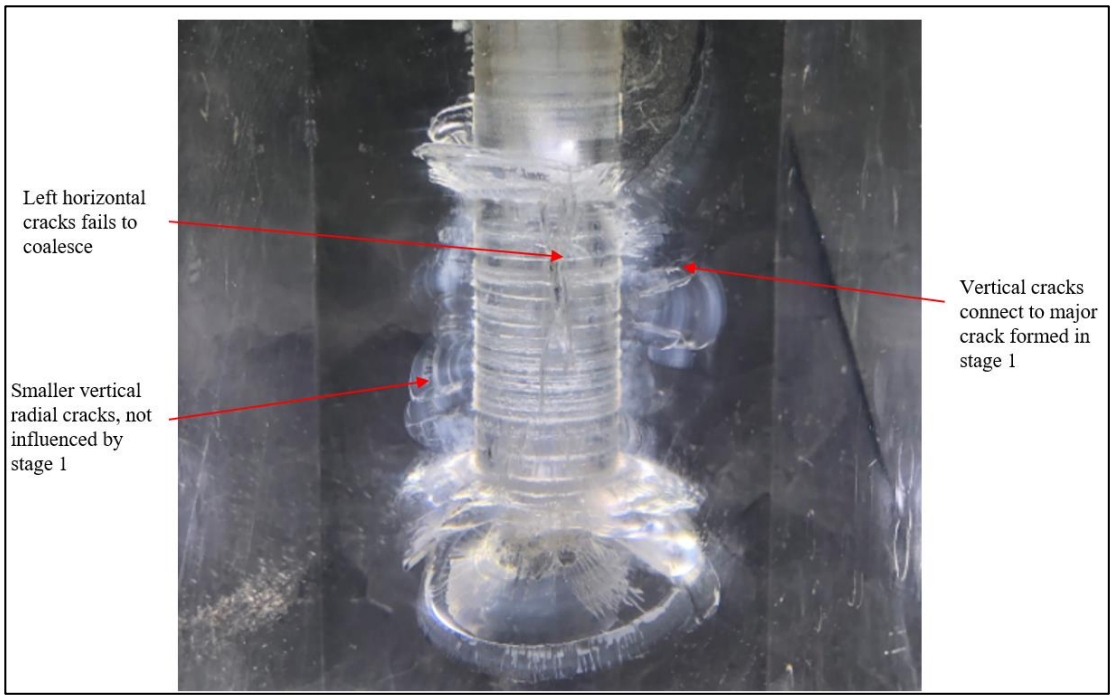

Figure 56: Left side view of Test 6, Stage 2

4.6.9 Test 6, Stage 3

Test 6 was pressurized quasi-statically to 8.27 MPa (1,200 psi) before two cracks formed and extended to the outer bottom surface. One of the cracks originated at the right horizontal crack, extending down the borehole before merging with the large circumferential cracks initiated by the pin impact in stage 1. The interaction with the circumferential crack directs the crack downward sharply to the bottom surface. Although the right crack down not expand all the way outward to the right surface, it experiences a significant amount of horizontal extension. The maximum distance reached from the borehole is 53 mm (2.09 in). Additionally, the right crack has a large width of 31 mm (1.22 in) when reaching the bottom surface. This is larger than the other

loaded condition tests, most likely because it is propagating in the vertical direction and not experiencing as much resistance from the in situ stress. The second crack is a circumferential expansion of the back most circumferential crack. The crack growth originates at the left most tip, expanding outwards circumferentially then downwards towards the bottom surface. Both cracks are outlined in red arrows in Figure 57. Additionally, the side view of each crack is presented in Figure 58.

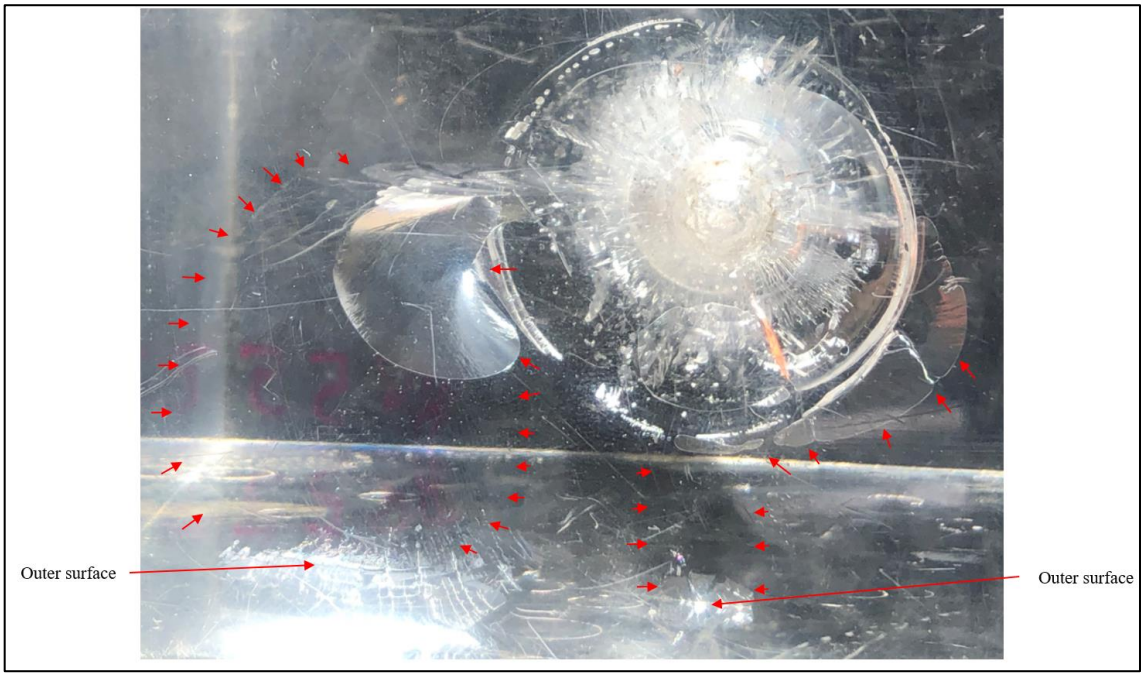

Figure 57: Back view of Test 6, Stage 3

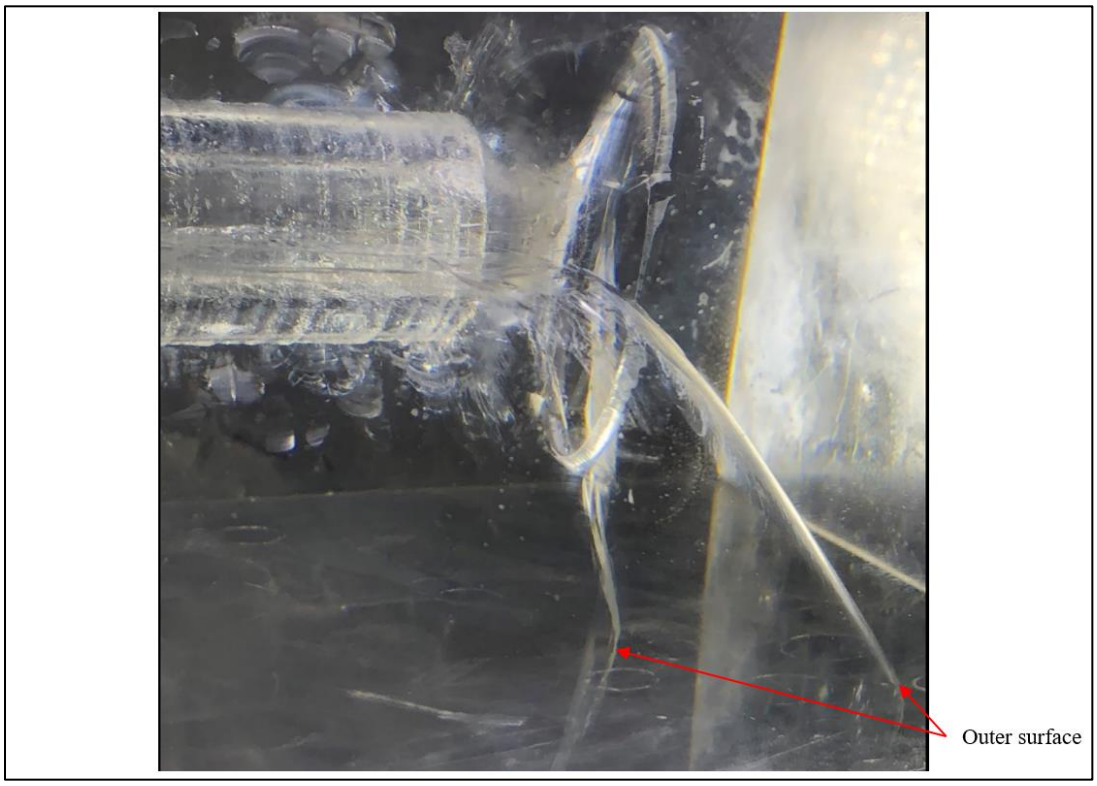

Figure 58: Right side view of Test 6, Stage 3

4.6.10 Discussion of Variations in Wedge Geometry

The variation in wedge blade angle appears to have an effect on the device's capability of ejecting the wedges and initiating crack growth in stage 1. Both Test 4 (20°) and Test 5 (10°) had a lesser degree of wedge ejection, compared to all tests conducted with a 30° wedge. This is likely due to the difference in mass and structure of the portion of the blade deforming the wellbore wall. The extreme of this is seen with Test 5, where the blade completely buckled and was unable to produce any significant horizontal cracks. The effect on Test 5 was less pronounced. The 20° wedges were capable of penetrating the borehole wall, but did not extend out from the borehole nearly

as far. One of the horizontal cracks developed was much smaller than average. However, when stage 2 was conducted on Test 4, the crack growth was comparable to those resulting from the 30° wedges, even the crack extending out from the small horizontal crack in stage 1. This observation shows that while blade angle impacts the ability to drive out the wedges, as long as the blades are capable of penetrating the borehole walls without buckling, the results will be comparable. However, due to the small cracks developed in stage 1 of Test 4, the recommended wedge angle for future tests is 30°, as it is shown to produce the best results at all stages of testing.

The most notable effect of wedge length is the ability to consistently initiate a single well-defined crack. As seen in Test 6, the blades successfully ejected to the same extent as the other 30°, however, the resulting cracks do not have the same characteristics. The left side crack is composed of a series of less defined cracks that do not coalesce during stage 2. The inability to merge and create a large defined crack is problematic when attempting to grow horizontally and overcome the in situ stress. For this reason, the 25.4 mm (1 in) blade is the recommended wedge length.

4.7 Sensitivity to borehole characteristics

The crack growth behavior displayed in the model testing described above shows a dependency on the borehole conditions. Specifically, the roughness of the borehole wall and the various discontinuities due to plugging and machining.

4.7.1 Borehole Wall Roughness

The borehole wall roughness does not seem to directly impact the ability of the device to eject the wedges. However, it does provide a potential flaw for non-horizontal cracks to grow from. These flaws can compete for crack growth with the desired horizontal cracks. This is undesirable, as it uses energy that could otherwise drive the horizontal cracks farther. Cracks growing from roughness flaws also are problematic if they become more well-defined than the horizontal cracks. If this occurs, it has the potential to interfere with the quasi-static expansion of the horizontal fractures. The borehole roughness seems to be most relevant during stage 2 of testing. When using water, the coupling is increased for the purpose of driving out the horizontal cracks. However, coupling also increases the tendency of the roughness flaws to initiate crack growth. For the tests that had successful blade ejection, the surface roughness is ordered most rough to least rough as follows: Test 4, Test 3, Test 2, Test 6, and Test 1. This is shown visually in Figure 59. Note that Test 2 roughness is difficult to see due to the machining oil occupying the small cracks on the surface. The reason for this observed roughness pattern is that the drill bit gradually deteriorated, then was sharpened new for Test 6. The amount of vertical crack development in stage 2 directly follows the pattern of roughness except for Test 3, the no-load condition. This shows that under the same stress field, surface roughness will dictate the extent of radial crack development in the undesired orientation. However, a noticeable decrease in vertical crack development is seen when the vertical compressive stress is absent.

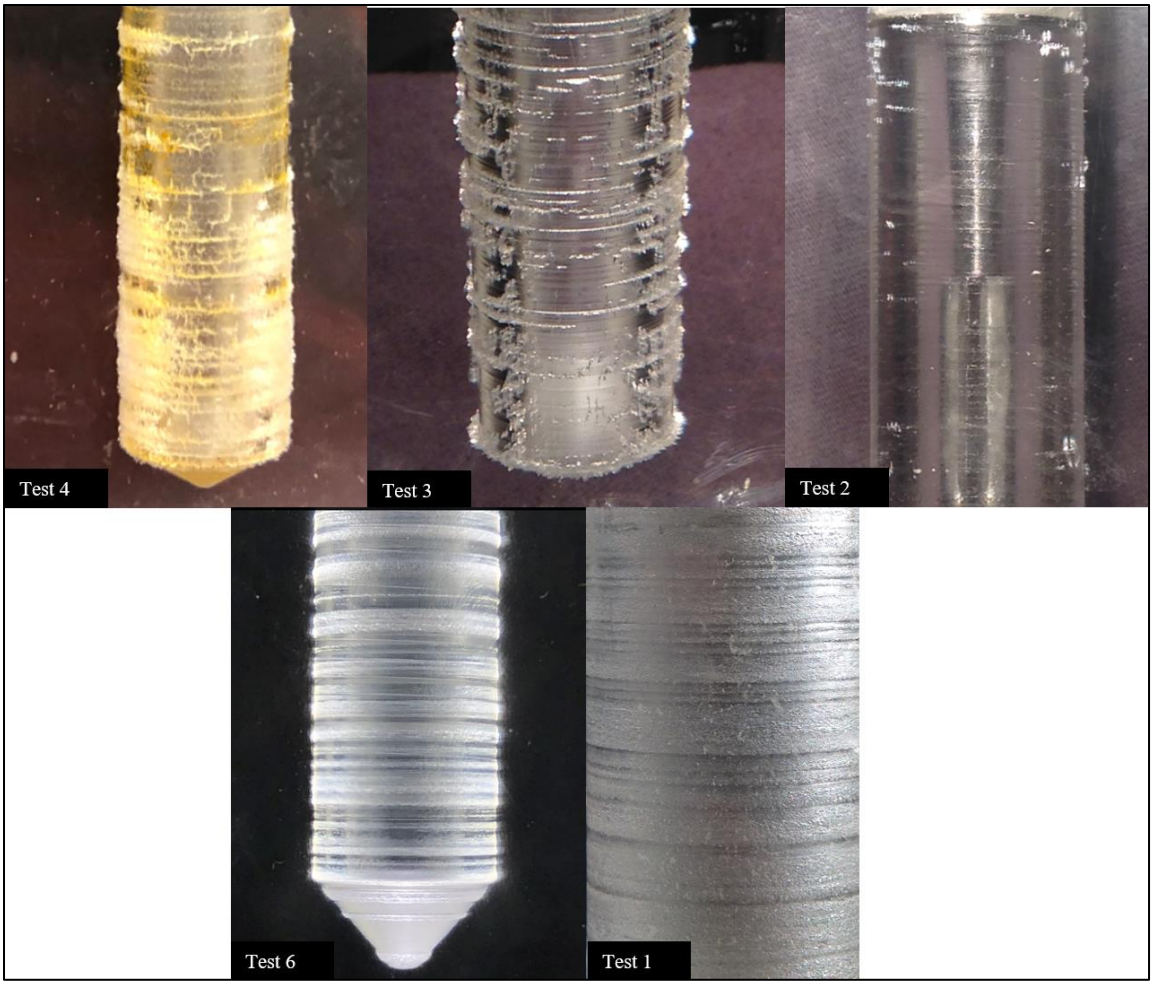

Figure 59: Roughness Comparison

4.7.2 Borehole Discontinuities

After reviewing the test results, the relationship between circumferential crack growth and discontinuities is obvious. When the pressure reaches a change in borehole diameter or plug bottom it increases and creates a circumferential crack. These cracks are mostly insignificant when attempting to grown horizontal fractures, but as seen in Test 6, they can change behavior if the cracks coalesce. In full-scale testing, plugging the

bottom of the borehole so that future circumferential crack growth does not occur is an option. Additionally, in a full-size wellbore there is more flexibility with longitudinal spacing. Placing the device farther away from the bottom of the borehole could avoid the problems observed in Test 6.

The circumferential crack development seen from the pin impacting the bottom of the borehole can also be mitigated. Comparing Test 6 with the models machined with a less steep drill bit shows that the angle affects the crack development from this impact. It is likely that a flat borehole end would best support the impact of the pin and cause less resulting crack growth. An alternative method of minimizing this growth is reducing the mass of the pin. For the purpose of model testing, a large pin head diameter was chosen for durability and the convenience of reusing components. However, the thin headed pin used for Test 1 and Test 2 was equally effective, while producing less of a crack due to impact.

4.8 Implications and Recommendations for Full-Size Testing

As mentioned in the discussion of wedge geometry, the best consistent results have been using the 30° wedge angle and 25.4 mm (1 in) length. The cross section of the wedges are scaled by relating the model borehole diameter to the borehole diameter of full-scale. Typical oil and gas borehole diameters range between 120 mm (4.7 in) and 400 mm (15.7 in) [30]. Assuming a medium sized borehole diameter of 200 mm (7.9 in), the length scaling factor will be 8.4. An engineering drawing and relevant dimensions of the components are shown in Figure 60, Figure 61, and Figure 62.

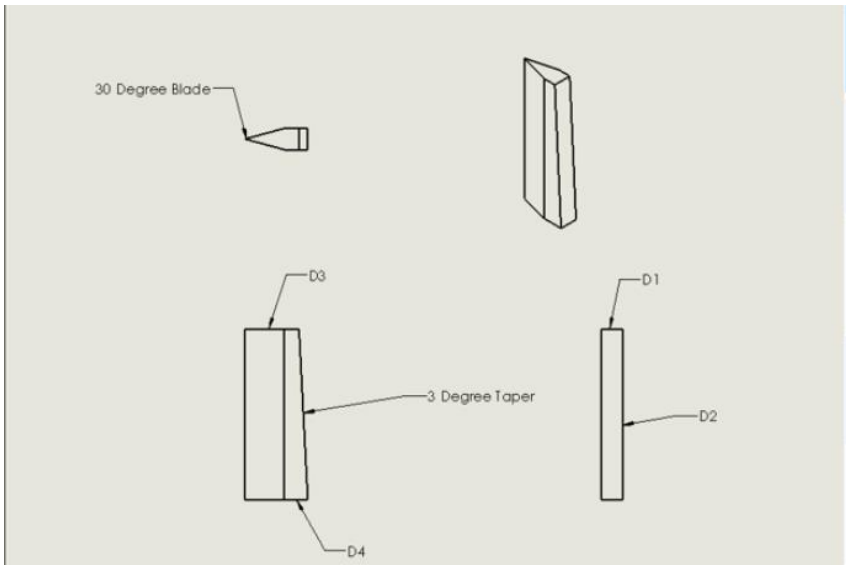

Dimension	Numerical Value [mm] (in)
D1	26.7 mm (1.05 in)
D2	213 mm (8.4 in)
D3	49.8 mm (1.96 in)
D4	80.2 mm (3.16 in)

Figure 60: Engineering Drawing of Scaled Wedge

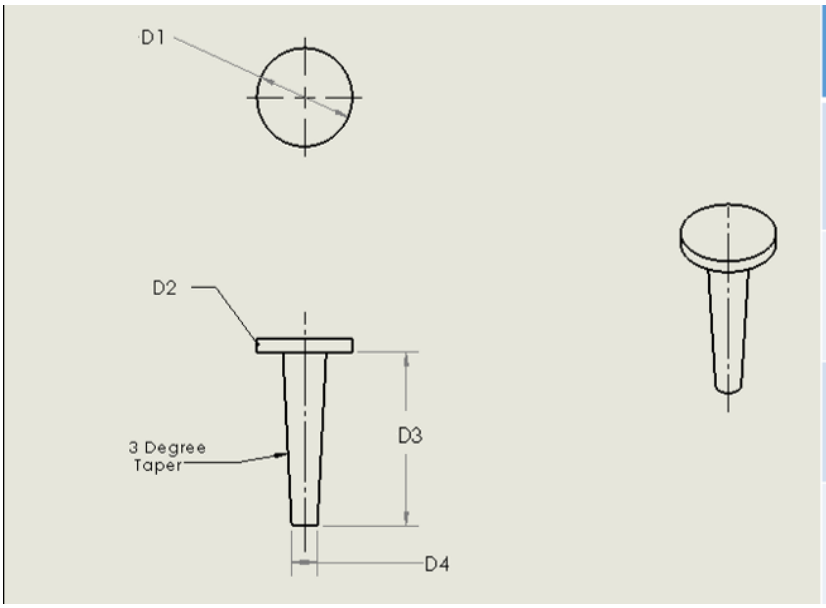

Dimension	Numerical Value [mm] (in)
D1	197 mm (7.75 in)
D2	13.3 mm (0.525 in)
D3	347 mm (13.7 in)
D4	53.3 mm (2.1 in)

Figure 61: Engineering Drawing of Scaled Pin

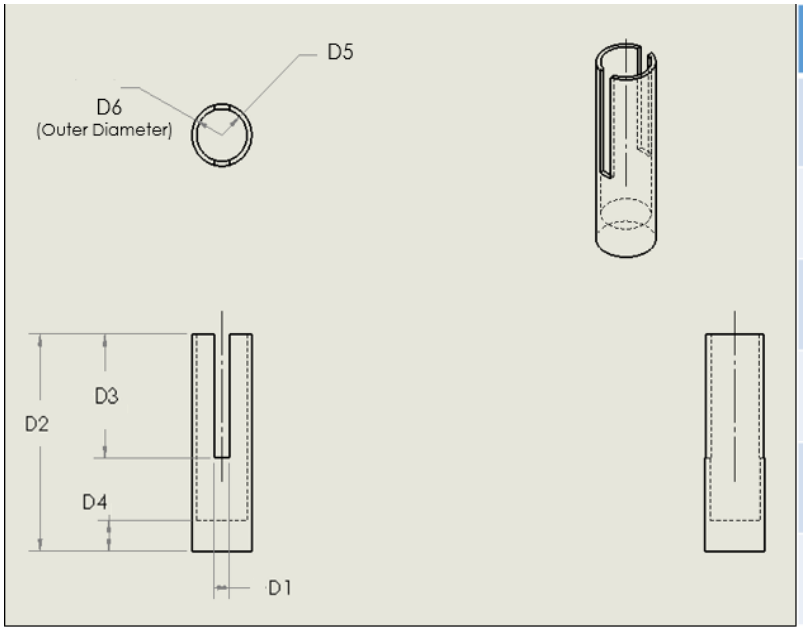

Dimension	Numerical Value [mm] (in)
D1	26.7 mm (1.05 in)
D2	373 mm (14.7 in)
D3	213 mm (8.4 in)
D4	53.3 mm (2.1 in)
D5	89.9 mm (3.54 in)
D6	107 mm (4.2 in)

Figure 62: Engineering Drawing of Scaled Rod

The charge size will use cube root scaling. Meaning for a length scaling factor of 8.4, the charge mass will be increased by a factor of 592.7. Including the initiating explosive, the total charge masses at model scale are 260 mg and 110 mg, for stage 1 and stage 2 respectively. Scaling to full-scale results in a first stage explosive mass of 154 grams, to be detonated in an aired filled borehole and a second stage explosive mass of 65 grams, to be detonated in a water filled borehole.

From the results observed during model testing, it is advised that the outside diameter of the pin head be lubricated prior to testing. This will ensure that it does not drag significantly against the borehole surface causing unwanted crack development, as seen in Test 6. It is also important that a sharp drill bit is used when creating the wellbore. Minimizing surface roughness will increase the effectiveness of the device in regards to controlling crack growth orientation.

Chapter 5: Conclusions and Future Work

5.1 Conclusion

The purpose of this research was to develop a mechanical device capable of initiating fracture growth in a horizontal wellbore, providing a more environmentally friendly method of accessing unconventional reservoirs. This problem was modeled by controlling the orientation of crack growth in a borehole loaded by an unfavorable in situ stress field. Preliminary testing was performed to explore mechanisms of initiating fractures, determine an appropriate size scale of explosives and device components, and assess optimal fluid medium for various stages of testing. The results from preliminary testing were used in an iterative process to make changes to the developing mechanical device until an acceptable design was determined.

After determining an initial design, six detailed tests were conducted. The repeatability of the device was proven and acceptable variation in the results was discussed. A no-load test was performed to study the effect of the applied in situ stress and observe the successfully functioning device with a high speed camera. Three variations in component geometry were manufactured and tested to determine which geometry produced optimal fracture growth. The sensitivity to changes in borehole conditions was discussed. Finally, the best performing device geometry was scaled and a schematic is prevented for full scale manufacturing and testing.

The results presented in this paper prove that using an insertable device is a promising method for the purpose of controlled fracture initiation. The ability to produce well-defined horizontal cracks in the presence of a vertical compressive stress

demonstrates the appeal of using this technique. The method presented is a potential alternative to the current methods used in hydraulic fracturing, but additional testing is recommended to assess the performance at a larger scale.

5.2 Suggested Future Work

With the successful development of a small-scale model device, the next step would be increasing the scale or complexity of the testing. This could include using the recommended scaled device to see if the results can be replicated in the real environment. A less aggressive and more economically feasible option might be to conduct a new series of model tests in a non-homogenous material. Using a lamina structure to mimic the joints found in rock would give insight into how interfaces and boundaries would affect crack propagation. Increasing the complexity of the model would undoubtedly be beneficial in further developing an insertable device for controlling crack growth orientation.

Another opportunity for continuing this work would be variation in material choices and pressurization methods of the current device, specifically manipulating the mechanical characteristics of the tapered wedge. Implementing a destructive wedge capable of initiating cracks before losing its structure would be very beneficial. Accomplishing this would alleviate the complications of removing the ejected wedges in full-scale modeling. Finally, considering implementing a fourth pressurization stage is an alternative method of improving the current process. An investigation into using

dynamic loading via explosives could be performed as a fourth stage to increase the roughness and crack quality of the cracks previously formed by quasi-static loading.

Bibliography

[1] "U.S. Energy Facts Explained: Consumption & Production," *U.S. Energy Information Administration*. [Online]. Available: https://www.eia.gov/energyexplained/?page=us_energy_home. [Accessed: 28-Dec-2017].

[2] "Annual Energy Outlook 2016: Marked Trends: Natural Gas," *U.S. Energy Information Administration*, 2016. [Online]. Available: https://www.eia.gov/outlooks/archive/aeo16/MT_naturalgas.cfm#natgasprod_exp. [Accessed: 28-Dec-2017].

[3] National Energy Technology Laboratory. "Modern Shale Gas Development in the United States: A Primer," *U.S. Department of Energy*, 2009. [Online]. Available: https://energy.gov/sites/prod/files/2013/03/f0/ShaleGasPrimer_Online_4-2009.pdf. [Accessed: 28-Dec-2017].

[4] House, Review of hydraulic fracturing technology and practices: hearing before the Committee on Science, Space, and Technology, House of Representatives, One Hundred Twelfth Congress, first session, Wednesday, May 11, 2011. Washington: U.S. G.P.O., 2011.

[5] Veatch, R.W., Jr., Moschovidis, Z.A., and Fast, C. R. 1989. An Overview of Hydraulic Fracturing. Recent Advances in Hydraulic Fracturing, ed J.L. Gidley, S.A. Holditch, D.E. Nierode, and R.W. Veatch Jr., Vol. 12. Richardson, Texas: Henry L. Doherty Monograph Series, SPE.

[6] Jennings, A.R., Jr., and Darden W. G. 1979. Gas Well Stimulation in the Eastern United States. SPE 7914.

[7] Stephenson, M.H. Shale gas and fracking: The science behind the controversy. Amsterdam (Holanda): Elsevier Science, 2015.

[8] Overbey, W.K., A.B. Yost, and D.A. Wilkins. 1988. Inducing Multiple Hydraulic Fractures from a Horizontal Wellbore. SPE 18249.

[9] Chesapeake Energy Corporation. Components of Hydraulic Fracturing, Presented to the NY DEC. October 2008.

[10] Wood, P. "Maryland General Assembly approves fracking ban," *Baltimore Sun*, 28-Mar-2017. [Online] Available: http://www.baltimoresun.com/news/maryland/politics/bs-md-fracking-ban-passes-20170327-story.html. [Accessed: 28-Dec-2017].

[11] Evensen, D., Jacquet, J.B., Clarke, C.E., and Stedman, R.C, 'What's the

'fracking' problem? One word can't say it all', *The Extractive Industries and Society*, vol. 1, no. 2, pp. 130-136, 2014.

[12] Zhang, D., and Yang, T, 'Environmental impacts of hydraulic fracturing in shale gas development in the United States', *Petroleum Exploration and Development*, vol. 42, no. 6, pp. 876-883, 2015.

[13] Howarth, R.W., Ingraffea, A., and Engelder, T., 'Natural gas: Should fracking stop?', *Nature*, vol. 477, no. 7364, pp. 271-275, 2011.

[14] Ellsworth, W L., 'Injection-induced earthquakes', *Science*, vol. 341, no. 6142, pp. 1225942-1–1225942-7, 2013.

[15] King, G E. 2012. Hydraulic fracturing 101: What every representative, environmentalist, regulator, reporter, investor, university researcher, neighbor and engineer should know about estimating frac risk and improving frac performance in unconventional gas and oil wells. SPE 152596.

[16] Osborn, S.G., Vengosh, A., Warner, N.R., et al., 'Methane contamination of drinking water accompanying gas-well drilling and hydraulic fracturing', *Proceedings of the National Academy of Sciences*, vol. 108, no. 20, pp. 8172-8176, 2011.

[17] Jackson, R.B., Vengosh, A., Darrah, T.H., et al., 'Increased stray gas abundance in a subset of drinking water wells near Marcellus shale gas extraction', *Proceedings of the National Academy of Sciences*, vol. 110, no. 28, pp. 11250-11255, 2013.

[18] Warner, N.R., Christie, C.A., Jackson, R.B., et al., 'Impacts of shale ga wastewater disposal on water quality in western Pennsylvania', *Environmental Science & Technology*, vol. 47, no. 20, pp. 11849-11857, 2013.

[19] Barker, D.B., Fourney W.L., and Dally, J.W., 'Fracture control in tunnel blasting: In tunneling and underground structures', *Transportation Research Record*, no. 684, 1978.

[20] McKown, A. F., Fourney, W.L., Sperry P. E., and Thompson, D.E., 'Field evaluation of fracture control in tunnel blasting,' Report No. 3060, U.S. Department of Transportation, Sep 1978.

[21] Fourney, W.L., and Leiste, U., 'Controlled explosive fracturing', *Blasting & Fragmentation*, vol. 9, no. 1, 2015.

[22] Fourney, W.L., and Barker, D.B., 'Characteristics of a crack driven by explosive loading', UMD Report to Department of Energy, Aug 1979.

[23] Fourney, W.L., Barker, D.B., and Holloway, D.C., 'Model studies of explosive well stimulation techniques', International Journal of Rock Mechanics and Mining Sciences & Geomechanics Abstracts, vol. 18, no. 2, pp. 113-127, 1981.

[24] Bieniawski, Z.T., 'Mechanism of brittle fracture of rock: Part I-theory of the fracture process', International Journal of Rock Mechanics and Mining Sciences & Geomechanics Abstracts, vol. 4, no. 4, pp. 395-404, 1967.

[25] Li, Q., Xing, H., Liu, J., and Liu, X., 'A review of hydraulic fracturing of unconventional reservoir', *Petroleum*, vol. 1, no. 1, pp. 8-15, 2015.

[26] Saharan, M.R., Mitri, H.S., and Jethwa, J.L., 'Rock fracturing by explosive energy: Review of state-of-the-art,' *Fragblast* The International Journal for Blasting and Fragmentation, vol. 10, no. 1-2, March-June 2006.

[27] Baker, W.E., Westine, P.S., and Dodge, F.T., *Similarity Methods in Engineering Dynamics: Theory and Practice of Scale Modeling*, Spartan Books, Haydon Book Company, Inc., Rochelle Park, New Jersey, 1973.

[28] Swisdak, M.M., 'Explosion Effects and Properties Part I - Explosion Effects in Air', NSWC-TR 75-116, Naval Surface Warfare Center, White Oak, MD, 1975.

[29] Fu, R., Lindfors, A., and Davis, J., 'Scaling for Internal Blast', AIP Conference. Proceedings, vol. 706, pp. 1440-1443, 2004.

[30] Lecampion, B., 'Modeling size effects associated with tensile fracture initiation from a wellbore', *International Journal of Rock Mechanics and Mining Sciences*, vol. 56, pp. 67-76, Dec 2012.